THE UNIVERSITY OF CALGARY

MODELLING THE DISSOLUTION OF A CO_2 BUBBLE INTO ATHABASCA BITUMEN

by

RICHARD J. DUNN

A THESIS

SUBMITTED TO THE FACULTY OF GRADUATE STUDIES

IN PARTIAL FULFILMENT OF THE REQUIREMENTS FOR THE

DEGREE OF MASTER OF ENGINEERING IN CHEMICAL ENGINEERING

DEPARTMENT OF CHEMICAL AND PETROLEUM ENGINEERING

CALGARY, ALBERTA

July, 1993

ISBN 0-315-88504-1

Name Richard James Dunn

Dissertation Abstracts International is arranged by broad, general subject categories. Please select the one subject which most nearly describes the content of your dissertation. Enter the corresponding four-digit code in the spaces provided.

Thesis title: Modelling the Dissolution of a CO_2 Bubble Into Athabasca Bitumen

SUBJECT TERM

0542

SUBJECT CODE

U·M·I

subject term - Chemical Engineering

Subject Categories

THE HUMANITIES AND SOCIAL SCIENCES

COMMUNICATIONS AND THE ARTS

Architecture 0729
Art History 0377
Cinema 0900
Dance 0378
Fine Arts 0357
Information Science 0723
Journalism 0391
Library Science 0399
Mass Communications 0708
Music 0413
Speech Communication 0459
Theater 0465

EDUCATION

General 0515
Administration 0514
Adult and Continuing 0516
Agricultural 0517
Art 0273
Bilingual and Multicultural 0282
Business 0688
Community College 0275
Curriculum and Instruction 0727
Early Childhood 0518
Elementary 0524
Finance 0277
Guidance and Counseling 0519
Health 0680
Higher 0745
History of 0520
Home Economics 0278
Industrial 0521
Language and Literature 0279
Mathematics 0280
Music 0522
Philosophy of 0998
Physical 0523

Psychology 0525
Reading 0535
Religious 0527
Sciences 0714
Secondary 0533
Social Sciences 0534
Sociology of 0340
Special 0529
Teacher Training 0530
Technology 0710
Tests and Measurements 0288
Vocational 0747

LANGUAGE, LITERATURE AND LINGUISTICS

Language
- General 0679
- Ancient 0289
- Linguistics 0290
- Modern 0291

Literature
- General 0401
- Classical 0294
- Comparative 0295
- Medieval 0297
- Modern 0298
- African 0316
- American 0591
- Asian 0305
- Canadian (English) 0352
- Canadian (French) 0355
- English 0593
- Germanic 0311
- Latin American 0312
- Middle Eastern 0315
- Romance 0313
- Slavic and East European 0314

PHILOSOPHY, RELIGION AND THEOLOGY

Philosophy 0422
Religion
- General 0318
- Biblical Studies 0321
- Clergy 0319
- History of 0320
- Philosophy of 0322

Theology 0469

SOCIAL SCIENCES

American Studies 0323
Anthropology
- Archaeology 0324
- Cultural 0326
- Physical 0327

Business Administration
- General 0310
- Accounting 0272
- Banking 0770
- Management 0454
- Marketing 0338

Canadian Studies 0385
Economics
- General 0501
- Agricultural 0503
- Commerce-Business 0505
- Finance 0508
- History 0509
- Labor 0510
- Theory 0511

Folklore 0358
Geography 0366
Gerontology 0351
History
- General 0578
- Ancient 0579
- Medieval 0581
- Modern 0582
- Black 0328
- African 0331
- Asia, Australia and Oceania 0332
- Canadian 0334
- European 0335
- Latin American 0336
- Middle Eastern 0333
- United States 0337

History of Science 0585
Law 0398
Political Science
- General 0615
- International Law and Relations 0616
- Public Administration 0617

Recreation 0814
Social Work 0452
Sociology
- General 0626
- Criminology and Penology 0627
- Demography 0938
- Ethnic and Racial Studies 0631
- Individual and Family Studies 0628
- Industrial and Labor Relations 0629
- Public and Social Welfare 0630
- Social Structure and Development 0700
- Theory and Methods 0344

Transportation 0709
Urban and Regional Planning 0999
Women's Studies 0453

THE SCIENCES AND ENGINEERING

BIOLOGICAL SCIENCES

Agriculture
- General 0473
- Agronomy 0285
- Animal Culture and Nutrition 0475
- Animal Pathology 0476
- Food Science and Technology 0359
- Forestry and Wildlife 0478
- Plant Culture 0479
- Plant Pathology 0480
- Plant Physiology 0817
- Range Management 0777
- Wood Technology 0746

Biology
- General 0306
- Anatomy 0287
- Biostatistics 0308
- Botany 0309
- Cell 0379
- Ecology 0329
- Entomology 0353
- Genetics 0369
- Limnology 0793
- Microbiology 0410
- Molecular 0307
- Neuroscience 0317
- Oceanography 0416
- Physiology 0433
- Radiation 0821
- Veterinary Science 0778
- Zoology 0472

Biophysics
- General 0786
- Medical 0760

EARTH SCIENCES

Biogeochemistry 0425
Geochemistry 0996

Geodesy 0370
Geology 0372
Geophysics 0373
Hydrology 0388
Mineralogy 0411
Paleobotany 0345
Paleoecology 0426
Paleontology 0418
Paleozoology 0985
Palynology 0427
Physical Geography 0368
Physical Oceanography 0415

HEALTH AND ENVIRONMENTAL SCIENCES

Environmental Sciences 0768
Health Sciences
- General 0566
- Audiology 0300
- Chemotherapy 0992
- Dentistry 0567
- Education 0350
- Hospital Management 0769
- Human Development 0758
- Immunology 0982
- Medicine and Surgery 0564
- Mental Health 0347
- Nursing 0569
- Nutrition 0570
- Obstetrics and Gynecology 0380
- Occupational Health and Therapy 0354
- Ophthalmology 0381
- Pathology 0571
- Pharmacology 0419
- Pharmacy 0572
- Physical Therapy 0382
- Public Health 0573
- Radiology 0574
- Recreation 0575
- Speech Pathology 0460
- Toxicology 0383

Home Economics 0386

PHYSICAL SCIENCES

Pure Sciences

Chemistry
- General 0485
- Agricultural 0749
- Analytical 0486
- Biochemistry 0487
- Inorganic 0488
- Nuclear 0738
- Organic 0490
- Pharmaceutical 0491
- Physical 0494
- Polymer 0495
- Radiation 0754

Mathematics 0405
Physics
- General 0605
- Acoustics 0986
- Astronomy and Astrophysics 0606
- Atmospheric Science 0608
- Atomic 0748
- Electronics and Electricity 0607
- Elementary Particles and High Energy 0798
- Fluid and Plasma 0759
- Molecular 0609
- Nuclear 0610
- Optics 0752
- Radiation 0756
- Solid State 0611

Statistics 0463

Applied Sciences

Applied Mechanics 0346
Computer Science 0984

Engineering
- General 0537
- Aerospace 0538
- Agricultural 0539
- Automotive 0540
- Biomedical 0541
- Chemical 0542
- Civil 0543
- Electronics and Electrical 0544
- Heat and Thermodynamics 0348
- Hydraulic 0545
- Industrial 0546
- Marine 0547
- Materials Science 0794
- Mechanical 0548
- Metallurgy 0743
- Mining 0551
- Nuclear 0552
- Packaging 0549
- Petroleum 0765
- Sanitary and Municipal 0554
- System Science 0790

Geotechnology 0428
Operations Research 0796
Plastics Technology 0795
Textile Technology 0994

PSYCHOLOGY

General 0621
Behavioral 0384
Clinical 0622
Developmental 0620
Experimental 0623
Industrial 0624
Personality 0625
Physiological 0989
Psychobiology 0349
Psychometrics 0632
Social 0451

THE UNIVERSITY OF CALGARY

FACULTY OF GRADUATE STUDIES

The undersigned certify that they have read, and recommend to the Faculty of Graduate Studies for acceptance, a thesis entitled "Modelling the Dissolution of a CO_2 Bubble Into Athabasca Bitumen", submitted by Richard J. Dunn in partial fulfilment of the requirements for the degree of Master of Engineering in Chemical Engineering.

Dr. A.K. Mehrotra, Supervisor
Department of Chemical and Petroleum Engineering

Dr. N.E. Kalogerakis
Department of Chemical and Petroleum Engineering

Dr. L.E. Turner
Department of Electrical Engineering

Date: August 5, 1993

ABSTRACT

The dissolution of a single CO_2 bubble into Athabasca bitumen was modelled for the cases of static and rising bubbles. The models developed for the dissolution of the static bubble included the more rigorous quasi-stationary model and the simpler molecular diffusion model. For the case of the rising bubble, the models developed were based upon Brian-Hales'/Levich's correlations and Higbie's penetration theory.

Molecular diffusion of the static bubble is shown to be enhanced by low temperatures and high pressures due to the higher CO_2 solubility and mass diffusivity at these conditions. Dissolution of the rising bubble is influenced by both molecular and convective diffusion effects. The numerical results show that, as a result of the combination of the diffusion effects, there exists a minimum in the bubble dissolution time with respect to temperature.

ACKNOWLEDGMENTS

The author wishes to express his sincere appreciation to Dr. Anil Mehrotra for his guidance and encouragement.

The completion of this project was made possible through the support and understanding of my wife, Bev, and our children, Carolyn, Fraser and Perrin. Thank you all very much.

This thesis

is dedicated to

my parents,

Mr. Bruce Dunn

and

Mrs. Florence Dunn

TABLE OF CONTENTS

LIST OF TABLES

LIST OF FIGURES

NOMENCLATURE

A = bubble area, m^2

a = bubble radius, m

c = molar concentration, $kmol/m^3$

C_D = drag coefficient

D_{AB} = mass diffusivity, m^2/s

d = bubble diameter, m

Fb = buoyant force, N

Fd = drag force, N

Fg = gravitational force, N

g = acceleration due to gravity, m/s^2

H = Henrys Law constant, kmol/m·N

$k1$ = $H \cdot R \cdot T$

$k2$ = $2\sigma/(a_0 p_0)$

k_c = convective mass transfer coefficient, m/s

m_b = bubble mass, kg

mw = molar mass, kg/kmol

N = molar flux, kmol/s cm^2

Na = time dependent parameter in Equation 3.1.13

Nb = time dependent parameter in Equation 3.1.14

P = pressure, Pa

R = universal gas constant, 8314 J/kmol K

r = radius, m

sol = solubility, m^3(@N.T.P.)/m^3

T = temperature, K or °C

t = time, s

$\overline{V}$ = partial specific volume, m^3/m^3

v = velocity, m/s

X = undersaturation parameter in Equation 3.1.15

x = mole fraction

z = height, m

zg = compressibility factor

a_1, a_2, a_3, a_4 = empirical constants for viscosity correlation - Equation 2.7.1

b_1, b_2, b_3, b_4 = empirical constants for solubility correlation - Equation 2.5.1

c_1, c_2, c_3 = constants for error function approximation - Equation 4.1.1

Subscripts

A = component A (typically gas)

avg = average

B = component B (typically liquid)

b = bubble (gas phase)

c = convection

D = drag

d = value at point of dissolution

exp = exposure (time)

g = gas phase (CO_2)

i = value at interphase

l = liquid phase (bitumen)

r = reduced value

s = system value

0 = value at $t = 0$

Greek letters

∞ = infinity

ρ = density, kg/m^3

σ = surface tension, mN/m

μ = dynamic viscosity of saturated bitumen, Pa·s

Dimensionless Parameters

Nu_{AB} = Mass transfer Nusselt number, $k_c d/D_{AB}$

Pe_{AB} = Mass transfer Peclet number ≡ $Re\ Sc$, vd/D_{AB}

Re = Reynolds number, $\rho vd/\mu$

Sc = Schmidt number, $\mu/\rho D_{AB}$

Transformations

C = reduced concentration, $C = (c-c_0)/(c_i-c_0)$

g_r = reduced bubble radius, $g_r = a/a_0$

gm_r = reduced bubble mass, $gm_r = m_b/m_{b,0}$

t_r = reduced time, $t_r = D_{AB}t/a_0^2$

y = reduced radius, $y = r/a_0$

y_1 = reduced delta radius, $y_1 = y - g_r$

θ = transformation $\theta = (y/g_r)C_A$

CHAPTER 1

INTRODUCTION

Bitumen is a viscous, dense fluid which is composed of a multitude of hydrocarbons. It is contained in extensive oil sand reserves in Alberta, principally in the Lloydminister, Cold Lake and Athabasca regions.

Knowledge of the processes involved in the diffusion of gases into bitumen is of interest, as it has application to the modelling and implementation of both in-situ enhanced oil recovery techniques, such as fire-flooding and CO_2 miscible flooding, and surface viscosity reduction treatments, including CO_2 injection/mixing.

Limited discussion of the diffusional process of gas into bitumen is available in the literature. In light of this, and the difficulty in performing actual experimental work due to logistical difficulties (including the potential for extremely long dissolution times) there is a need to provide both quantitative and qualitative insights into the diffusional process through a theoretical investigation.

As a first step in providing these insights, it was decided to look at the dissolution of a single bubble of CO_2 gas into a

surrounding mass of bitumen. Different modelling approaches were used, simulating both static bubble and rising bubble dissolution.

Modelling the dissolution of a static bubble was performed using the more rigorous quasi-stationary differential approach, following the work performed by several authors involved in analyzing the dissolution of gas bubbles (CO_2 and O_2) in glass melts. Additionally, a less rigorous lumped approach for modelling the dissolution of a static bubble was performed, where the mass-transfer Nusselt number for mass transfer from a single sphere was set to a value of 2.0 (a theoretical value for purely molecular diffusion) thereby ignoring convective effects.

Modelling the dissolution of a rising bubble considered the system where the rising bubble (described by Stokes' law) is assumed to be at terminal velocity conditions, while mass transfer from the single sphere is described by either Higbie's penetration theory or by Brian-Hales' or Levich's correlation (dependent upon Peclet number).

In addition to assessing the effect of translatory motion on bubble dissolution, the following parameters were also varied in order to consider their impact upon CO_2 dissolution into bitumen:

- temperature,
- pressure,
- initial bubble radius/bubble mass, and
- initial gas concentration in the bitumen.

Properties of the CO_2-bitumen system incorporated into the models include:

- surface tension,
- mass diffusivity,
- bitumen density,
- gas solubility, and
- gas saturated bitumen viscosity.

As system properties were readily available in the literature for the CO_2-Athabasca bitumen system, this system was taken as a representative gas-bitumen system. The Peng-Robinson equation of state was used to calculate the gas phase PVT properties. Empirical or semi-empirical methods, available in the literature, were used for other physical and transport properties.

CHAPTER 2

LITERATURE REVIEW

In this Chapter, details regarding selected dissolution models, applicable to both static and rising bubble cases, are introduced and some of the relevant work is discussed. Additionally, a review of literature concerning physical and transport properties of the CO_2-Athabasca bitumen system is given.

2.1 Quasi-Stationary Model

The quasi-stationary approximation has been used extensively by a number of workers, including Epstein and Plesset (1950), Weinberg et al. (1980) and Weinberg (1981), in analyzing the dissolution of isolated gas bubbles, consisting of O_2 and CO_2, into glass melts.

The quasi-stationary model assumes the following:

- bubble boundary motion ignored,
- bubble motion due to gravitational effects (Stokes' law) ignored,
- time dependent solute concentration field calculated for

fixed radius,

- negligible viscous effects influencing bubble shrinkage,
- solute diffusivity independent of solute concentration, and
- negligible partial specific volume of solute.

Epstein and Plesset (1950) noted that inclusion of bubble boundary motion into the diffusion equation complicated the analysis, precluding a simple analytical solution. They argued that the size of the bubble had little effect on the gas concentration in the solution and therefore their development of the quasi-stationary approximation was valid if:

- the diffusion field in the solution is very much larger than the bubble radius, and
- the concentration of gas in the liquid is much smaller than the gas density in the bubble.

Epstein and Plesset (1950) noted that ignoring translatory motion of the gas bubble could significantly affect the results from the quasi-stationary analysis.

For glass melts under specific conditions Weinberg et al. (1980) extended the Epstein and Plesset (1950) approach through the inclusion of surface tension effects. Additionally, Weinberg et al. (1980) compared the results of

the complete set of partial differential equations for mass transfer with the results from the relatively simple quasi-stationary approximation.

Weinberg et al. (1980) agreed with Epstein and Plesset's (1950) conditions regarding the appropriateness of the quasi-stationary model, and further noted that the approximation was valid where the diffusional flow and bubble boundary motion occur on diverse time scales. They concluded that over the majority of the time domain of bubble dissolution, the quasi-stationary method provides comparable results to the more complex complete set of partial differential equations.

As would be anticipated, Weinberg et al. (1980) found that surface tension played a significant role in the dissolution process where the melt was close to saturation and where the bubble radius was very small. Additionally, they concluded that O_2 bubbles dissolve much more rapidly than CO_2 bubbles due to two factors:

- The diffusivity of O_2 in glass melts is much larger than that of CO_2, and
- The solubility of O_2 in glass melts is much larger than the solubility of CO_2, thereby increasing the degree of undersaturation in any given model.

Weinberg (1981) reviewed the effects of surface tension on the dissolution of O_2 and CO_2 bubbles and concluded that, mathematically, the primary reason the inclusion of surface tension affected the dissolution model was the modification of the time-dependent parameter *Na*. Accordingly, it was concluded that the model should be characterized by the undersaturation parameter, *X*, rather than by the value of Na_0.

The ordinary differential equation describing the quasi-stationary dissolution is developed in the literature as:

$$\frac{dg_r}{dt_r} = -Na\left[1 - \frac{1}{3\left(1+\left(\frac{a_0 P_s}{2\sigma}\right) g_r\right)}\right]^{-1}\left[\frac{1}{\sqrt{\pi t_r}} + \frac{1}{g_r}\right] \qquad \textbf{(2.1.1)}$$

IC: $g_{r,0} = 1.0$

where, g_r is the reduced radius, t_r is reduced time, and *Na* is a time-dependent parameter (as a result of surface tension effects) which reflects the degree of undersaturation of the solution.

2.2 Molecular Diffusion Model (Lumped Approach)

As given in Welty et al. (1983), assuming purely molecular diffusion, the mass-transfer Nusselt number (Nu_{AB}) for a sphere diffusing into a large volume of stagnant fluid theoretically approaches a value of 2.0. Utilizing a lumped approach, upon relating Nu_{AB} to the mass flux (N_A), and multiplying mass flux and the bubble surface area, the following ordinary differential equation is obtained for the bubble dissolution:

$$\frac{dm_b}{dt} = -\,2.0\;\pi\;d_b\;D_{AB}\;(c_{A,i}-c_{A,\infty})\;mw_g \qquad \textbf{(2.2.1)}$$

2.3 Brian-Hales'/Levich's Correlations

Correlations for the mass-transfer Nusselt number for a single sphere include terms for both mass transfer by purely molecular diffusion and by convective effects (Welty et al., 1983). The mass-transfer Nusselt number theoretically approaches a value of 2.0 when convective effects are ignored, and the generalized equation for Nusselt number becomes:

$$Nu_{AB} = 2.0 + C\,Re^{m}\,Sc^{1/3} \qquad \textbf{(2.3.1)}$$

where, C and m are correlating constants for the convective term.

For mass transfer into liquid streams where the mass-transfer Peclet number, Pe_{AB}, is less than 10000, Brian and Hales (1969) proposed the following correlation:

$$Nu_{AB} = (4.0 + 1.21\,Pe_{AB}^{2/3})^{1/2} \qquad \textbf{(2.3.2)}$$

When Pe_{AB} is greater than 10000, Levich (1962) proposed the following correlation:

$$Nu_{AB} = 1.01\,Pe_{AB}^{1/3} \qquad \textbf{(2.3.2)}$$

2.4 Higbie's Penetration Theory Model

Higbie proposed the theoretically derived penetration theory model to explain the mass transfer of a gas into a liquid phase where the gas penetrates only a short distance into the solvent due to a slow rate of diffusion and/or because the

time of contact between phases is relatively short (Welty et al., 1983). The model considers the mass transfer occurring from the gas phase into a liquid phase via unsteady state molecular transport. The model envisions mass transfer occurring as an infinitely deep liquid packet slides along the surface of the gas bubble.

The mass flux at the interface between the phases is given as:

$$N_A = \sqrt{\frac{D_{AB}}{\pi t_{exp}}} \, (C_{A,i} - C_{A,\infty}) \qquad \textbf{(2.4.1)}$$

Integrating over the exposure time, and subsequently dividing through by the exposure time, provides the average mass flux at the interface during the time of exposure:

$$N_{A_{avg}} = 2 \sqrt{\frac{D_{AB}}{\pi t_{exp}}} \, (C_{A,i} - C_{A,\infty}) \qquad \textbf{(2.4.2)}$$

Exposure time, t_{exp}, is assumed to be the time a bubble takes to rise a distance equal to its diameter. Sources of values for the interface gas concentration in the liquid, $C_{A,i}$, and mass diffusivity, D_{AB}, are discussed in Sections 2.5 and 2.6, respectively.

2.5 Gas Solubility Correlation for CO_2 Saturated Athabasca Bitumen

The solubility of CO_2 in bitumen was found by Svrcek and Mehrotra (1982) to vary inversely with absolute temperature and directly with pressure up to 6.0 MPa. Mehrotra and Svrcek (1982), using non-linear regression techniques for a least-square minimization, developed the following correlation:

$$sol = b_1 + b_2 P + b_3 \frac{P}{T} + b_4 \left(\frac{P}{T}\right)^2 \qquad (2.5.1)$$

sol = solubility (m^3 @ NTP / m^3)

T = temperature (K)

P = pressure (MPa)

b_1, b_2, b_3, b_4 = empirical correlation constants

The correlation gave a satisfactory fit between experimental data (Svrcek and Mehrotra, 1982) and predicted values of CO_2 solubility, providing an average deviation of 6.3%. The correlation was developed from data over a temperature range of 296 to 369 K and a pressure range of 1.7 to 6.4 MPa.

When comparing solubility data of CO_2 with N_2 and CH_4, it was determined that, within the range of conditions studied, the solubility of CO_2 was significantly higher than that of N_2 or CH_4. It was further noted that while the solubility of all

gases exhibited a strong dependency upon pressure, the solubility of CO_2 showed a much stronger inverse relationship to temperature than did the other gases.

Figure 2.5.1, taken from Mehrotra and Svrcek (1982), provides iso-solubility contours as a function of pressure and temperature.

2.6 Mass Diffusivity of CO_2 in Athabasca Bitumen

Predictions for mass diffusivity, D_{AB}, of CO_2 into Athabasca bitumen were obtained from Mehrotra et al. (1987). In this study, the infinite dilution and the mutual diffusion coefficients for the CO_2-bitumen system were predicted using the Umesi-Danner correlation and Teja's corresponding states method, respectively.

The Umesi-Danner correlation was selected on the basis that it gave the best match with experimental data for five gas-liquid systems. The correlation was combined with Teja's method for the prediction of the mutual diffusion coefficient for the CO_2-bitumen system. The results were compared with the predicted mutual diffusion coefficient using the best correlation for a liquid-liquid system, the Sridhar-Potter correlation for prediction of infinite dilution.

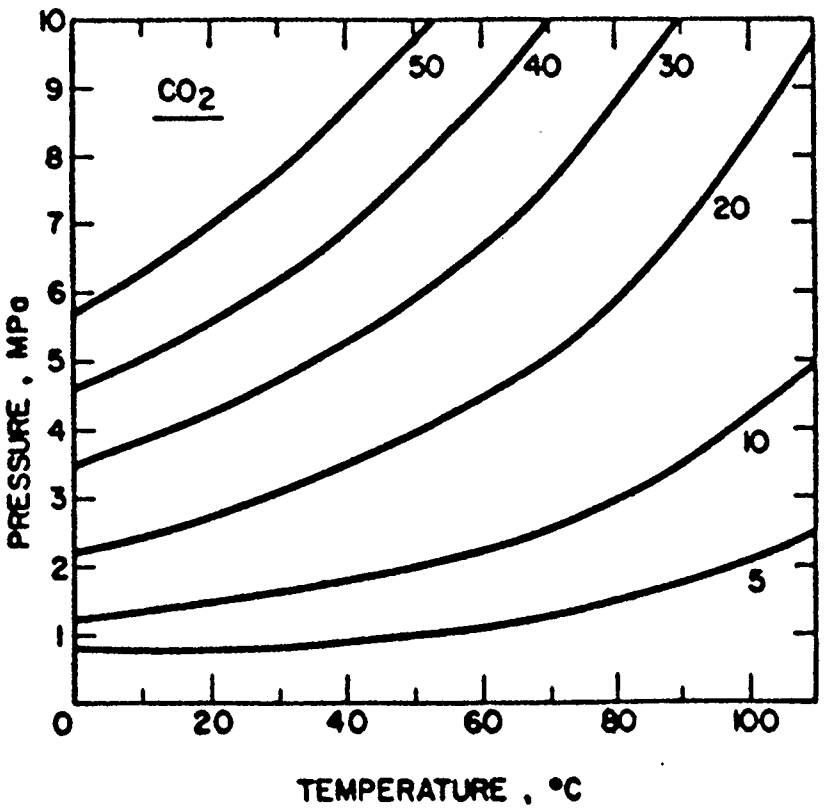

Figure 2.5.1 Iso-solubility contours for CO_2-saturated bitumen. (Solubility units: m^3 of CO_2 at N.T.P. per m^3 of bitumen). Taken from Mehrotra and Svrcek (1982)

When compared to experimental results of the mutual diffusion coefficient for the CO_2-Athabasca bitumen system (Schmidt et al., 1982), the Umesi-Danner correlation provided more satisfactory results, confirming that the CO_2-bitumen system behaves like a gas-liquid system over the range of pressures and temperatures considered in this study.

The value of the CO_2-Athabasca bitumen diffusion coefficient using the Umesi-Danner correlation is predicted to slightly increase with increasing temperature (due to an inverse relationship with bitumen viscosity) and increasing mole fraction of CO_2. Experimental values of Schmidt et al. (1982) showed little correlation between mass diffusivity and CO_2 mole fraction, a variance from the predictions using the Umesi-Danner correlation, especially at CO_2 mole fractions less than 0.05.

A plot taken from Mehrotra et al. (1987), relating predicted mass diffusivity to temperature and mole fraction of CO_2, is included as Figure 2.6.1.

2.7 Solution Dynamic Viscosity Correlation for CO_2 saturated Athabasca Bitumen

Using graphical techniques, Mehrotra and Svrcek (1982)

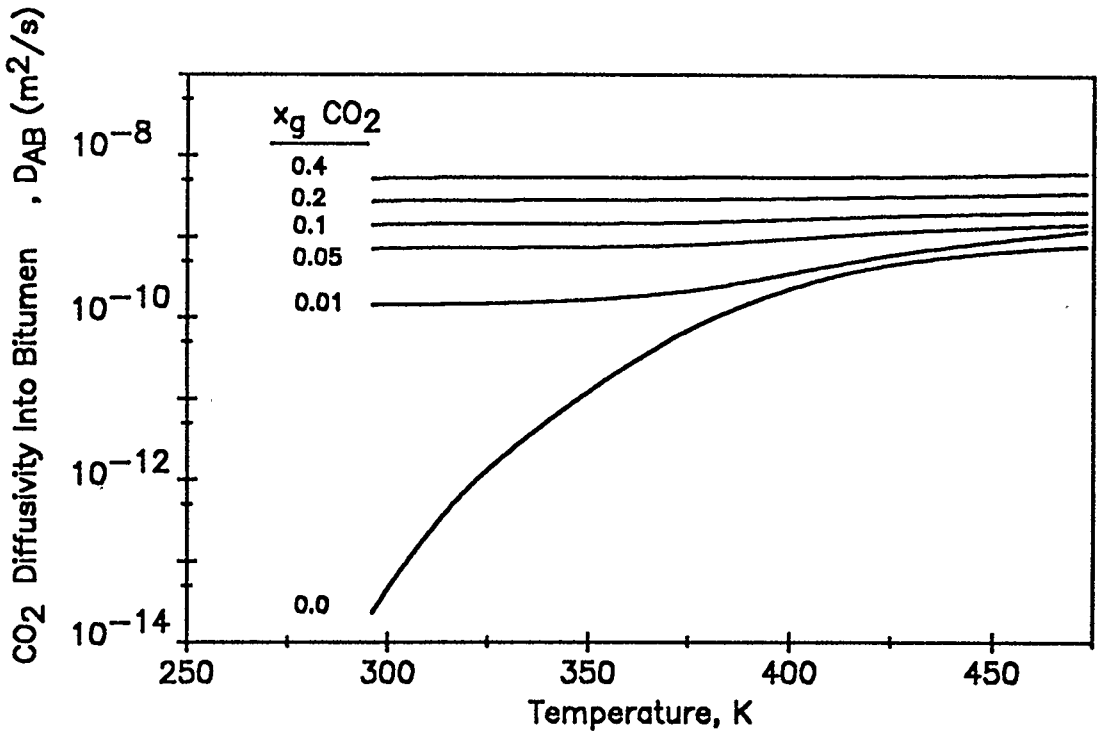

Figure 2.6.1 Effect of temperature upon CO_2 diffusivity into bitumen at various mole fractions of CO_2 , (Mehrotra et al. 1987)

utilized the Walther equation to develop a viscosity correlation for Athabasca bitumen saturated with various gases, including CO_2. The following equation was utilized:

$$\log \log (\mu) = a_1 + a_2 T + a_3 P + a_4 \frac{P}{(273.16+T)} \qquad (2.7.1)$$

μ = dynamic viscosity (mPa s)

T = temperature (°C)

P = pressure (MPa)

a_1, a_2, a_3, a_4 = empirical correlation constants

The correlation provided a satisfactory fit between experimental data (Svrcek and Mehrotra, 1982) and predicted values of CO_2 saturated bitumen viscosity, with an average deviation of 6.5%. The correlation was developed from data over a temperature range of 303 to 369 K and a pressure range of 1.7 to 6.4 MPa.

It was noted that, in addition to temperature, the viscosity of CO_2 saturated Athabasca bitumen has a strong dependency on pressure, a result somewhat different than the other gases for which viscosity correlations were developed, CH_4 and N_2. Additionally, while the viscosity of dead (gas-free) bitumen is dependent upon temperature, of note is that conversely, the viscosity of dead bitumen is relatively unaffected by pressure, thereby demonstrating the relationship between the

amount of dissolved CO_2 and the viscosity reduction of the bitumen.

The results presented in Figure 2.7.1 (taken from Mehrotra and Svrcek, 1982) provide predicted iso-viscosity contours for CO_2 saturated bitumen as a function of pressure and temperature.

2.8 Solution Density of CO_2 Saturated Athabasca Bitumen

As concluded by Mehrotra and Svrcek (1982), the effect of pressure, and therefore mole fraction of gas, on the density of bitumen saturated with CO_2 is insignificant. There is, however, a strong correlation between density and the inverse of absolute temperature.

Experimental values (Svrcek and Mehrotra, 1982) for bitumen density (averaged over a range of sample pressures) versus temperature were input into the ACSL Table command in order to generate a function for density. Values between breakpoints in the table are interpolated linearly.

Figure 2.8.1, plots data provided by Svreck and Mehrotra (1982), providing the relationship between bitumen density and temperature.

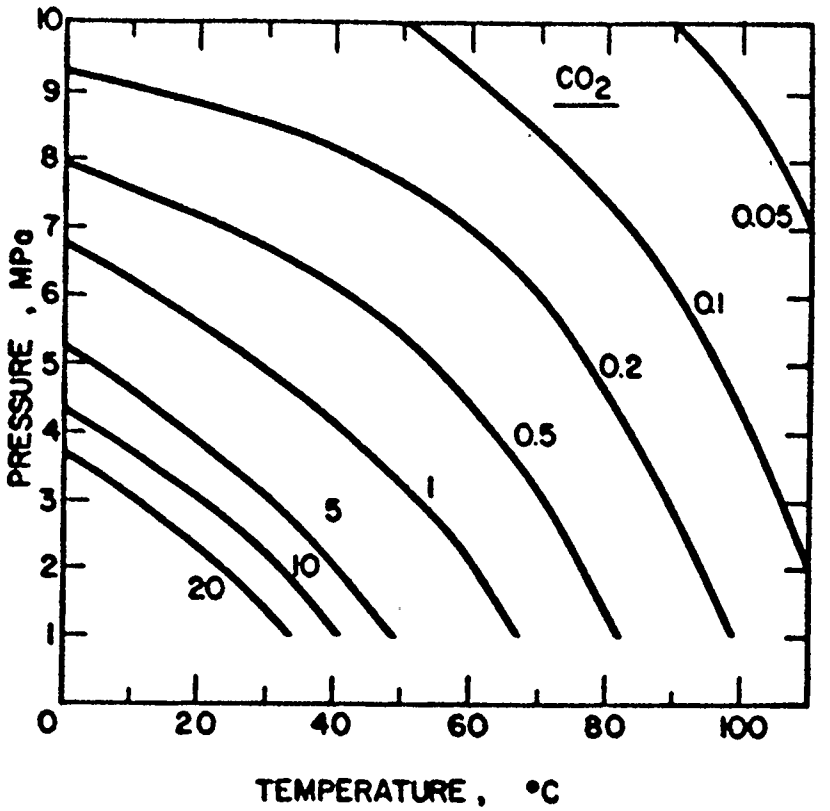

Figure 2.7.1 Iso-viscosity contours for CO_2-saturated bitumen. (Viscosity units: Pa.s). Taken from Mehrotra and Svrcek (1982).

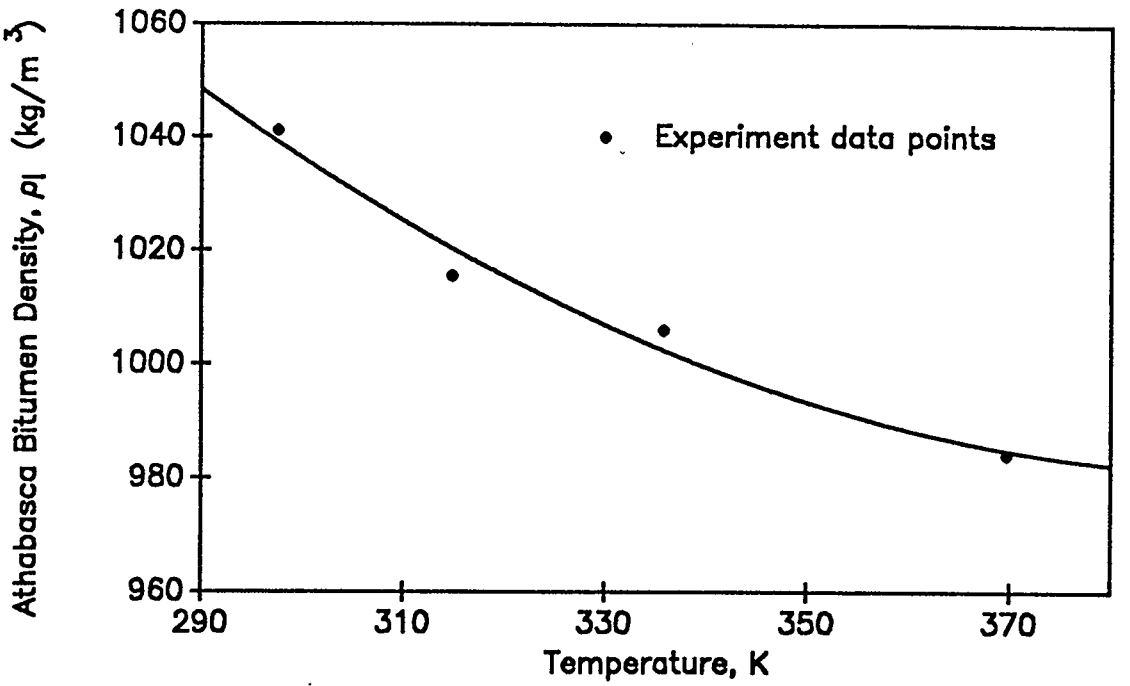

Figure 2.8.1 Temperature dependence of CO_2–saturated bitumen density. (Svrcek and Mehrotra, 1982)

2.9 Surface Tension of Athabasca Bitumen

Mehrotra et al. (1985) investigated several approaches for the prediction of bitumen surface tension. They determined that surface tension predictions by use of the principle of corresponding states were in general agreement with limited published experimental data by Bowman (1967) and Isaacs and Smolek (1983).

The predicted values for surface tension versus temperature were input into the ACSL Table command in order to generate a function for surface tension. Surface tension showed a slight increase with decreasing temperature in the range of temperature reviewed (337 to 385 K).

Experimental work performed by Bowman (1967) reported that below 333 K the surface tension increases significantly with decreasing temperature.

Figure 2.9.1, provides Mehrotra et al.'s (1985) predictions for surface tension of Athabasca bitumen as a function of temperature, as well as smoothed curves of experimental data provided by Bowman (1967) and Isaacs and Smolek (1983).

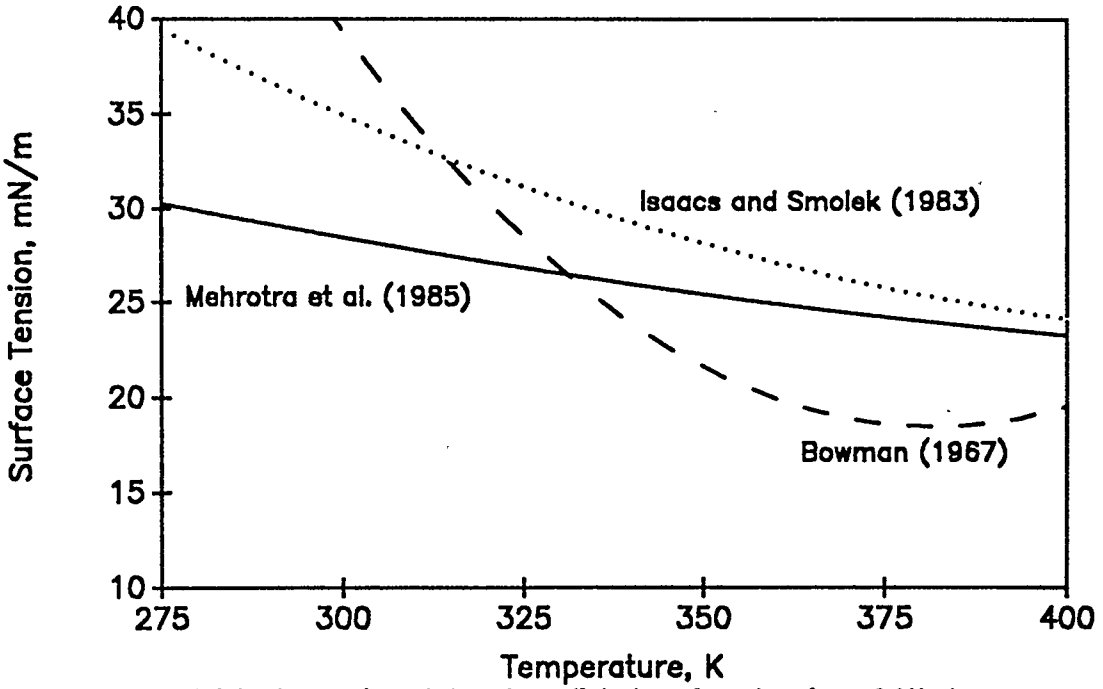

Figure 2.9.1 Published experimental and predicted surface tension of Athabasca Bitumen, (Mehrotra et al., 1985).

CHAPTER 3

MODEL DEVELOPMENT

3.1 Quasi-Stationary Model (Differential Approach)

Starting with the equation of continuity in spherical coordinates, assuming constant ρ and D_{AB}, allowing for the effects of the partial specific volume of the solute and ignoring terms involving θ and ϕ, the differential equation of diffusivity becomes (Ready and Cooper, 1966):

$$\frac{\partial c_A}{\partial t} = \frac{1}{r^2}\frac{\partial}{\partial r}\left(D_{AB} r^2 \frac{\partial c_A}{\partial r}\right) + \frac{a^2}{r^2}\left(\overline{V_A} c_{A,b} - 1\right)\frac{\partial a}{\partial t}\frac{\partial c_A}{\partial r} \qquad \textbf{(3.1.1)}$$

Assuming time dependent concentration profiles for a fixed bubble radius, Equation 3.1.1 modifies to:

$$\frac{\partial c_A}{\partial t} = \frac{1}{r^2}\frac{\partial}{\partial r}\left(D_{AB}\, r^2\, \frac{\partial c_A}{\partial r}\right) \qquad \textbf{(3.1.2)}$$

Assuming constant diffusivity, Equation 3.1.2 is equivalent to:

$$\frac{\partial c_A}{\partial t} = D_{AB}\frac{\partial^2 c_A}{\partial r^2} + \frac{2D_{AB}}{r}\frac{\partial c_A}{\partial r} \qquad (3.1.3)$$

The concentration gradient at the interface is calculated and substituted into a form of Fick's Law, representing the conservation of mass in the system. Equation boundary conditions are of the first kind and include:

- solute concentration at an infinite radius is assumed to remain at the initial melt concentration throughout the entire dissolution period, and
- gas concentration at the bubble interface is assumed to be at its equilibrium value (via Henry's law) at all times. (If surface tension effects are ignored, interfacial boundary concentration is assumed constant throughout the bubble dissolution.)

$$\frac{da}{dt} = \frac{D_{AB}}{c_A(1-c_{A,i}\overline{V_A})}\left(\frac{\partial c_A}{\partial r}\right)_{r=a} \qquad (3.1.4)$$

IC: $c_A(0,r) = c_{A,0}$

BC I: $c_A(t,\infty) = c_{A,0}$

BC II: $c_A(t,a) = c_{A,i}$

The following transformations are applied in order to enable

an analytic solution to the modified differential equation of diffusivity, thereby enabling the simplification of the conservation of mass problem from one requiring the solution of a partial differential equation to one requiring the solution of an ordinary differential equation:

$$C_A = \frac{C_A - C_{A,0}}{C_{A,i} - C_{A,0}} \tag{3.1.5}$$

$$t_r = \frac{D_{AB} t}{a_0^2} \tag{3.1.6}$$

$$y = \frac{r}{a_0} \tag{3.1.7}$$

$$g_r = \frac{a}{a_0} \tag{3.1.8}$$

$$y_1 = y - g_r \tag{3.1.9}$$

$$\theta_{(t_r, y_1)} = \frac{y}{g_r} C_{A_{(t_r, y_1)}} \tag{3.1.10}$$

Equation 3.1.3 transforms to:

$$\frac{\partial C_A}{\partial t_r} = \frac{\partial^2 C_A}{\partial y^2} + \frac{2}{y} \frac{\partial C_A}{\partial y} \tag{3.1.11}$$

IC: $C_A(0, y) = 0$

BC I: $C_A(t_r, \infty) = 0$

BC II: $C_A(t_r, a) = 1$

Equation 3.1.4 transforms to:

$$\frac{dg_r}{dt_r} = Na\ Nb\ \left(\frac{\partial C_A}{\partial y}\right)_{(t_r, y=g_r)} \qquad (3.1.12)$$

Assuming that the concentration of gas at the bubble interface, throughout the dissolution process, is at its equilibrium value given by Henry's law:

$$Na = \frac{C_{A,i} - C_{A,0}}{\rho_b} = \frac{HRT\left[g_r(1-X) + \frac{2\sigma}{a_0 P_s}\right]}{\left[g_r + \frac{2\sigma}{a_0 P_s}\right]} \qquad (3.1.13)$$

For simplicity of display we let:

$$Nb = \left[1 - \frac{1}{3\left(1 + \left(\frac{a_0 P_s}{2\sigma}\right) g_r\right)}\right]^{-1} \qquad (3.1.14)$$

The undersaturation parameter, X, is defined as the ratio of the initial solution molar concentration of gas to the molar concentration of gas in a saturated solution, i.e.

$$X = \frac{C_0}{H\ P_0} \qquad (3.1.15)$$

Equation 3.1.11 transforms to:

$$\frac{\partial\theta}{\partial t_r} = \frac{\partial^2\theta}{\partial y_1^2} \qquad (3.1.16)$$

IC: $\theta(0,y_1) = 0$

BC I: $\theta(t_r,\infty) = 0$

BC II: $\theta(t_r,0) = 1$

The analytical solution for Equation 3.1.16 is given by (Carslaw and Jaeger, 1959):

$$\theta = erfc\left(\frac{y_1}{2\sqrt{t_r}}\right) = erfc\left(\frac{y-g_r}{2\sqrt{t_r}}\right) \qquad (3.1.17)$$

Therefore by definition (Equation 3.1.10) the concentration profile becomes:

$$C_A = \frac{g_r}{y} erfc\left(\frac{y-g_r}{2\sqrt{t_r}}\right) \qquad (3.1.18)$$

As:

$$\left.\frac{\partial C_A}{\partial y}\right|_{(y=g_r)} = \frac{\partial\theta}{\partial y} - \frac{C_A}{y} = -\left[\frac{1}{\sqrt{\pi t_r}} + \frac{1}{g_r}\right] \qquad (3.1.19)$$

Following from Equations 3.1.12 and 3.1.19:

$$\frac{dg_r}{dt_r} = -Na\ Nb\left[\frac{1}{\sqrt{\pi t_r}} + \frac{1}{g_r}\right] \qquad \textbf{(3.1.20)}$$

IC: $g_{r,0} = 1$

Equation 3.1.20 is a time-dependent, non-linear ordinary differential equation; solvable in a straightforward manner through use of a continuous system simulator such as ACSL - Advanced Continuous Simulation Language.

Epstein and Plesset (1950) further simplified Equation 3.1.20 by dropping the time dependent term in the brackets, an approach which has been used by Chen and Wang (1989). While this approach simplifies the mathematics, enabling an analytic solution to the dissolution problem and provides results reasonably similar to the quasi-stationary results (within 10% for air bubbles dissolving in water), the use of a simulator such as ACSL precludes the need to further simplify the problem.

3.2 Molecular Diffusion Model (Lumped Approach)

As discussed in Section 2.2, assuming purely molecular diffusion, experimental work has determined that the mass-transfer Nusselt number, Nu_{AB}, for a sphere diffusing into a large volume of stagnant fluid approaches the theoretical value of 2.0.

Given:

$$k_c = \frac{Nu_{AB}\, D_{AB}}{d_b} \qquad (3.2.1)$$

$$N_A = k_c\, (c_{A,i} - c_{A,\infty}) \qquad (3.2.2)$$

$$A_b = 2\, \pi\, d_b^2 \qquad (3.2.3)$$

The rate of mass transfer is determined by multiplying the mass flux times the bubble surface area. Hence, the resultant ordinary differential equation for mass transfer from the bubble is:

$$\frac{dm_b}{dt} = -\, 2.0\, \pi\, d_b\, D_{AB}\, (c_{A,i} - c_{A,\infty})\, mw_g \qquad (3.2.4)$$

3.3 Brian-Hales'/Levich's Correlations

As given in Section 2.3, both Brian and Hales' and Levich's correlations for Nu_{AB}, reflect the contributions to diffusion by both molecular and convective forces. The correlations and the appropriate conditions, are respectively:

$$Nu_{AB} = (4.0 + 1.21\ Pe_{AB}^{2/3})^{1/2} \qquad \textbf{(3.3.1)}$$
$$Pe_{AB} < 10000$$

$$Nu_{AB} = 1.01\ Pe_{AB}^{1/3} \qquad \textbf{(3.3.2)}$$
$$Pe_{AB} > 10000$$

Similar to the development of Equation 3.2.4 , the equation for mass transfer from the bubble becomes:

$$\frac{dm_b}{dt} = -\pi\ d_b\ D_{AB}\ (c_{A,i}-c_{A,\infty})\ Nu_{AB}\ mw_g \qquad \textbf{(3.3.3)}$$

Equation 3.3.3 is solved using the appropriate expression for the mass-transfer Nusselt number, determined by the Peclet number.

3.4 Higbie's Penetration Theory Model

As discussed in Section 2.4, the average molar flux (with respect to time) due to convective effects from a rising bubble, is described by Higbie's penetration theory model as:

$$N_{A_{avg}} = 2 \sqrt{\frac{D_{AB}}{\pi t_{exp}}} \; (C_{A,i} - C_{A,\infty}) \qquad \textbf{(3.4.1)}$$

The exposure time (t_{exp}) is assumed to be:

$$t_{exp} = \frac{d_b}{v_b} \qquad \textbf{(3.4.2)}$$

Accordingly the differential equation describing mass transfer from the bubble becomes:

$$\frac{dm_b}{dt} = -2 \; mw_g \; (C_{A,i} - C_{A,\infty}) \; d_b \; (D_{AB} \; \pi \; v_b \; d_b)^{1/2} \qquad \textbf{(3.4.3)}$$

An important point to note is that Higbie's penetration theory model assumes the mass flux varies with the square root of diffusivity. This dependence is opposed to both the molecular diffusion model presented in Section 3.2 (where mass flux is proportional to diffusivity) and Brian-Hales'/Levich's

correlations presented in Section 3.3 (where the dependence of mass flux upon diffusivity varies between being directly proportional to varying to the 2/3 power of diffusivity, dependent upon the influence of convective effects as indicated by the Peclet number).

3.5 Other Considerations

3.5.1 Rising Bubble Velocity Model Development

The initial approach in the development of a velocity model assumed a simple force balance on the bubble. It was assumed that the rising bubble is spherical and that the Stokes' law is applicable.

A force balance on the rising bubble gives:

$$m_b \frac{dv_b}{dt} = Fb - Fg - Fd$$

$$Fb = m_b\, g\, \frac{\rho_1}{\rho_b} \qquad \textbf{(3.5.1)}$$

$$Fg = m_b\, g$$

$$Fd = 0.5\, C_D\, v_b^2\, A_b\, \rho_1$$

Equation 3.5.1 leads to the differential equation for velocity being:

$$\frac{dv_b}{dt} = g\left(\frac{\rho_l}{\rho_b} - 1\right) - \frac{0.5\ \rho_l\ C_D\ v_b^2\ A_b}{m_b} \qquad \textbf{(3.5.2)}$$

When solving this ordinary differential equation for bubble velocity in conjunction with the appropriate ordinary differential equation describing bubble dissolution, it was determined that the equations were extremely tightly coupled, severely limiting computational speed.

Model runs were performed and, as shown in Figure 3.5.1, it was determined that the bubble reached terminal velocity conditions in the viscous bitumen mixture extremely rapidly. Accordingly the assumption of terminal bubble velocity at all times in the dissolution process has a minimal impact upon the bubble dissolution model results.

At the terminal velocity the derivative of velocity with respect to time is zero; hence, the equation for bubble velocity becomes:

$$v_{b\,(term)} = \left(\left(\frac{\rho_l}{\rho_b} - 1\right)\left(\frac{g\ m_b}{0.5\ \rho_l\ C_D\ A_b}\right)\right)^{0.5} \qquad \textbf{(3.5.3)}$$

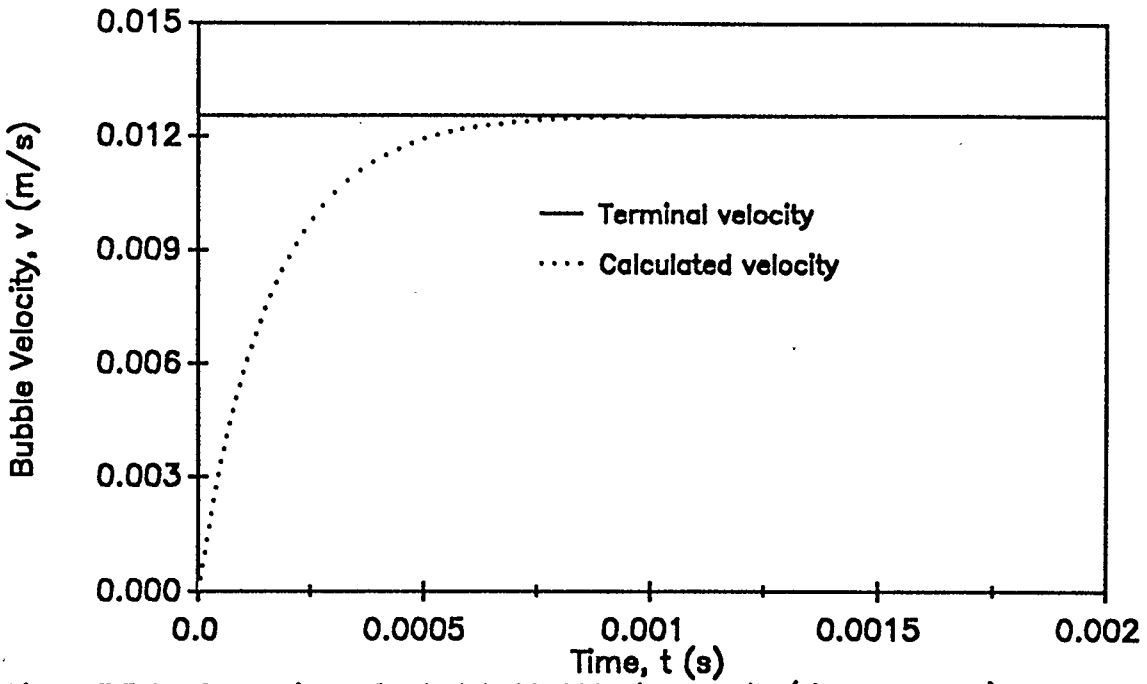

Figure 3.5.1 Comparison of calculated bubble rise velocity (via Stokes' law) to terminal velocity. T = 350 K, P = 6.0 MPa, $m_{b,0} = 5.0 \times 10^{-7}$ kg

Solving the equation for terminal bubble velocity enables the calculation of the rise of the bubble through integration of:

$$\frac{dz}{dt} = v_b \qquad (3.5.4)$$

3.5.2 Bubble Pressure

Including both hydrostatic and surface tension effects, the bubble pressure can be written as:

$$P_b = P_\infty - \rho_l \, g \, z + \frac{2\sigma}{a} \qquad (3.5.5)$$

3.5.3 Bubble Density and Mass

Equations for gas density and bubble mass are:

$$\rho_b = \frac{P_b \, mw_g}{zg \, R \, T} \qquad (3.5.6)$$

$$m_b = \frac{4}{3}\pi a^3 \rho_b \qquad (3.5.7)$$

3.5.4 Drag Coefficient

Bird et al. (1960) showed the drag coefficient around a sphere to be dependent upon Reynolds number as follows:

$$\begin{aligned} &For\ 0 < Re < 2 \qquad C_D = \frac{24}{Re} \\ &For\ 2 < Re < 500 \qquad C_D = \frac{18.5}{Re^{0.6}} \end{aligned} \qquad (3.5.8)$$

For Reynolds number less than 2, flow is assumed to be in the creeping flow regime. Flows around spheres with Reynolds numbers between 2 and 500 are deemed to be in the intermediate regime.

3.6 ACSL Software

The Advanced Continuous Simulation Language, ACSL, allows the modelling and solution of continuous systems described by time dependent, non-linear ordinary differential equations. Program

coding structure includes:

- an initial section where variable values are assigned prior to running the program.
- a dynamic/derivative section where the fortran based dynamic model is executed at every communications interval. The model limits (for example maximum model run time, minimum bubble diameter or mass) are tested at every communications interval and if the limits are not exceeded, the integration is initiated again according to the code in the derivative block in order to evaluate the state variable derivatives.
- a terminal section which is reached upon exiting from the dynamic section. From this section, data collected can be displayed in tabular or graphical format, or the model can be re-run with modified variables.

A flowsheet detailing the ACSL program, taken from the vendor's reference manual (Mitchell and Gauthier, 1986), is included as Figure 3.6.1. Level 9C of ACSL was used which is suitable for running on personal computers. Microsoft Fortran, Version 5.1, was used in conjunction with the ACSL program.

Integration algorithms available in ACSL include both the Runge-Kutta algorithm (first, second or fourth order) and Gear's Stiff algorithm which is a variable step, variable

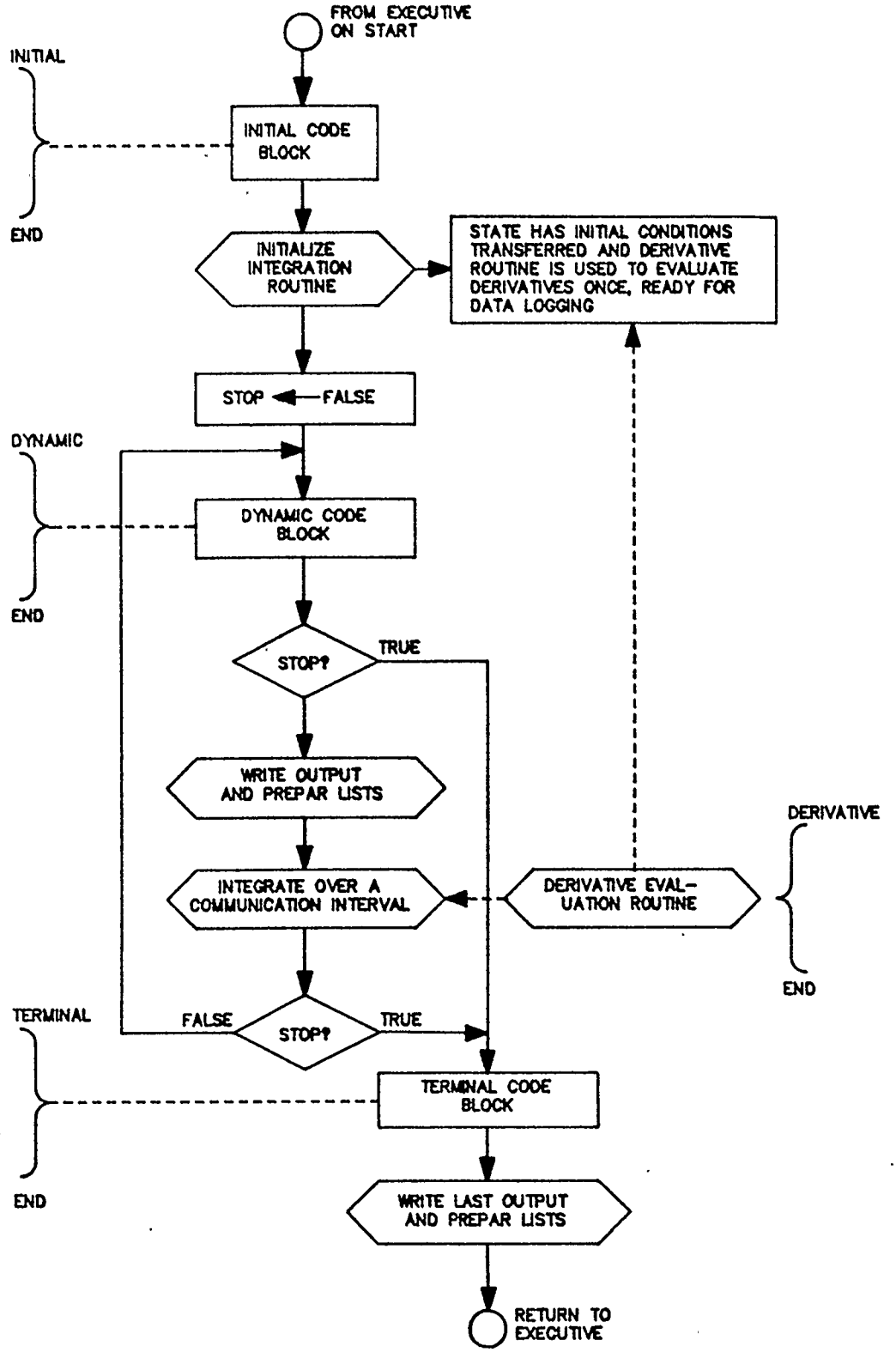

Figure 3.6.1 Main Program Loop of ACSL Model. From Mitchell and Gauthier Associates (1986)

order algorithm.

The second order Runge-Kutta algorithm was used to evaluate the static bubble dissolution models, as it provided good accuracy along with acceptable speed of computation.
The Gear's Stiff algorithm was chosen for evaluating the early time response of the rising bubble models (for confirmation of acceptability of the assumption of terminal velocity), as it is an efficient algorithm for stiff systems where model time constants differ significantly.

CHAPTER 4

DISCUSSION OF RESULTS

4.1 Verification of Model and Solution Algorithm

To confirm the correct interpretation of the referenced works and the proper functioning of the model, the calculations of Weinberg et al. (1980) on the dissolution of O_2 and CO_2 bubbles in a glass melt were reproduced. Physical constants used in the simulations (for the conditions of T = 1673 K, P = 101.3 kPa and X = 0.9349) are given in Table 4.1.1.

The listing for the ACSL model simulating the quasi-stationary dissolution of a oxygen bubble in a glass melt, DIFFUS1, is included as Appendix A.

The approximation for the complementary error function required for the reduced concentration profile is given by Hastings (1955):

$$erfc(x) = (c_1 t + c_2 t^2 + c_3 t^3)\ e^{-x^2} \qquad (4.1.1)$$

$$t = \frac{1}{1 + 0.47047x}$$

Table 4.1.1.

Physical Constants of a CO_2-Glass Melt System (Weinberg et al., 1980)

Model Conditions - T = 1673 K, P = 101.3 kPa, X = 0.9349

Gas	Solubility, *sol* (m^3/m^3)	Diffusivity, D_{AB} (m^2/s)	Henry's Law Constant, H (kmol/Pa m^3)	Surface Tension, σ (mN/m)
O_2	5.01×10^{-1}	5.00×10^{-10}	2.21×10^{-7}	300
CO_2	2.55×10^{-3}	5.00×10^{-11}	1.12×10^{-9}	300

4.1.1 Dissolution of O_2 Into a Glass Melt

Weinberg et al.'s (1980) results and the results of the ACSL model for the quasi-stationary approximation for the dissolution of a 1.0 mm radius oxygen bubble, both with and without surface tension, are included as Table 4.1.2. Comparison of the results shows good agreement between Weinberg et al.'s (1980) published results and the ACSL model, lending credibility to the latter.

The *S* shape of the reduced bubble radius, g_r, versus reduced time, t_r, and real time, t, as evident in Figures 4.1.1 and 4.1.2 respectively, is characteristic of quasi-stationary dissolution. The characteristic response is explained as follows:

- Initially, at small values of t_r, a large concentration gradient exists at the bubble interface, resulting in a rapid early dissolution of the bubble. The reduced concentration profiles for the solute at various points in the dissolution process are given in Figure 4.1.3. Inspection of the early time concentration profiles (t_r = 0.0, 0.05) confirms the steep concentration gradients. Additionally, of note is the limited distance which the solute has diffused into the melt at early times.

Table 4.1.2.

Comparison of the ACSL Model and Weinberg et al.'s (1980) Results for the Quasi-Stationary Dissolution of a Static Oxygen Bubble Into a Sub-Saturated Glass Melt

Model Conditions - a_0 = 1.0 mm, T = 1673 K, P = 101.3 kPa, X = 0.9349

t_r	g_r Weinberg σ=0 mN/m	g_r ACSL Model σ=0 mN/m	g_r Weinberg σ=300 mN/m	g_r ACSL Model σ=300 mN/m
0.011	0.974	0.975	0.972	0.973
0.038	0.948	0.949	0.944	0.945
0.125	0.893	0.895	0.883	0.885
0.250	0.831	0.832	0.814	0.816
0.400	0.764	0.765	0.739	0.740
0.575	0.687	0.688	0.648	0.651
0.770	0.600	0.601	0.543	0.546
0.985	0.495	0.496	0.406	0.408
1.225	0.356	0.358	0.131	0.146
1.500	0.063	0.069	Dissolved	Dissolved

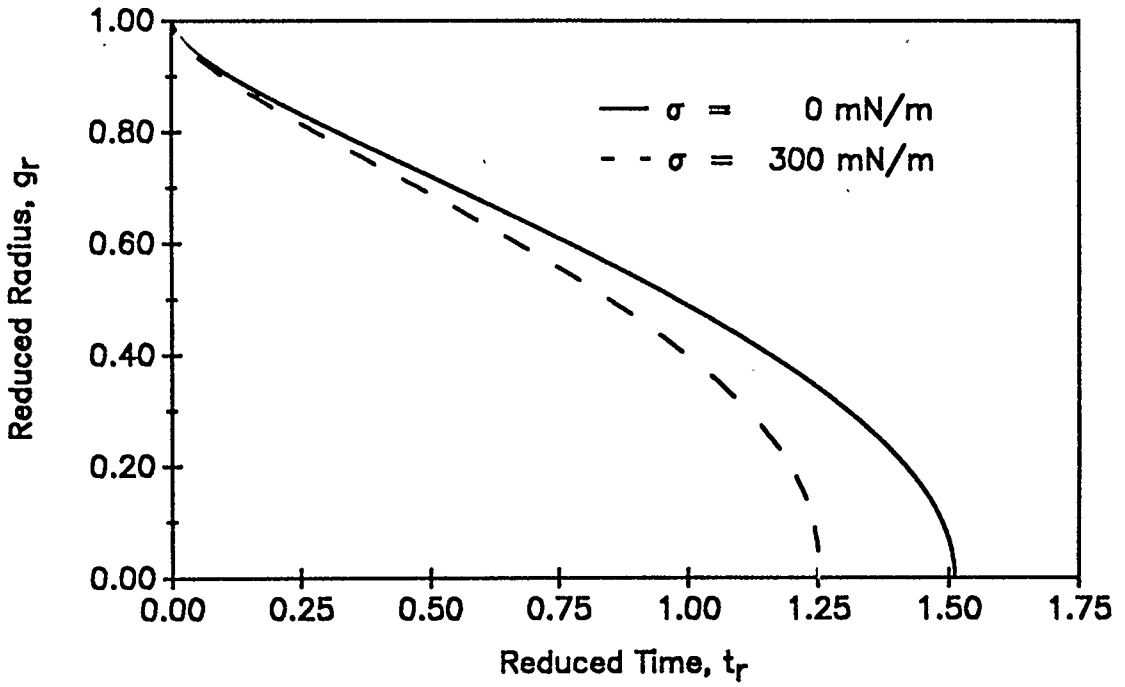

Figure 4.1.1 Quasi–stationary dissolution of a 1.0 mm radius O_2 bubble in a glass melt. T= 1673 K, P = 101.3 kPa, X = 0.9349

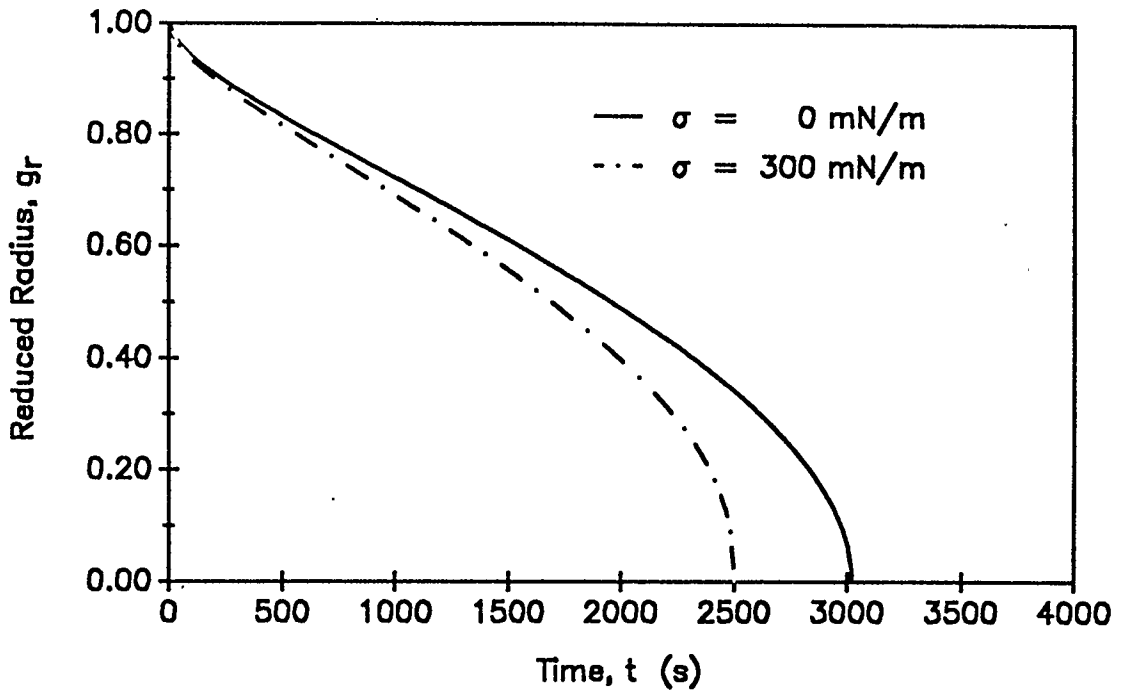

Figure 4.1.2 Quasi–stationary dissolution of a 1.0 mm radius O_2 bubble in a glass melt. T = 1673 K, P = 101.3 kPa, X = 0.9349

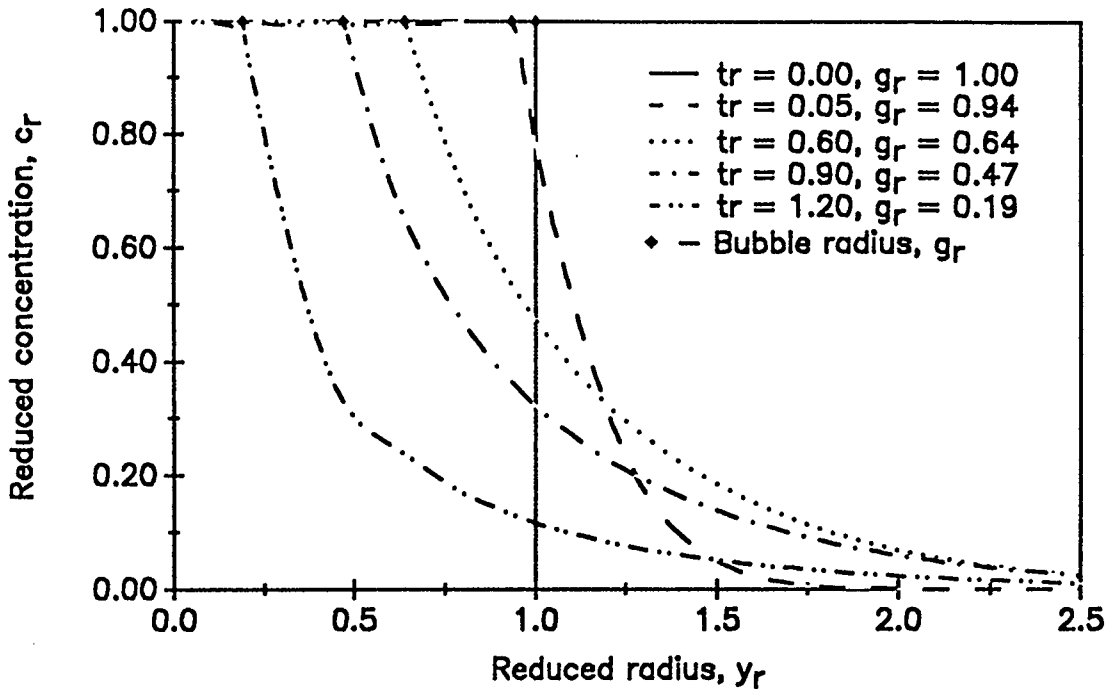

Figure 4.1.3 Solute concentration profiles at various points in the quasi-stationary dissolution of an O_2 bubble in a glass melt. T = 1673 K, P = 101.3 kPa, X = 0.9349, σ = 300 mN/m

- At intermediate times, the rate of bubble dissolution slows from the initial rapid dissolution to a relatively steady rate as the concentration gradient at the bubble interface is reduced due to the increasing concentration of solute in the glass melt. Inspection of the intermediate time curves of Figure 4.1.3 (t_r = 0.6, 0.9) reveals both the reduced concentration gradients and the increased distance into the melt which the gas has diffused at intermediate times.

  Mathematically, an inspection of Equation 3.1.20 shows that the rate of dissolution is approximately proportional to $t_r^{-1/2}$ during short to intermediate times when the second term in the brackets, (g_r^{-1}), is less significant than the first, $(t_r^{-1/2})$, term. Figure 4.1.3 confirms this relationship.

$$\frac{dg_r}{dt_r} = -Na\ Nb\left[\frac{1}{\sqrt{\pi t_r}} + \frac{1}{g_r}\right] \qquad \textbf{(3.1.20)}$$

IC: $g_{r,0} = 1.0$

- At later times when the bubble radius and surface area is small the rate of dissolution again increases. Again, inspection of Equation 3.1.20 shows that, as the dissolution progresses, the second bracketed term (g_r^{-1})

dominates the first term ($t_r^{-1/2}$) and the rate of change of bubble radius becomes significantly larger.

Physically, the increase in dissolution at longer times is due to:

- the mass flux being increased by the relative increase in the volume of the diffusional zone to the area of the bubble surface (an effect which results in steeper concentration gradients at the bubble interface as evidenced in the t_r = 1.2 curve in Figure 4.1.3) and;
- surface tension effects increasing the concentration gradient at the bubble interface.

Surface tension increases bubble pressure above the system pressure, as per Equation 3.5.5, and therefore the gas solubility in the solute via Henry's law. Surface tension effects are significant over the entire time of dissolution in the modelled case as can be seen through inspection of the curves (with and without surface tension effects) in Figures 4.1.1 and 4.1.2. Surface tension effects are significant as:

- the undersaturation of the gas in the melt is low, (X = 0.9349),
- the system pressure is low, (P = 101.3 kPa), and

- the initial bubble radius is small, (a_0 = 1.0 mm)

The importance of surface tension in the dissolution of O_2 in solutions close to saturation is evident through consideration of the dimensionless parameter *Na*, described by Equation 3.1.13. In Equation 3.1.20, *Na* affects the rate of bubble dissolution linearly. If surface tension is ignored, as the undersatuation parameter *X* (Equation 3.1.15) approaches 1.0 (a saturated solution), *Na* approaches a value of 0.0, and the bubble remains in a stable, non-dissolving state. Inclusion of surface tension however (Equation 3.1.13), in the case of a saturated solution (X = 1.0), results in a positive value for *Na*, and the bubble is driven towards dissolution.

4.1.2 Dissolution of CO_2 Into a Glass Melt

Quasi-stationary dissolution of a CO_2 bubble in a glass melt was modelled in order to compare the results with the case of the O_2 bubble dissolution in a glass melt and to provide a reference case for comparison of the quasi-stationary dissolution of a CO_2 bubble in bitumen. Dissolution time results, for the dissolution of O_2 and CO_2 bubble cases are provided in Table 4.1.3.

Table 4.1.3.

Quasi-Stationary Dissolution of Static Bubbles (CO_2 and O_2) Into a Sub-Saturated Glass Melt

Model Conditions - a_0 = 1.0 mm, X = 0.9349
T = 1673 K, P = 101.3 kPa

	X	$t_{r,d}$ σ = 0 mN/m	t_d (s) σ = 0 mN/m	$t_{r,d}$ σ = 300 mN/m	t_d (s) σ = 300 mN/m
O_2	0.9349	1.51	3023	1.2	2500
CO_2	0.9349	475	9.5×10^6	409	8.2×10^6
CO_2	0.0	27.5	5.6×10^5	27.6	5.5×10^5

As is evident through comparison of Figures 4.1.2 and 4.1.4, the dissolution of an O_2 bubble in a glass melt is significantly faster (by a factor of approximately 3300) than the dissolution of a CO_2 bubble. The slower dissolution of the CO_2 bubble is attributable to:

- the solubility, and hence Henry's law coefficient, of CO_2 in the glass melt is less than one-hundredth of O_2; and
- the mass diffusivity of CO_2 in the glass melt is one-tenth of O_2.

In order to assess the effect of solvent under-saturation, the dissolution of a 1.0 mm CO_2 bubble in a completely sub-saturated glass melt solution was studied. The results are presented in Figure 4.1.5 and Table 4.1.3. While the reduction of the undersaturation parameter, X, from 0.9349 (Figure 4.2.1) to 0.0, reduces the dissolution time of the bubble significantly (by a factor of approximately 15 - from 8.2×10^6 s to 5.5×10^5 s), of note is the extremely limited tendency of the CO_2 bubble to dissolve in the glass melt, even in completely sub-saturated conditions.

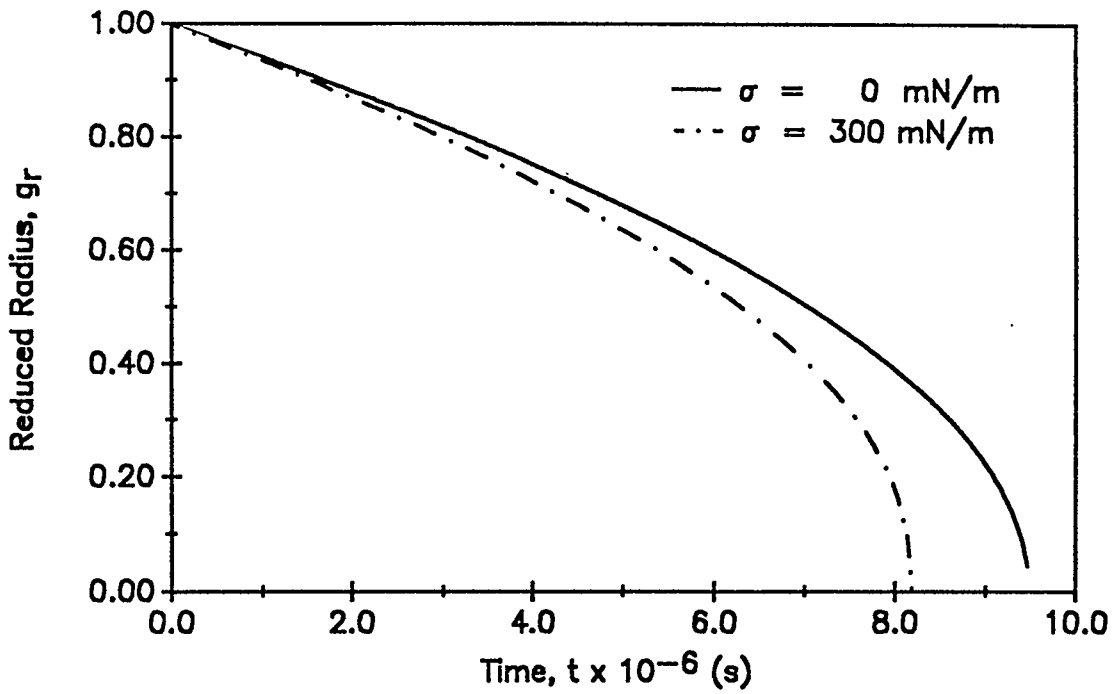

Figure 4.1.4 Quasi–stationary dissolution of a 1.0 mm radius CO_2 bubble in a glass melt. T = 1673 K, P = 101.3 kPa, X = 0.9349

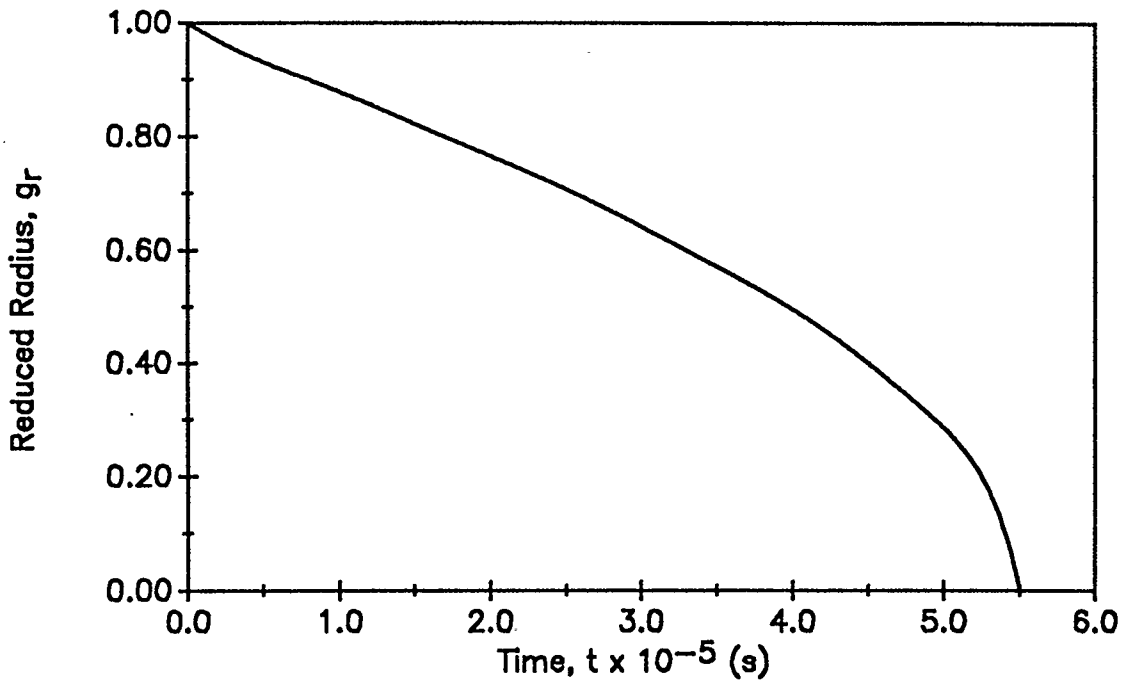

Figure 4.1.5 Quasi–stationary dissolution of a CO_2 bubble in a completely sub–saturated glass melt. T = 1673 K, P = 101.3 kPa, a_0 = 1.0 mm

4.2 Considerations in the Modelling of the Dissolution of CO_2 into Bitumen

With confidence obtained in the ACSL quasi-stationary model, based upon a good reproduction for the results of the dissolution of bubbles into glass melts, the work was extended and alternative models were developed to address the dissolution of both static and rising CO_2 bubbles into CO_2-Athabasca bitumen solutions. The source code for the models are provided in Appendix B through E respectively, and include the programs:

- DIFFUS2 - Static Bubble - Quasi-Stationary (Differential) Model,
- DIFFUS3 - Static Bubble - Molecular Dissolution (Lumped) Model, Nu_{AB} = 2.0
- DIFFUS4 - Rising Bubble - Dissolution assuming Nu_{AB} determined via Brian and Hales' or Levich's correlation, dependent upon Pe_{AB}.
- DIFFUS5 - Rising Bubble - Higbie's Penetration Theory

As required, the models include ACSL table statements, utilizing data provided in the literature, for the following properties of the CO_2-Athabasca bitumen system:

- the mass diffusivity,

- the gas-saturated bitumen density, and
- the surface tension.

Similarly as necessary, the models use correlations provided in the literature to describe the following system properties:

- the dynamic viscosity of saturated bitumen, and
- the solubility of CO_2.

The Peng-Robinson equation of state, an appropriate EOS for the PVT properties of CO_2 over the ranges of pressure and temperature conditions of interest to this work, was used for estimating gas compressibility values. This cubic equation of state (Walas, 1985) was solved directly using a method given in Perry's Handbook (1984).

4.3 Quasi-Stationary Dissolution

4.3.1 Fixed Initial Radius

The dissolution of a 1.0 mm radius bubble of CO_2 in a completely sub-saturated solution of Athabasca bitumen was the first system to be modelled. Representative of conditions which might be encountered in practical applications, while also working within the temperature and pressure ranges for

which correlations and/or data are available for system properties, temperature was considered over the range of 300 to 400 K, while pressure was varied from 1.0 to 6.0 MPa. Values of system properties, including solubility (and the associated interfacial molar gas concentration), mass diffusivity, dynamic viscosity, surface tension and liquid density, over the temperature and pressure ranges evaluated, are provided in Table 4.3.1. Sources for the system physical and transport property data and correlations used were discussed in Sections 2.5 through 2.9.

Graphical examples of the results from a typical model run, (T = 350 K, P = 1.0 MPa), providing:

- reduced mass and bubble radius vs reduced time,
- reduced mass and bubble radius vs time, and
- bubble mass vs time;

are presented as Figures 4.3.1 through 4.3.3, respectively.

Inspection of the reduced radius versus time curve in Figure 4.3.1 shows the anticipated S shape plot (typical of quasi-stationary dissolution - as discussed in Section 4.1.1). In contrast with the decline in reduced radius, the reduced mass follows a rapid, smooth decline as shown in Figure 4.3.3 (due to the cubic relationship between bubble radius and bubble

Table 4.3.1.

Values of Selected Properties of the CO_2-Athabasca Bitumen System (Mehrotra et al., 1985; Mehrotra et al., 1987; Mehrotra and Svrcek, 1982)

T (K)	P_s (MPa)	sol (m^3/m^3)	x_g	D_{AB} (m^2/s)	μ (mPa·s)	σ (mN/m)	ρ_l (kg/m^3)
300	1.0	6.68	0.148	2.06×10^{-9}	35380	0.028	1037
350	1.0	3.61	0.088	1.31×10^{-9}	677	0.025	997
400	1.0	1.30	0.035	7.66×10^{-10}	56	0.023	964
300	2.0	13.48	0.261	3.56×10^{-9}	14580	0.028	1037
350	2.0	7.30	0.164	2.38×10^{-9}	491	0.025	997
400	2.0	2.67	0.069	1.25×10^{-9}	51	0.023	964
300	4.0	27.41	0.425	5.57×10^{-9}	3070	0.028	1037
350	4.0	14.93	0.271	4.06×10^{-9}	270	0.025	997
400	4.0	5.60	0.135	2.16×10^{-9}	43	0.023	964
300	6.0	41.79	0.537	6.93×10^{-9}	837	0.028	1037
350	6.0	22.90	0.390	5.30×10^{-9}	157	0.025	997
400	6.0	8.77	0.197	3.01×10^{-9}	36	0.023	964

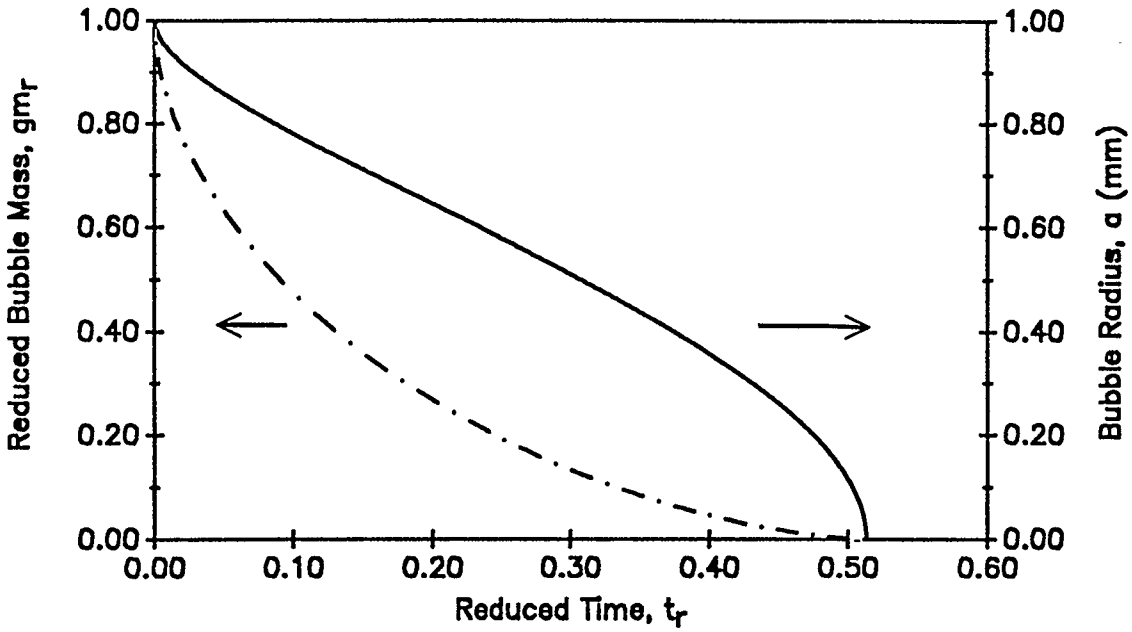

Figure 4.3.1 Quasi–stationary dissolution of a CO_2 bubble into completely sub–saturated Athabasca bitumen. T = 350 K, P = 1.0 MPa, a_0 = 1.0 mm

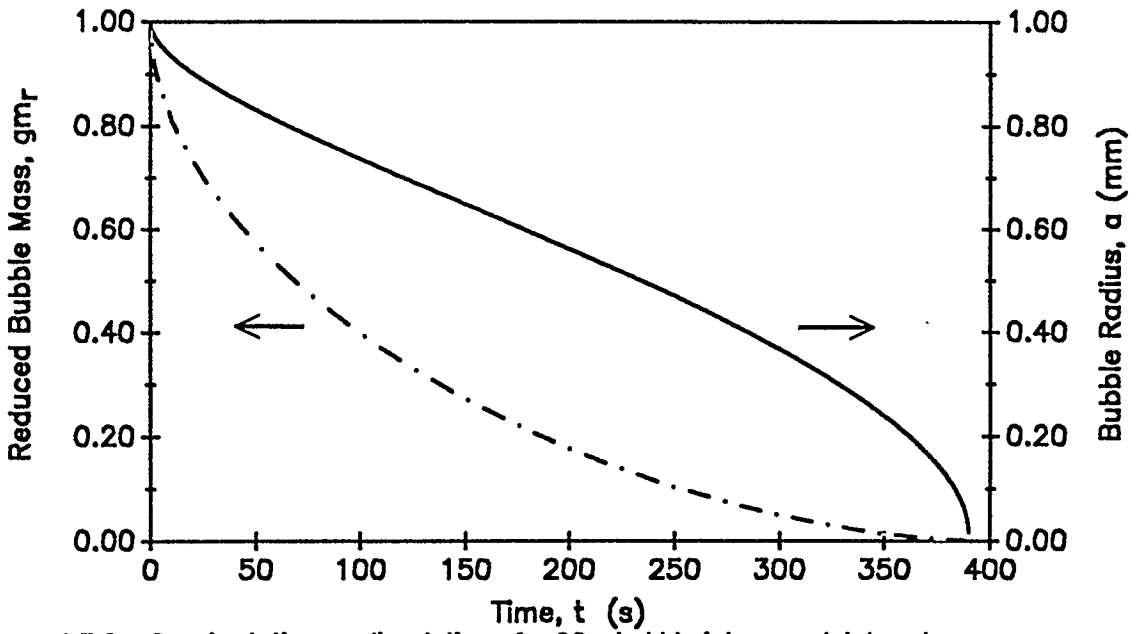

Figure 4.3.2 Quasi–stationary dissolution of a CO_2 bubble into completely sub–saturated Athabasca bitumen. T = 350 K, P = 1.0 MPa, a_0 = 1.0 mm

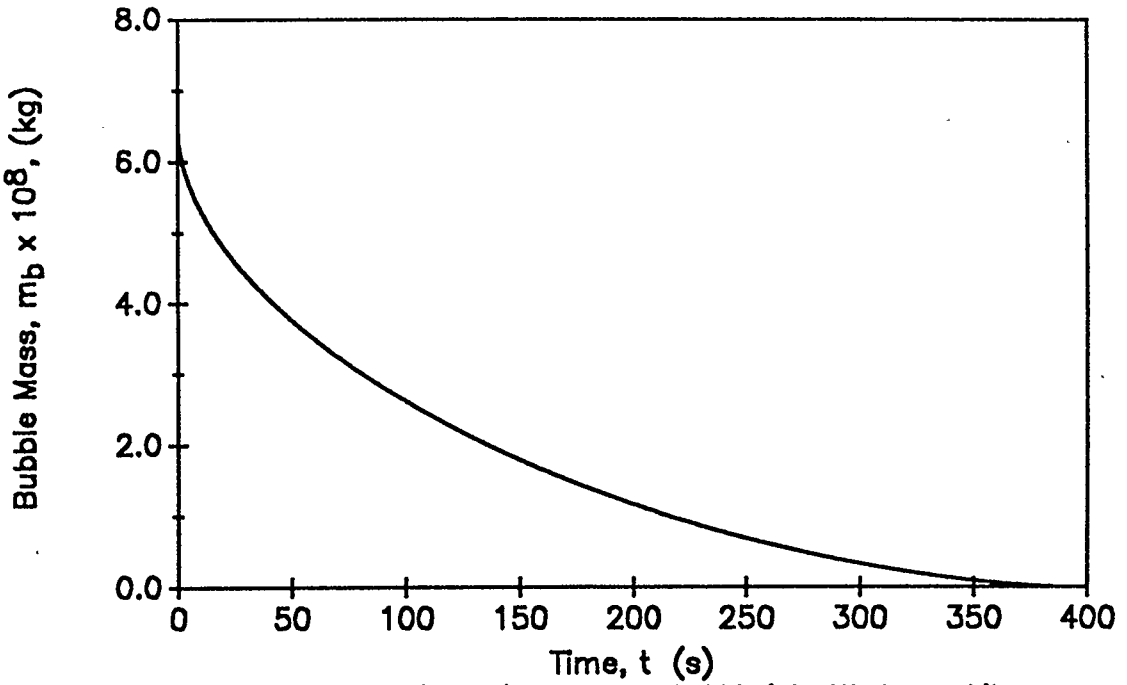

Fig. 4.3.3 Quasi–stationary dissolution of a CO_2 bubble into Athabasca bitumen
T = 350 K, P = 1.0 MPa, X = 0.0, a_0 = 1.0 mm

volume or mass).

Results of the reduced and actual dissolution times, over the temperature and pressure ranges evaluated, for the quasi-stationary dissolution of the fixed initial radius bubble, are given in Table 4.3.2.

Over the range of conditions evaluated, the most rapid dissolution was achieved at the lowest temperature and highest pressure considered (t_d = 37 s, T = 300 K, P = 6.0 MPa). Conversely, the slowest dissolution was achieved at the highest temperature and lowest pressure considered (t_d = 2036 s, T = 400 K, P = 1.0 MPa). The difference in dissolution times was achieved even though the bubble's initial mass in the fastest dissolution case (7.8×10^{-7} kg) was greater by a factor of fourteen than the slowest dissolution case (5.7×10^{-8} kg).

The conditions favouring dissolution of a static bubble (high pressure and low temperature) are easily anticipated through inspection of Fick's rate equation, knowledge of the solubility and diffusivity properties of CO_2 in Athabasca bitumen, and understanding of the model assumptions.

Inspection of Equation 3.1.4, a form of Fick's law, shows the rate of mass transfer from the bubble is related to the

Table 4.3.2

Quasi-Stationary Dissolution of a Static CO_2 Bubble Into a Completely Sub-Saturated CO_2-Athabasca Bitumen Solution, Considering Constant Initial Bubble Radius

Model Conditions - a_0 = 1.0 mm, X = 0.0

T (K)	P_s (MPa)	$t_{r,d}$	t_d (s)	$m_{b,0}$ (kg x 10^7)
300	1.0	0.275	133.2	0.78
350	1.0	0.510	388.2	0.66
400	1.0	1.560	2036.1	0.57
300	2.0	0.272	76.3	1.67
350	2.0	0.504	211.8	1.36
400	2.0	1.520	1215.3	1.16
300	4.0	0.266	47.7	3.93
350	4.0	0.490	120.6	2.93
400	4.0	1.443	666.7	2.41
300	6.0	0.260	37.5	7.84
350	6.0	0.476	89.8	4.79
400	6.0	1.367	453.9	3.77

magnitude of the diffusivity and concentration gradient at the bubble surface.

$$\frac{da}{dt} = \frac{D_{AB}}{c_A(1-c_{A,i}\overline{V_A})}\left(\frac{\partial c_A}{\partial r}\right)_{r=a} \qquad \textbf{(3.1.4)}$$

Svrcek and Mehrotra (1982) determined that CO_2 solubility in Athabasca bitumen increases with increasing pressure and decreasing temperature (Section 2.5). Additionally, as discussed in Section 2.6, Mehrotra et al. (1987) predicted that the mass diffusivity of CO_2 into bitumen (D_{AB}) has a strong dependence upon the gas mole fraction (x_g) in the solution (Figure 2.6.1), especially at lower values of x_g, and only a slight direct dependence upon temperature (at constant mole fractions of gas). However, as the models used in analyzing bubble dissolution assume equilibrium gas concentration at the bubble interface (interface gas concentration determined via Henry's law), both pressure and temperature through their relationships with Henry's law constant/gas solubility (direct and inverse relationships respectively), have significant effect upon mass diffusivity.

Graphical examples showing the effect of temperature on dissolution times are included as Figures 4.3.4 and 4.3.5. As shown in Figure 4.3.5 (the early time response of the bubble

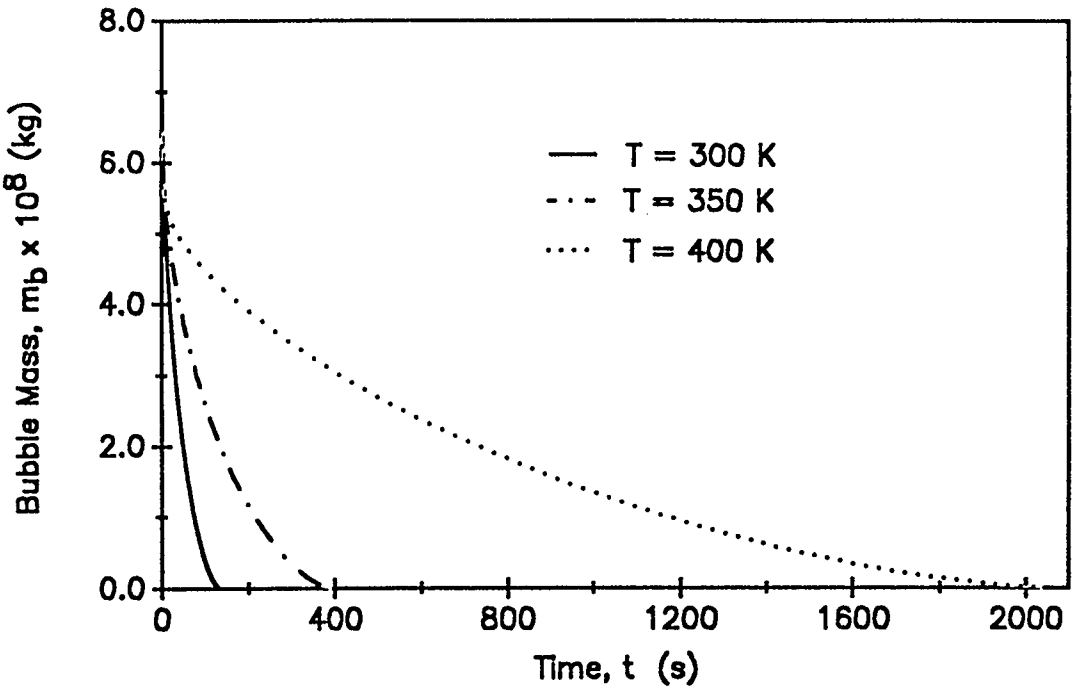

Fig. 4.3.4 Comparison of quasi–stationary dissolution of a CO_2 bubble at various temperatures. P = 1.0 MPa, X = 0.0, a_0 = 1.0 mm

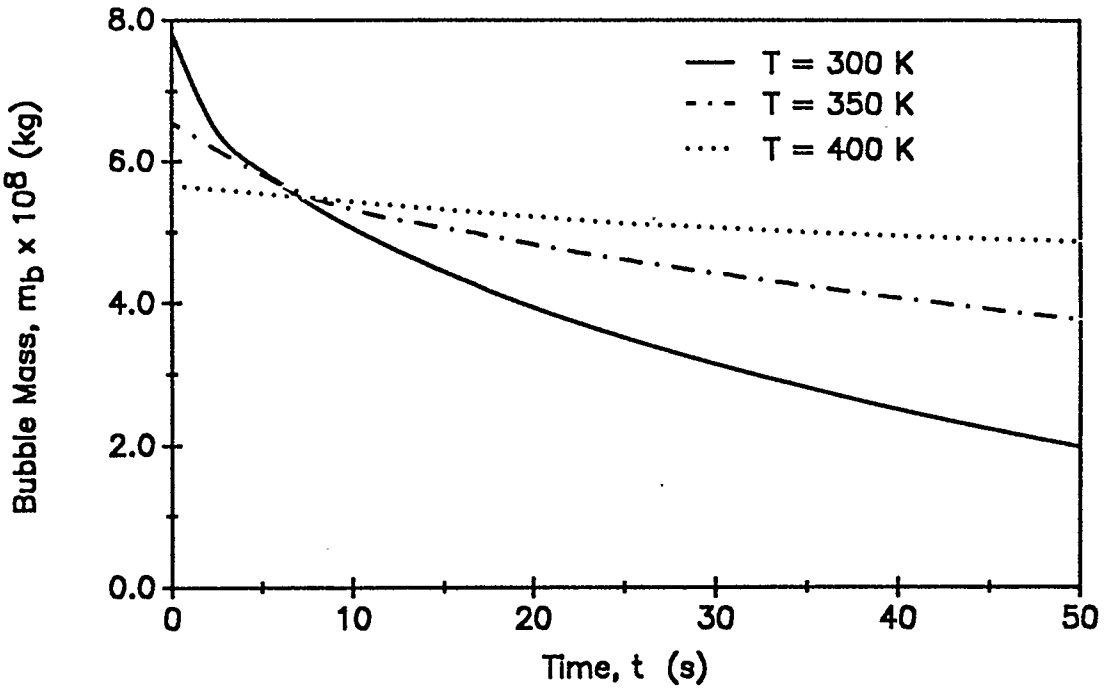

Fig. 4.3.5 Early time response at various temperatures of quasi–stationary dissolution of a CO_2 bubble. P = 1.0 MPa, X = 0.0, a_0 = 1.0 mm

dissolution), the bubbles reach a common mass extremely early in the dissolution process, indicating the strong difference in tendency towards dissolution over the temperature range considered.

At pressure of 1.0 MPa, increasing the temperature from 300 to 400 K, changes the dissolution time of a 1.0 mm radius CO_2 bubble in a completely sub-saturated solution, from 133 s to 2036 s (Figure 4.3.4). The longer bubble dissolution time occurs despite a decrease in initial bubble mass, (from 7.8 x 10^{-8} kg to 5.7 x 10^{-8} kg). Increasing the temperature from 300 to 400 K, decreased solubility from 6.68 to 1.3 m^3/m^3, with accompanying mass diffusivity reduced from 2.06 x 10^{-9} to 7.66 x 10^{-10} m^2/s.

At a temperature of 350 K, increasing the pressure from 1.0 to 6.0 MPa reduces the dissolution time of a 1.0 mm radius CO_2 bubble in a completely sub-saturated solution, from 388 s to 90 s (Figure 4.3.6), even though the initial bubble mass increased from 0.66 x 10^{-7} kg to 4.79 x 10^{-7} kg. Increasing the pressure from 1.0 to 6.0 MPa increases the solubility from 3.6 to 22.9 m^3/m^3, while mass diffusivity increased by a factor of approximately four, from 1.3 x 10^{-9} to 5.3 x 10^{-9} m^2/s.

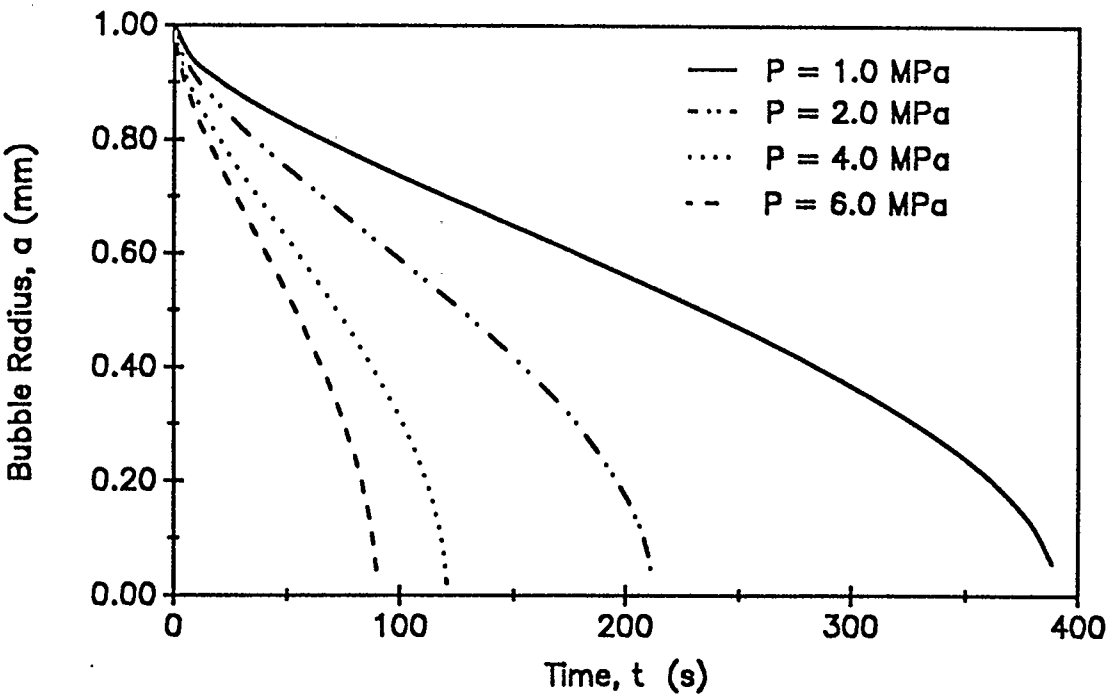

Figure 4.3.6 Effect of system pressure upon the quasi–stationary dissolution of a CO_2 bubble into bitumen. T = 350 K, X = 0.0

In addition to the assumption of equilibrium conditions at the bubble interface, other assumptions pertaining to mass diffusivity in the model include:

- solution diffusivity is based upon interface gas concentration, and
- constant diffusivity throughout the solution (bitumen) phase.

It is emphasized that the assumption of constant diffusivity in the solution is a reasonable simplification. Inspection of Table 4.3.1 shows that, for the majority of cases considered, the gas mole fraction at the interface ($x_{g,i}$) is well into the range ($x_g > 0.05$) where diffusivity shows only moderate dependence upon x_g. Additionally the diffusional process occurring at the interface has the greatest influence upon the dissolution process as:

- the concentration gradients are the highest at the interface, and
- the shell through which diffusion occurs is the smallest in the system,

Both considerations result in the largest molar fluxes in the system being at the interface. It is probable that over-estimating the diffusivity further out in the solution (gas molar concentrations being lower than at the interface), where

the diffusional shell is much larger, will not significantly impact the validity of the results.

It is interesting to note that, for a given temperature, increasing the system pressure has a minimal effect upon the reduced time to dissolution, $t_{r,d}$, while there is a significant decrease in the actual time of dissolution, t_d. Physically, as discussed, the decrease in time for bubble dissolution with increased system pressure is attributable to the increase in mass solubility and diffusivity. Mathematically, however, the decrease in actual time to dissolution, while reduced time remains relatively constant, is attributable to the inverse relationship between the actual time and mass diffusivity contained within the transformation from reduced time to actual time (Equation 3.1.6).

The CO_2 bubble diffuses much faster into bitumen than the glass melt for the pressure and temperature conditions considered in each instance. The reason for the vastly different dissolution rates can be seen through comparison of typical mass diffusivity and solubility values, given in Tables 4.1.1 and 4.3.1. Inspection shows that, for the conditions considered, the diffusivity and solubility values for the CO_2-bitumen system are significantly higher than the values for the CO_2-glass melt system.

4.3.2 Constant Initial Bubble Mass

Quasi-stationary dissolution of a CO_2 bubble with a fixed initial mass (5.0×10^{-7} kg) in a completely sub-saturated bitumen solution was studied. System temperature and pressure were again varied from 300 to 400 K and from 1.0 to 6.0 MPa respectively. Obviously, the bubble diameter will be governed by the PVT relationship for the constant mass of CO_2.

Model results are summarized in Table 4.3.3. Typical bubble dissolution curves, over a pressure range of 1.0 to 6.0 MPa, at a temperature of 350 K are shown as Figure 4.3.7.

As anticipated, bubble dissolution is promoted by higher pressures and lower temperatures. Dissolution times varied over the cases from a low of 28 s, (at conditions of T = 300 K and P = 6.0 MPa), to a high of 8795 s, (at conditions of T = 400 K and P = 1.0 MPa).

The effect of pressure and temperature variations upon bubble dissolution times is shown in Figures 4.3.8 and 4.3.9 respectively. As shown there consistently are dramatic increases in dissolution time at the upper end of the temperature range considered and similarly at the lower end of the pressure range considered, reflecting solubility and mass diffusivity relationships.

Table 4.3.3.

Quasi-Stationary Dissolution of a Static CO_2 Bubble Into a Completely Sub-Saturated CO_2-Athabasca Bitumen Solution, Considering Constant Initial Bubble Mass

Model Conditions - $m_{b,0} = 5.0 \times 10^{-7}$ kg, $X = 0.0$

T (K)	P_s (MPa)	$t_{r,d}$	t_d (s)	a_0 (mm)
300	1.0	0.275	459.1	1.85
350	1.0	0.513	1512.8	1.96
400	1.0	1.578	8795.0	2.07
300	2.0	0.272	158.7	1.44
350	2.0	0.504	505.1	1.54
400	2.0	1.520	3226.0	1.63
300	4.0	0.266	56.0	1.08
350	4.0	0.490	172.1	1.19
400	4.0	1.443	1084.0	1.27
300	6.0	0.260	27.8	0.86
350	6.0	0.476	91.3	1.01
400	6.0	1.367	547.0	1.10

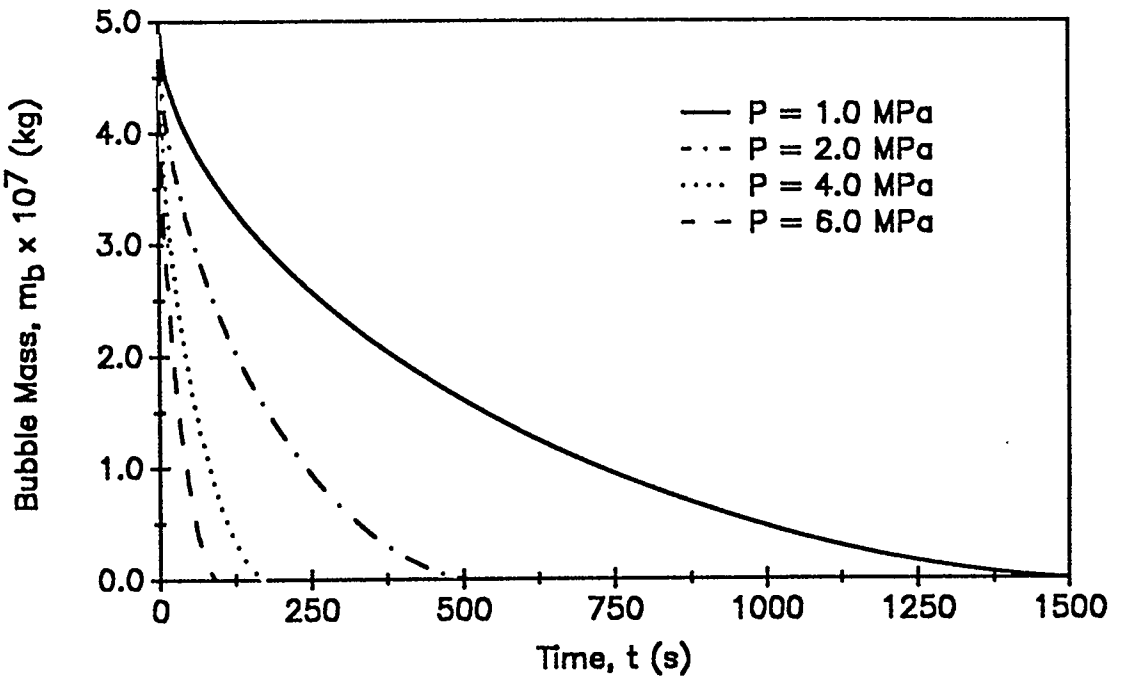

Figure 4.3.7 Effect of system pressure upon the quasi–stationary dissolution of a CO_2 bubble into bitumen. $m_{b,0}$ = 5.0 x 10^{-7}kg, T = 350 K, X = 0.0

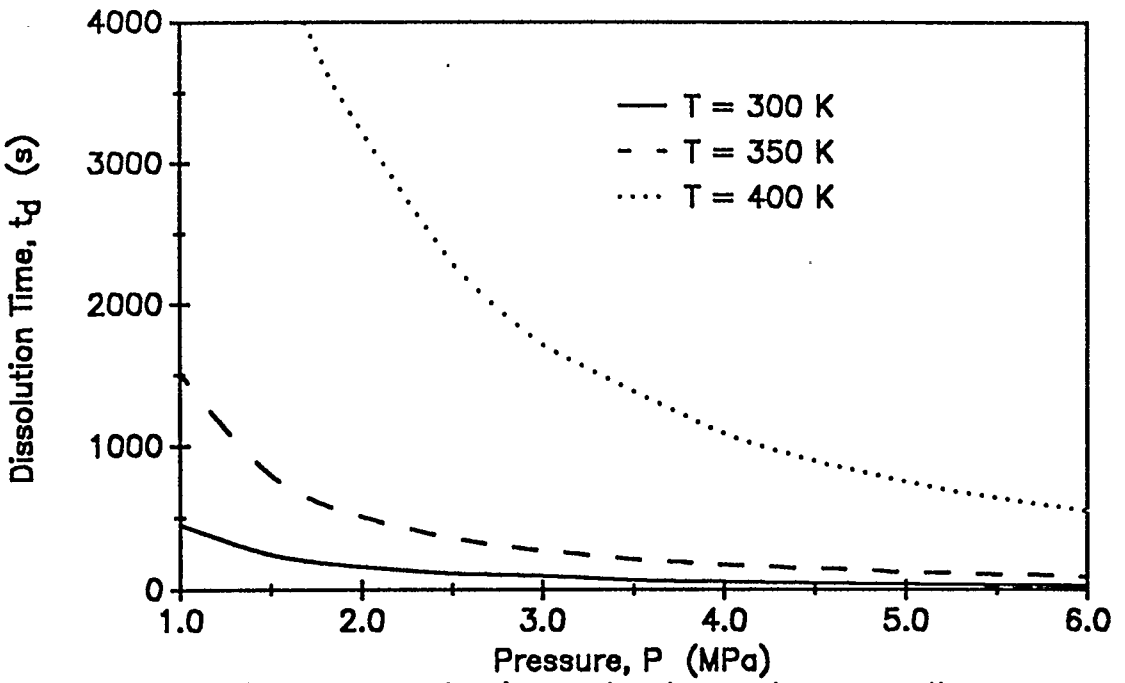

Figure 4.3.8 Effect of pressure, at various system temperatures, upon the dissolution of a CO_2 bubble into bitumen assuming Quasi-stationary dissolution. $m_{b,0} = 5.0 \times 10^{-7}$ kg, X = 0.0.

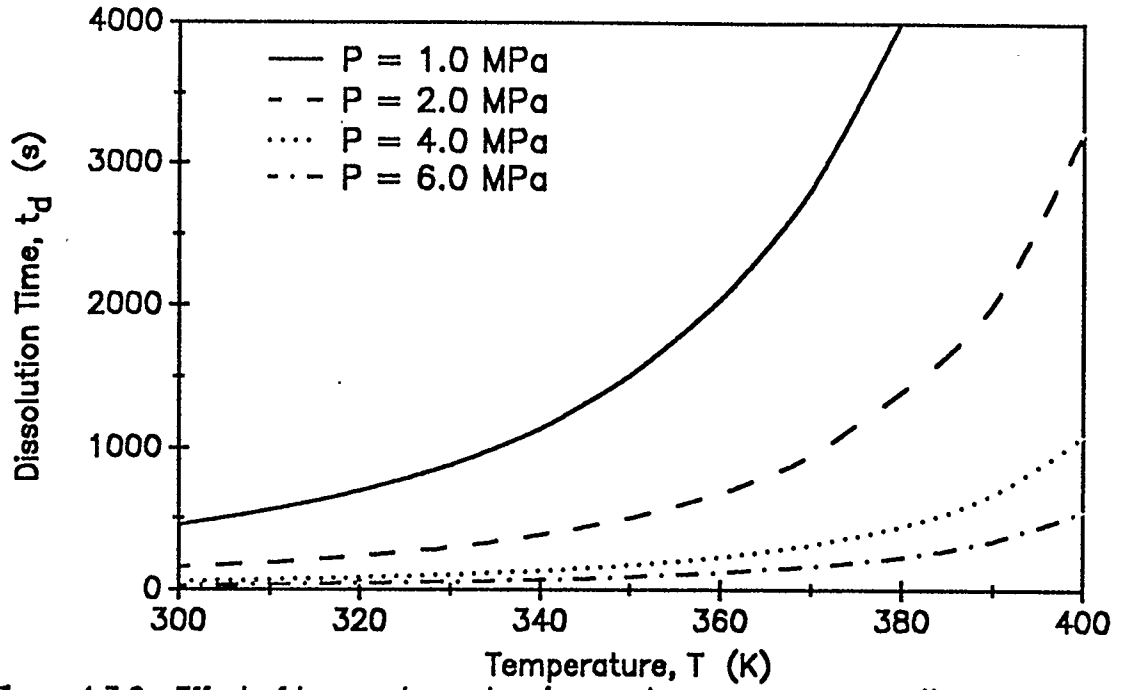

Figure 4.3.9 Effect of temperature, at various system pressures, upon the dissolution of a CO_2 bubble into bitumen assuming Quasi–stationary dissolution. $m_{b,0} = 5.0 \times 10^{-7}$ kg, X = 0.0

Review of the results from the cases where initial bubble radius was held constant (Table 4.3.2), with the results of the constant initial mass case (Table 4.3.3), shows that for specified temperature and pressure conditions, the reduced time to dissolution for different initial bubble radius/mass cases does not change, while the actual time to dissolution does vary. Inspection of the quasi-stationary dissolution equations (Equations 3.1.13, 3.1.14 and 3.1.20) shows that the same reduced times to dissolution would be anticipated where the surface tension effects are minimal. Mathematically, the difference in actual times to dissolution between cases of different initial bubble radius or mass at the same system conditions is attributable to the transformation from reduced time to actual time, Equation 3.1.6, in which actual time is proportional to the square of initial bubble radius.

The relationship between results of quasi-stationary dissolution models at the same system conditions of temperature and pressure but with different initial parameters (i.e. bubble radius or mass) makes the prediction of the results of alternative cases a relatively simple matter.

4.3.3 Concentration Profile and Mass Flux

The profiles for reduced molar concentration of CO_2 at various times in the dissolution process, for the conditions of T = 350 K, P = 1.0 MPa, and $m_{b,0}$ = 5.0 x 10^{-7} kg, are included as Figure 4.3.10. The explanation for the shape of the concentration profiles at the various points of the bubble dissolution is consistent with the discussion on concentration profiles for the dissolution of the O_2 bubble into the glass melt (Section 4.1.1).

The semi-log plot of mass transfer rate from the bubble versus time, at the given conditions, is shown as Figure 4.3.11. Inspection shows a high rate of mass transfer during the early stages of the bubble dissolution. This would be anticipated from previous discussions of the early time bubble behaviour in glass melts (Section 4.1.1); that is the rapid early dissolution is attributable to the large concentration gradient at the bubble surface.

During intermediate times the mass transfer rate declines exponentially (straight line relationship on the semi-log plot). The long term behaviour of the rate of change of bubble mass is somewhat surprising, however, as the mass transfer rate tends to decrease dramatically as the bubble approaches complete dissolution and finally disappears.

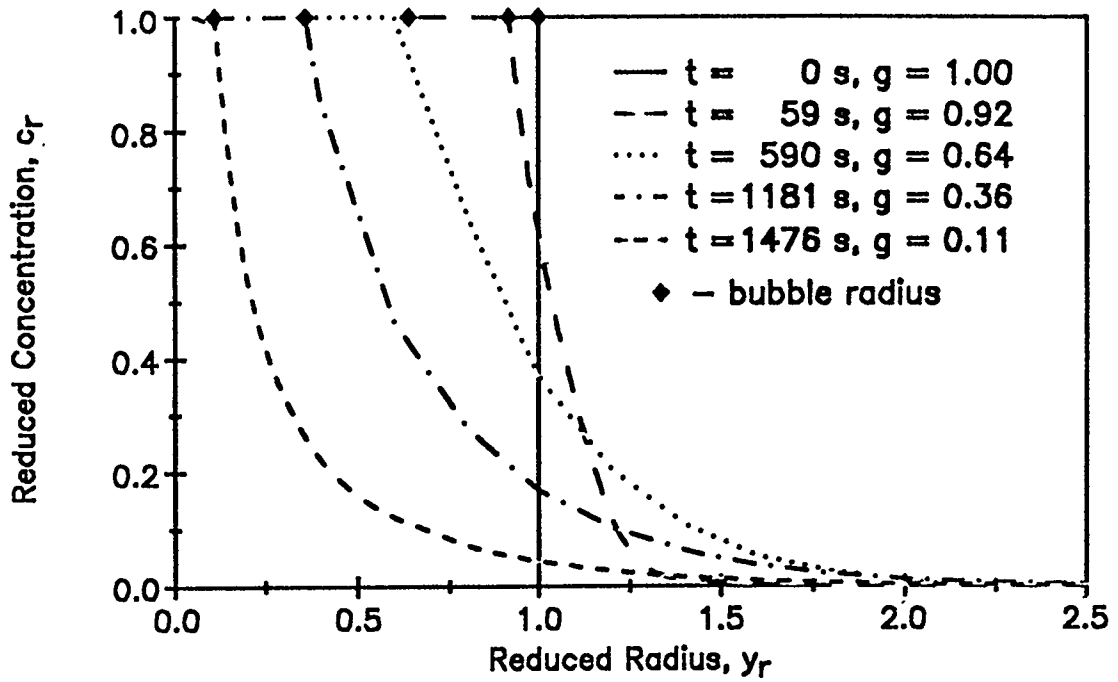

Figure 4.3.10 Solute concentration profiles during the dissolution of a CO_2 bubble into bitumen assuming quasi–stationary dissolution. T = 350 K, P = 1.0 MPa, $m_{b,0} = 5.0 \times 10^{-7}$ kg

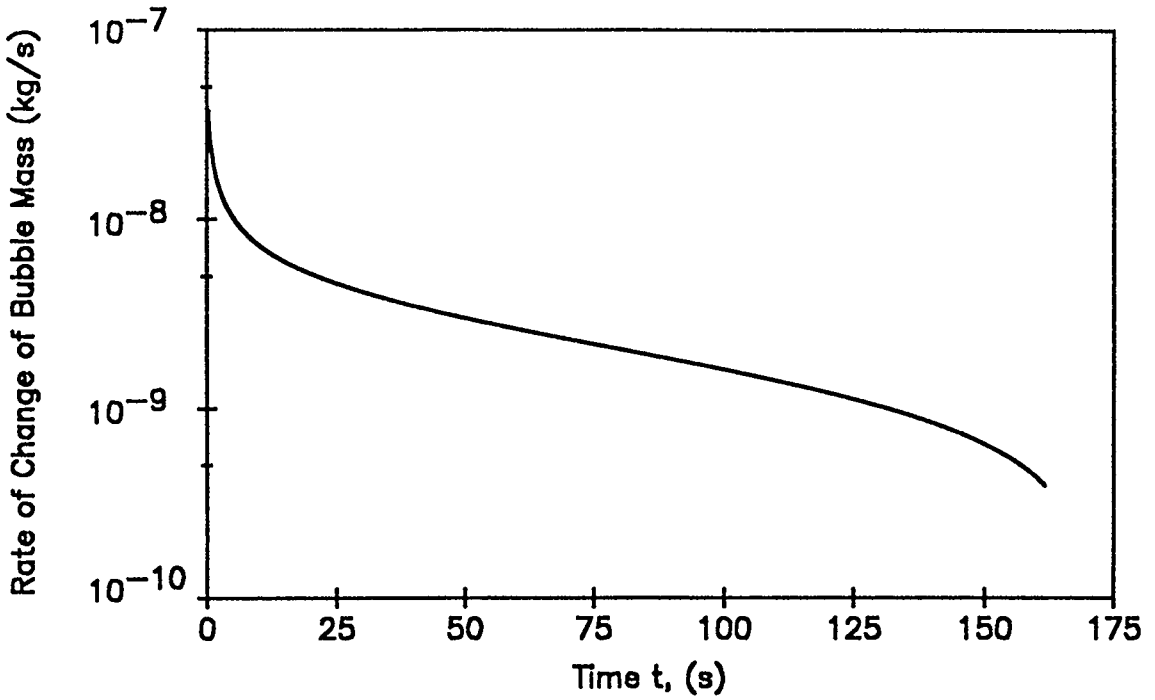

Figure 4.3.11 Mass transfer from a static CO_2 bubble into Athabasca bitumen using quasi–stationary assumptions. T = 350 K, P = 4.0 MPa, $m_{b,0} = 5.0 \times 10^{-7}$ kg, X = 0.0.

The semi-log plot of mass flux from the bubble (N_A) versus time is shown as Figure 4.3.12. As seen previously, at early times the high mass flux, coupled with the relatively large surface area results in rapid early dissolution. At intermediate times the mass flux is relatively constant, indicative of a trade-off between declining mass transfer rate and the shrinking bubble surface area.

At longer times, the mass flux increases once again. In comparing Figures 4.3.12 and 4.3.13, it is apparent that the increase in the mass flux corresponds with the rapid reduction of bubble radius. The effect upon bubble radius is enhanced by the cubic relationship between radius and bubble mass or volume.

As discussed previously, the increase in mass flux or dissolution rate at longer times is attributable to:

- increased area (relative to the diminishing bubble surface area) available for diffusion, and in lesser part due to,
- increased bubble pressure (due to surface tension) acting to increase the gas concentration at the bubble interface and thereby increasing the concentration gradient across the solution phase.

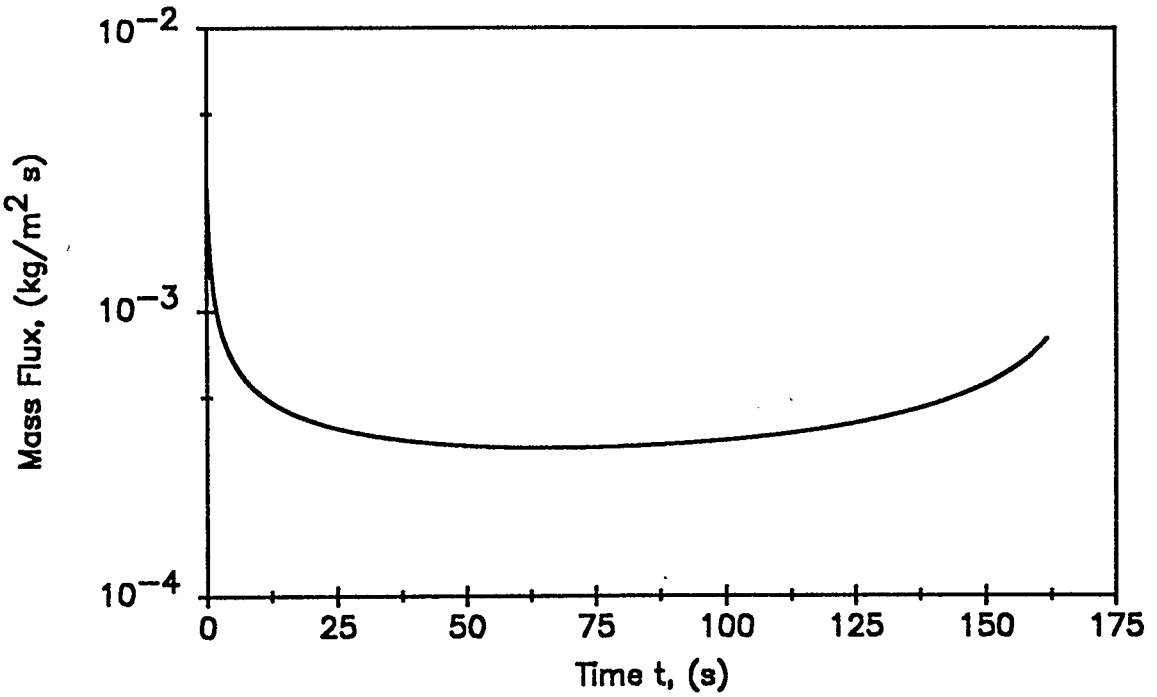

Figure 4.3.12 Mass flux from the dissolution of a static CO_2 bubble into bitumen using the quasi-stationary model. T = 350 K, P = 4.0 MPa, X = 0.0 $m_{b,0} = 5.0 \times 10^{-7}$ kg

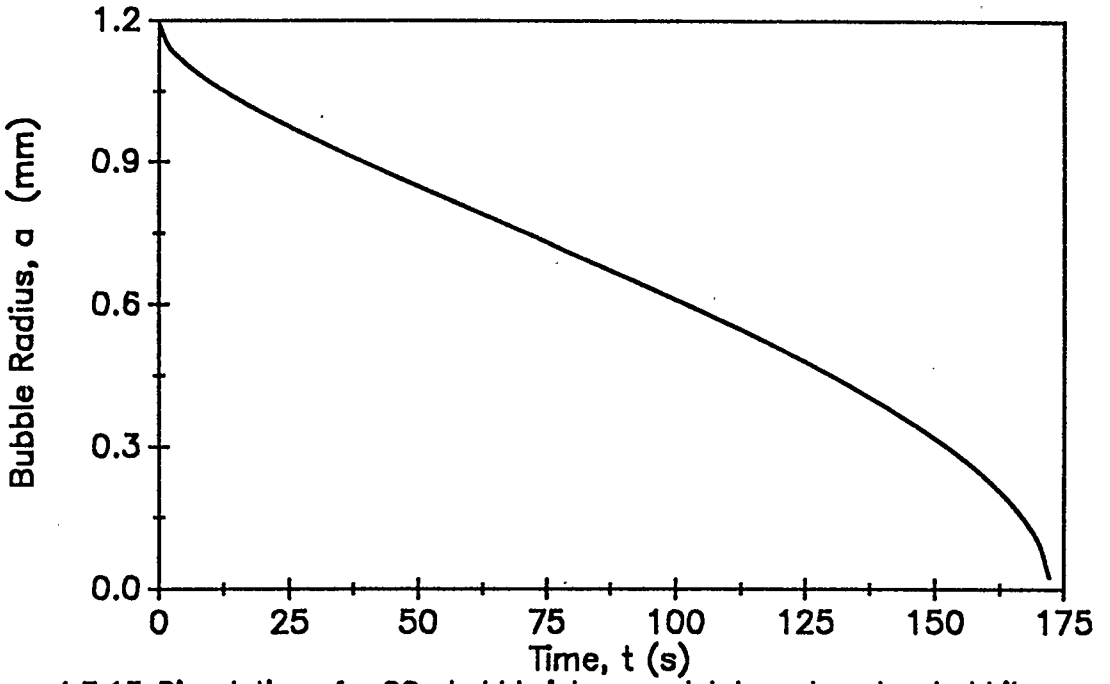

Figure 4.3.13 Dissolution of a CO_2 bubble into completely undersaturated bitumen bitumen using the quasi–stationary model. T = 350 K, P = 4.0 MPa, $mb_0 = 5.0 \times 10^{-7}$ kg.

Surface Tension Effects

Surface tension effects were considered for a number of cases, and these provided a range of dissolution times (Table 4.3.4).

As compared to the glass melt system previously reviewed, the CO_2-Athabasca bitumen system under consideration has relatively low values of surface tension and, at the same time, relatively high system pressures. Accordingly, as would be anticipated, surface tension effects are minimal in the CO_2-Athabasca bitumen system.

For the system modelled (P = 1.0 MPa, T varied from 300 to 400 K), inclusion of the surface tension effects decreased the dissolution time by only approximately 0.1 %. Although the surface tension effects are minimal (and therefore have not been shown graphically), the results indicate:

- surface tension plays a more significant role where bubble dissolution is slower (simply from being in effect longer),
- although higher system temperatures result in longer bubble dissolution times, the increased effect of surface tension in this case is offset by a reduction in the value of surface tension with temperature, and

Table 4.3.4.

Quasi-Stationary Dissolution of a Static CO_2 Bubble Into a Completely Sub-Saturated CO_2-Athabasca Bitumen Solution, Considering the Effects of Surface Tension

Model Conditions - $m_{b,0}$ = 5.0 x 10^{-7} kg, P_s = 1.0 MPa, X = 0.0

T (K)	P_b (MPa)	$t_{r,d}$	t_d (s)
Surface tension effects not included			
300	1.0	0.275	459.5
350	1.0	0.513	1514.9
400	1.0	1.578	8804.2
Surface tension effects included (Mehrotra et al., 1985)			
300	1.0009	0.275	459.1
350	1.0015	0.513	1512.8
400	1.0015	1.578	8795.0
Surface tension effects included (Bowman, 1967)			
300	1.0010	0.275	459.0
350	1.0014	0.513	1513.0
400	1.0011	1.578	8797.0

- over the range of conditions studied, the use of Bowman's (1967) data for surface tension, as opposed to using predictions provided by Mehrotra et al. (1985), produced little change in the results.

4.3.5 Sub-Saturated CO_2-Bitumen Solution

As shown by the typical results displayed in Table 4.3.5 (T = 350 K, P varied between 1.0 to 6.0 MPa) increasing the initial CO_2 concentration in a sub-saturated CO_2 bitumen solution (thereby reducing the molar concentration gradient between the bubble interface and the solution) decreases the rate of dissolution of the bubble/increases bubble dissolution time. In an actual dissolution situation, the effect of the reduced concentration gradient would be partially offset by the increased mass diffusivity in the solution (mass diffusivity increasing with the degree of saturation - Section 2.6). However, that effect is not considered significant nor is it addressed in the quasi-stationary model developed in Chapter 3.

Inspection of Equations 3.1.13 and 3.1.15 shows that increasing $c_{A,0}$ increases the value of the undersaturation parameter, X. (A value of X = 1.0 indicates a saturated CO_2

Table 4.3.5.

Quasi-Stationary Model Dissolution of a Static CO_2 Bubble Into a Sub-Saturated CO_2-Athabasca Bitumen Solution, Considering the Effects of Variation of $c_{A,0}$

Model Conditions - $m_{b,0} = 5.0 \times 10^{-7}$ kg, $T = 350$ K

X	P_s (MPa)	$t_{r,d}$	t_d (s)
$c_{A,0} = 0.0$ kg/m^3			
0.000	1.0	0.51	1513
0.000	2.0	0.50	505
0.000	4.0	0.49	172
0.000	6.0	0.48	91
$c_{A,0} = 0.03218$ kg/m^3			
0.200	1.0	0.68	2007
0.099	2.0	0.57	576
0.048	4.0	0.52	183
0.032	6.0	0.49	96
$c_{A,0} = 0.06436$ kg/m^3			
0.400	1.0	0.99	2888
0.198	2.0	0.67	671
0.097	4.0	0.56	195
0.063	6.0	0.52	100
$c_{A,0} = 0.12872$ kg/m^3			
0.800	1.0	3.74	10993
0.395	2.0	0.97	971
0.193	4.0	0.65	227
0.126	6.0	0.57	109
$c_{A,0} = 0.150$ kg/m^3			
0.932	1.0	12.72	37419
0.460	2.0	1.11	1070
0.225	4.0	0.68	238
0.147	6.0	0.59	114

-bitumen solution, while $X = 0.0$ is indicative of a completely sub-saturated solution). Increasing the value of X decreases the magnitude of Na, thereby reducing the rate of dissolution, as given by Equation 3.1.20.

As X approaches 1.0, dissolution times get extremely long. For example for the conditions of $T = 350$ K, $P = 1.0$ MPa and $m_{b,0} = 5.0 \times 10^{-7}$ kg, increasing $c_{A,0}$ from 0.0 to 0.15 kg/m^3 (i.e., changing X from 0.0 to 0.932) increases the bubble dissolution time by a factor of 25 from 1500 to 37500 s.

The results (for the conditions $P = 1.0$, $T = 350$ K) of bubble radius versus time for varying initial concentrations are shown in Figure 4.3.14. The plot shows the significant increase in dissolution times as the initial gas concentration in the solution approaches saturation.

As discussed in Section 4.1.1, in a completely saturated solution ($X = 1.0$) the additional bubble pressure resulting from surface tension promotes the dissolution process. The early time response for the completely saturated case, where only surface tension provides the driving force for the dissolution of the CO_2 bubble, is shown in Figure 4.3.15. The very slow rate of dissolution supports the previous conclusion that surface tension has a minimal effect upon the CO_2 bubble dissolution process.

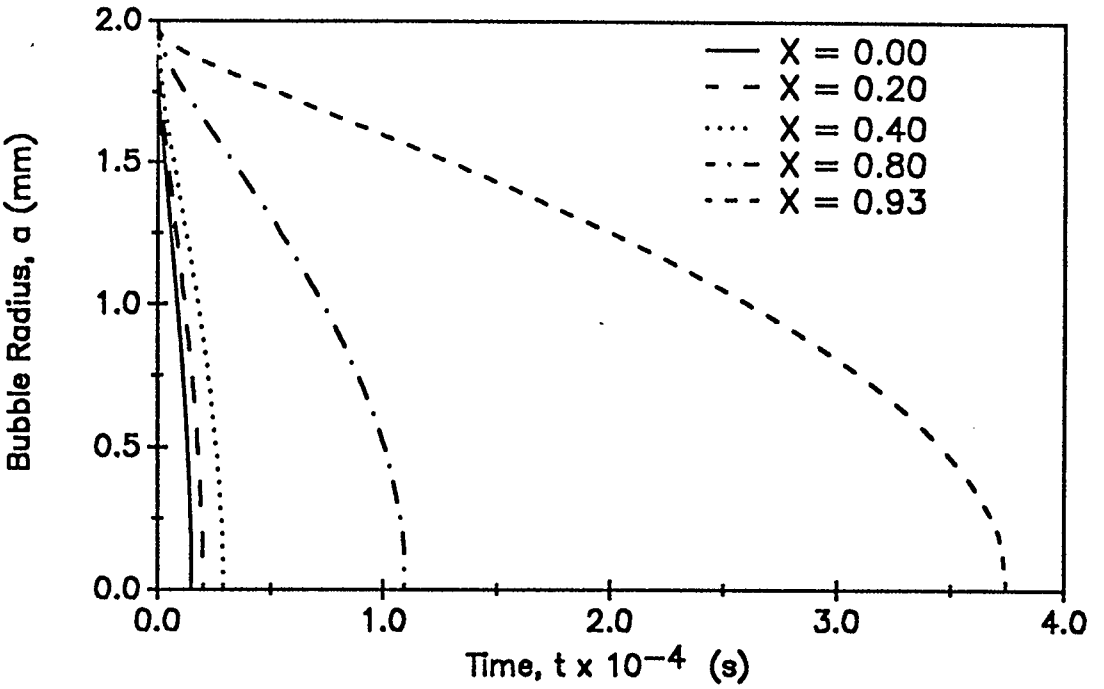

Figure 4.3.14 Quasi–stationary dissolution of a CO_2 bubble at varying solution undersaturations. T = 350 K, P = 1.0 MPa, $m_{b,0} = 5.0 \times 10^{-7}$ kg

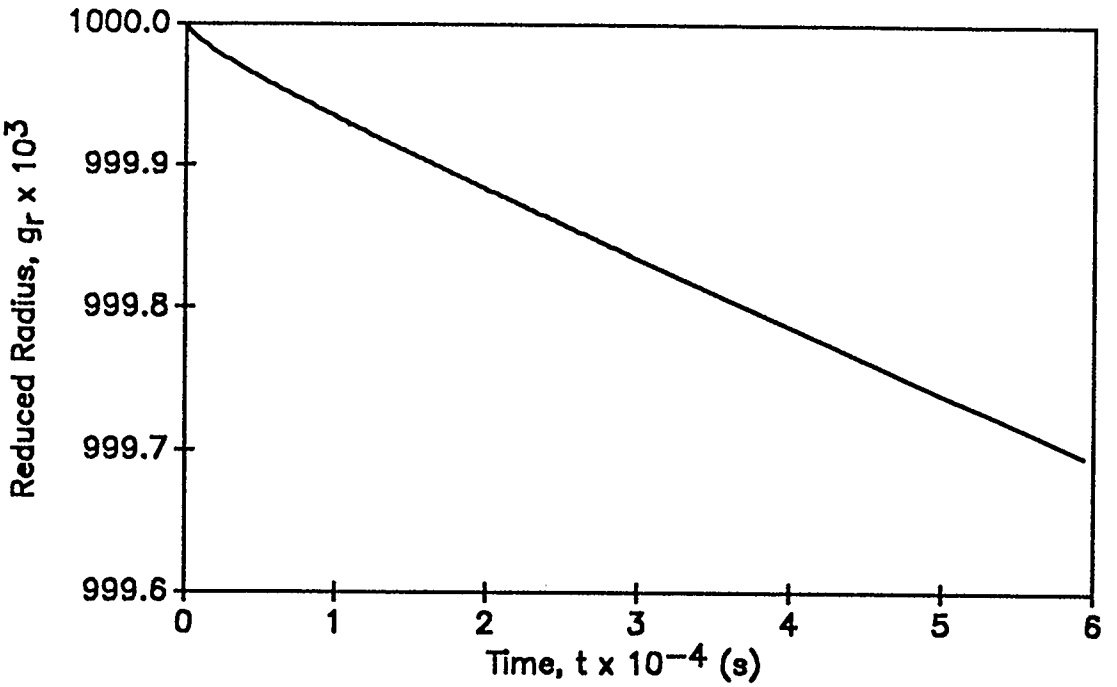

Figure 4.3.15 Early time response of the dissolution of a CO_2 bubble into a completely saturated bitumen solution. σ = 0.025 mN/m, T = 350 K, P = 1.0 MPa, X = 1.0

4.4 Molecular Diffusion of a Static CO_2 Bubble; Lumped Approach

The second model to be applied to study the dissolution of a static gas bubble was the rather simple molecular diffusion model. As discussed previously in Section 2.2, this lumped model assumes that diffusion occurs by molecular means only, with the mass-transfer Nusselt number, Nu_{AB}, set to the theoretical value of 2.0.

The results for the constant initial mass case ($m_{b,0}$ = 5.0 x 10^{-7} kg) over a range of temperature and pressure conditions, are given in Table 4.4.1.

Trends in dissolution time for the lumped molecular diffusion model are similar to the quasi-stationary models; that is, lower temperatures and higher pressures promote faster dissolution. Trends for the lumped model temperature and pressure effects are shown in Figures 4.4.1 and 4.4.2. Similar to the quasi-stationary model trends (included in the figures), dissolution time dramatically increases at both the upper end of the temperature range and lower end of the pressure range under consideration.

When compared with the results from the analytically formulated quasi-stationary model, the predicted dissolution

Table 4.4.1.

Molecular Diffusion Model (Nu_{AB} = 2.0) Dissolution of a Static CO_2 Bubble Into a Completely Sub-Saturated CO_2-Athabasca Bitumen Solution, Considering Constant Initial Bubble Mass

Model Conditions - $m_{b,0}$ = 5.0 x 10^{-7} kg, X = 0.0

T (K)	P_s (MPa)	t_d (s)
300	1.0	1171
350	1.0	3259
400	1.0	14753
300	2.0	430
350	2.0	1131
400	2.0	5500
300	4.0	180
350	4.0	410
400	4.0	1951
300	6.0	120
350	6.0	245
400	6.0	1045

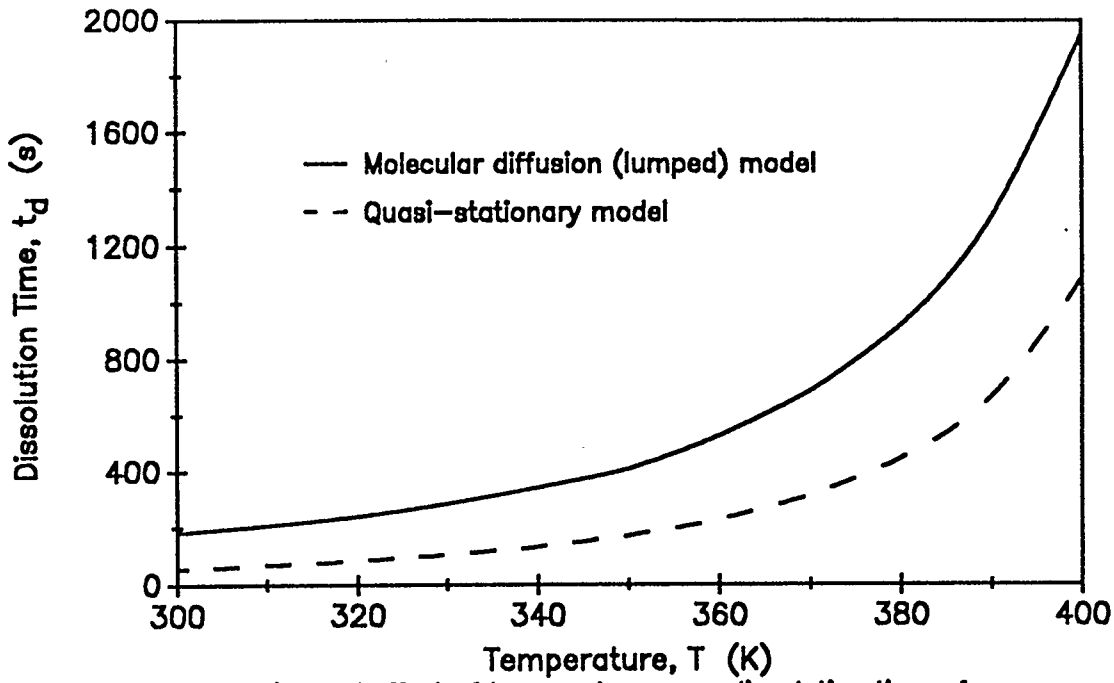

Figure 4.4.1 Comparison of effect of temperature upon dissolution time of a static CO_2 bubble under alternative models. $m_{b,0} = 5.0 \times 10^{-7}$ kg, P = 4.0 MPa, X = 0.0.

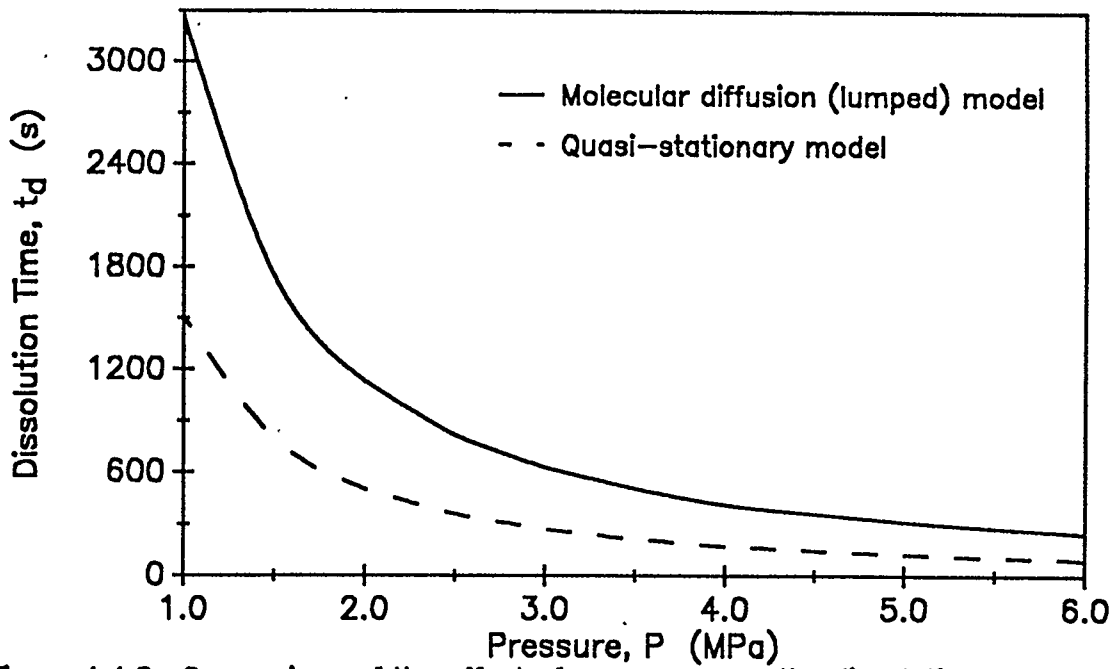

Figure 4.4.2 Comparison of the effect of pressure upon the dissolution of a static CO_2 bubble under alternative dissolution models. $m_{b,0} = 5.0 \times 10^{-7}$kg, T = 350 K, X = 0.0.

times of the lumped model are significantly slower (by a factor of 1.7 to 4.3) as shown graphically in Figures 4.4.3 and 4.4.4.

The shape of the lumped model dissolution curves are rather monotonous and smooth, with the most significant difference in the dissolution profiles of the two methods being the lumped model's lack of early time effects and resultant *S* shaped bubble radius decline curve, typical of the quasi-stationary approach (which assumes a high early time concentration gradient at the bubbles surface).

Mass flux results from the bubble for both the lumped and quasi-stationary models are shown as Figure 4.4.5. The mass flux values reflect the more rapid dissolution predicted by the quasi-stationary analytic model. In contrast with the quasi-stationary dissolution model, the lumped model does not provide high early-time rates of dissolution or mass flux. The lumped model predicts mass flux to increase gradually until the bubble approaches the point of dissolution, whereupon mass flux increases dramatically.

The rationale for the increase in mass flux as the bubble approaches dissolution under lumped model assumptions is the same as discussed for the quasi-stationary model, i.e.:

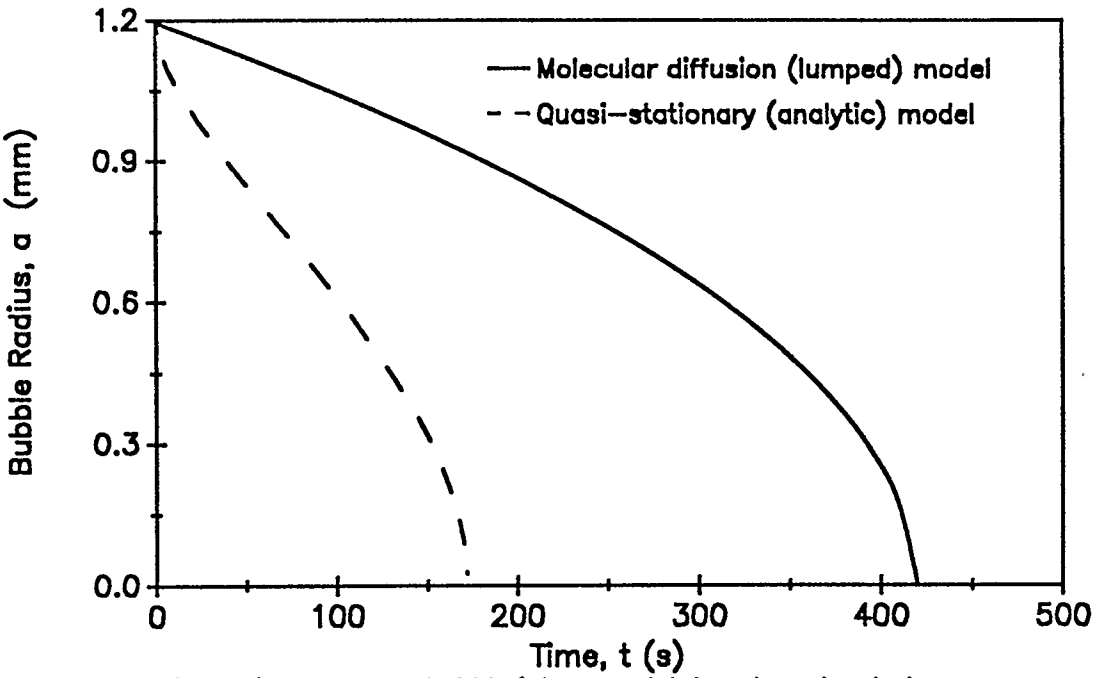

Figure 4.4.3 Dissolution of a CO_2 bubble into completely sub-saturated bitumen using alternative models. T = 350 K, P = 4.0 MPa, $m_{b,o} = 5.0 \times 10^{-7}$kg.

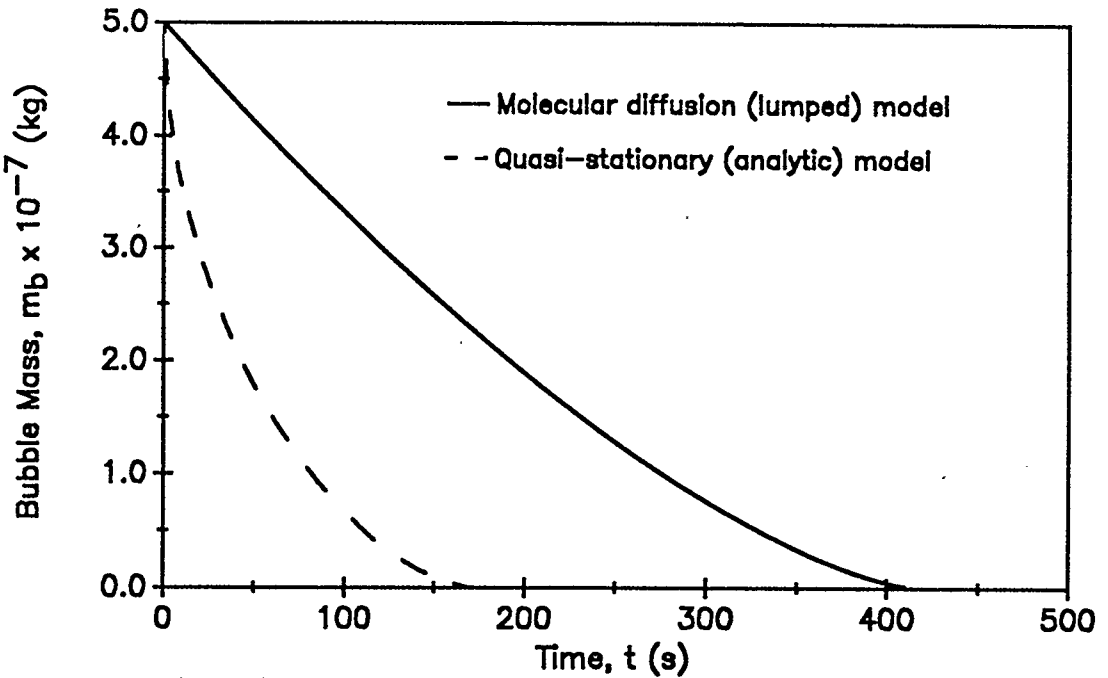

Figure 4.4.4 Dissolution of a CO_2 bubble into completely sub–saturated bitumen using alternative models. T = 350 K, P = 4.0 MPa.

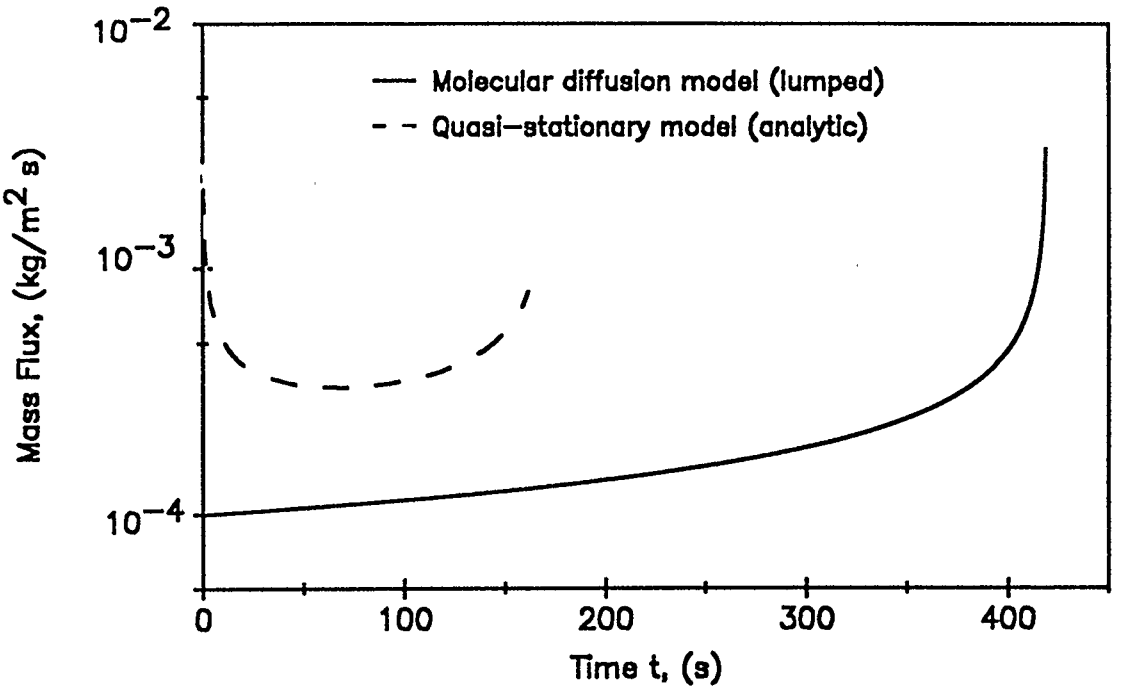

Figure 4.4.5 Mass flux from the dissolution of a static CO_2 bubble into bitumen using alternative models. T = 350 K, P = 4.0 MPa, X = 0.0

- increased area (relative to the diminishing bubble surface area) available for diffusion, and to a lesser extent:
- increased bubble pressure (due to surface tension) acting to increase the gas concentration at the bubble interface and thereby increasing the concentration gradient across the solution.

4.5 Brian-Hales'/Levich's Correlations

As it is probable that convective effects would have a significant bearing upon bubble dissolution, the understanding of system dynamics gained through the analysis of static bubble dissolution was extended to study the dissolution of a rising bubble. The first model selected for the analysis was the mass transfer Nusselt number (Nu_{AB}) correlations provided by Brian and Hales (1969) and Levich (1962). Both correlations are dependent upon Pe_{AB}. As discussed in Section 2.3, the correlations take into account convective effects, in addition to the purely molecular diffusional forces which were modeled in Section 4.4 with the lumped approach towards modelling the static bubble dissolution. Accordingly, it would be anticipated that the Brian-Hales and Levich correlations for the rising bubble would result in more rapid bubble dissolution than for the lumped analysis of the static bubble dissolution.

Results of dissolution time and bubble height for the dissolution of a rising CO_2 bubble ($m_{b,0}$ = 5.0 x 10^{-7} kg) into a completely sub-saturated CO_2-Athabasca bitumen solution, over the same range of system properties (T and P) considered in the analysis of the static bubble, are included as Table 4.5.1. Dissolution times varied over the cases from a low of 47 s, (at conditions of T = 300 K and P = 6.0 MPa), to a high

Table 4.5.1.

Brian-Hales' / Levich's Correlations for the Dissolution of a Rising CO_2 Bubble Into a Completely Sub-Saturated CO_2-Athabasca Bitumen Solution, Considering Constant Initial Bubble Mass

Model Conditions - $m_{b,0}$ = 5.0 x 10^{-7} kg, X = 0.0

T (K)	P_s (MPa)	t_d (s)	z_d (m)
300	1.0	462.0	0.040
350	1.0	352.8	1.560
400	1.0	761.0	34.780
300	2.0	190.5	0.024
350	2.0	162.9	0.600
400	2.0	337.8	11.530
300	4.0	75.3	0.024
350	4.0	74.9	0.290
400	4.0	162.9	4.280
300	6.0	46.8	0.031
350	6.0	47.8	0.210
400	6.0	105.0	2.400

of 462 s, (at conditions of T = 300 K and P = 1.0 MPa).

Typical dissolution curves, showing bubble radius and mass declines, are shown as Figures 4.5.1 and 4.5.2 respectively. Both sets of curves exhibit smooth, monotonous early and middle time declines with a rapid decline in bubble radius experienced at very late times in the process.

At a given temperature (Figure 4.5.3) increasing the pressure decreases the dissolution time. From previous discussions in Section 4.3, this result would be anticipated through understanding of pressure effects upon solubility and mass diffusivity. However, the extent of the relative change in the reduction of dissolution time, as compared to the static bubble models (Figure 4.5.4), is moderated by:

- the Brian-Hales/Levich models having slightly less dependence upon diffusivity (rate of mass transfer varies between directly proportional at low Pe_{AB} to varying to the 2/3 power at higher Pe_{AB}) than the static models (rate of mass transfer directly proportional to diffusivity - Section 3.1 - Equation 3.1.4, Section 3.2 - Equation 3.2.4), and
- convective effects.

For a given initial mass of bubble, as the system pressure

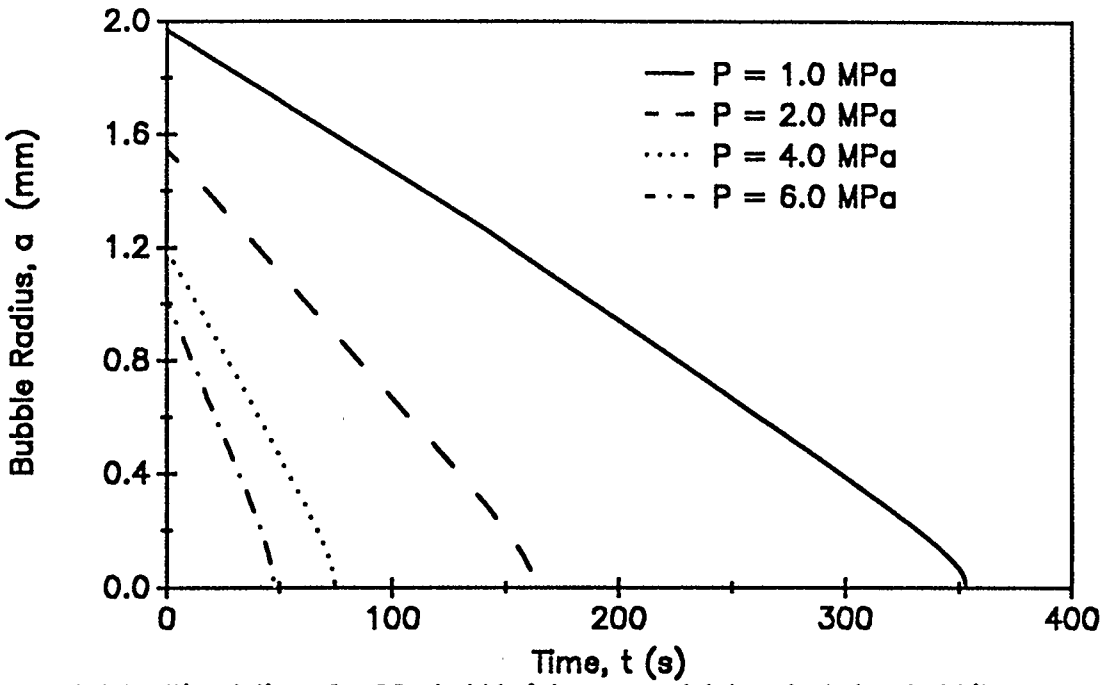

Figure 4.5.1 Dissolution of a CO_2 bubble into a completely sub-saturated bitumen solution over a range of pressures via Brian-Hales'/Levich's correlations. T = 350 K, $m_{b,0} = 5.0 \times 10^{-7}$ kg.

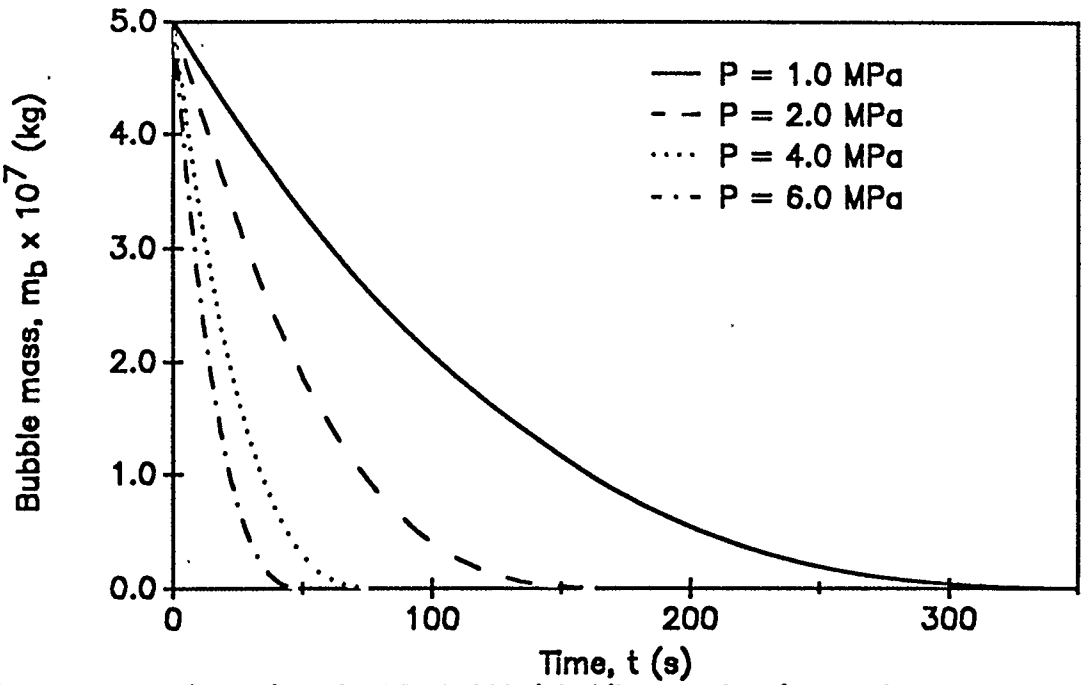

Figure 4.5.2 Dissolution of a CO_2 bubble into bitumen at various system pressures via Brian–Hales'/Levich's correlations. T = 350 K, X = 0.0

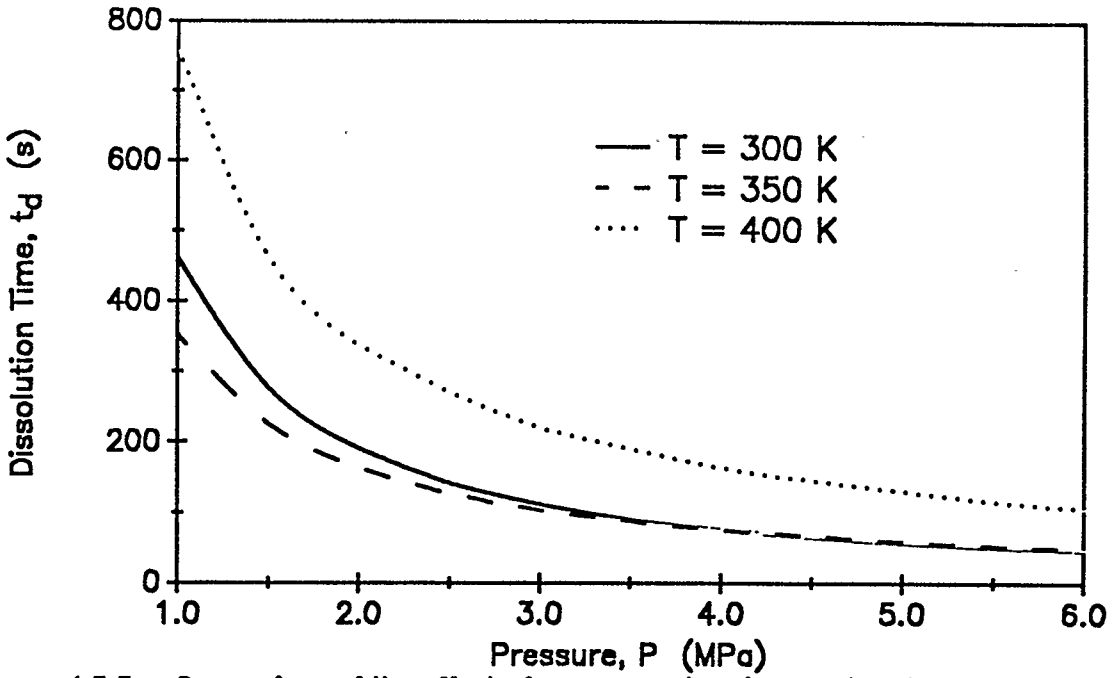

Figure 4.5.3 Comparison of the effect of pressure, at various system temperatures, upon the dissolution of a CO_2 bubble into bitumen assuming Brian–Hales'/Levich's correlations. $m_{b,0} = 5.0 \times 10^{-7}$kg, X = 0.0.

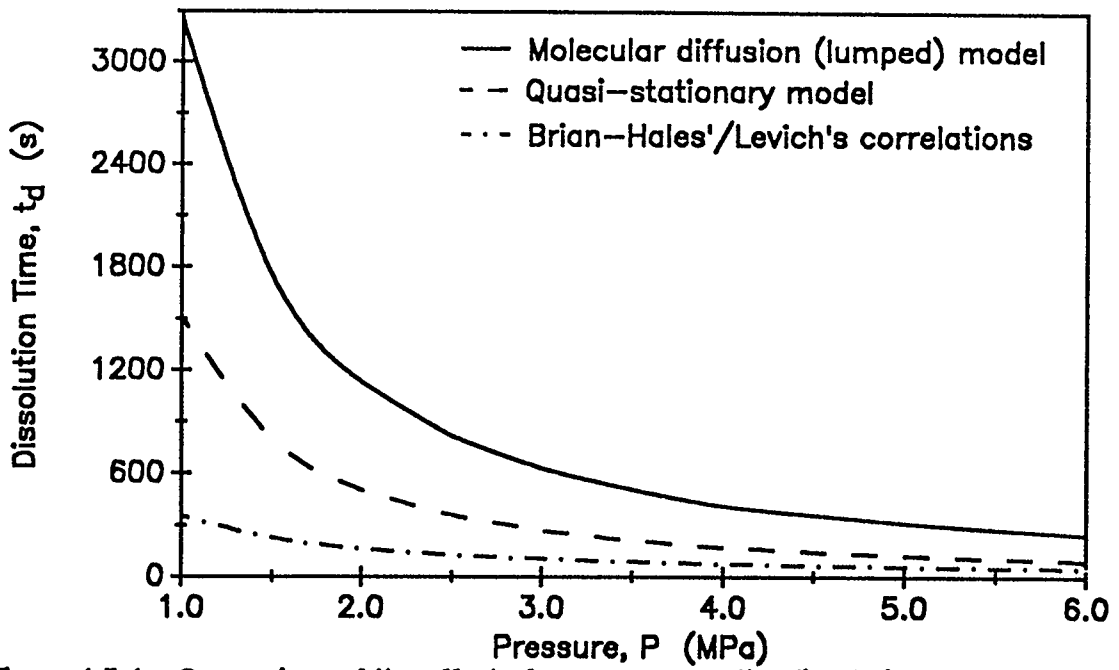

Figure 4.5.4 Comparison of the effect of pressure upon the dissolution of a CO_2 bubble under alternative dissolution models. $m_{b,0} = 5.0 \times 10^{-7}$ kg, T = 350 K, X = 0.0.

increases the bubble radius decreases. At a given system temperature, Stokes' law dictates that the smaller bubble will have a slower rise velocity, with associated decrease in convective diffusion effects. For example, when only molecular diffusion is considered in the case of the static bubble modeled by the lumped approach, increasing the system pressure from 1.0 MPa to 4.0 MPa (T = 350 K) reduces the dissolution time by 87 % (3259 s to 410 s). While the absolute dissolution times for the rising bubble are much shorter than for the static bubble, the relative reduction in dissolution time when system pressure is increased from 1.0 to 4.0 MPa is 78 % (353 s to 75 s).

At a given pressure (Figure 4.5.5), bubble dissolution time moderately increases at both ends of the temperature range under consideration. Hence, a mid-range temperature which corresponds to a minimum dissolution time is seen. The curvature demonstrating the mid-range minimum is much more pronounced at lower system pressures.

The mid-range temperature minimum dissolution time predicted by use of Brian-Hales'/Levich's correlations contrasts with the static bubble dissolution (Figure 4.5.6), where increased temperature consistently resulted in significantly longer dissolution times. For example, at conditions of $m_{b,0}$ = 5.0 x 10^{-7} kg and P = 4.0 MPa, increasing the system temperature from

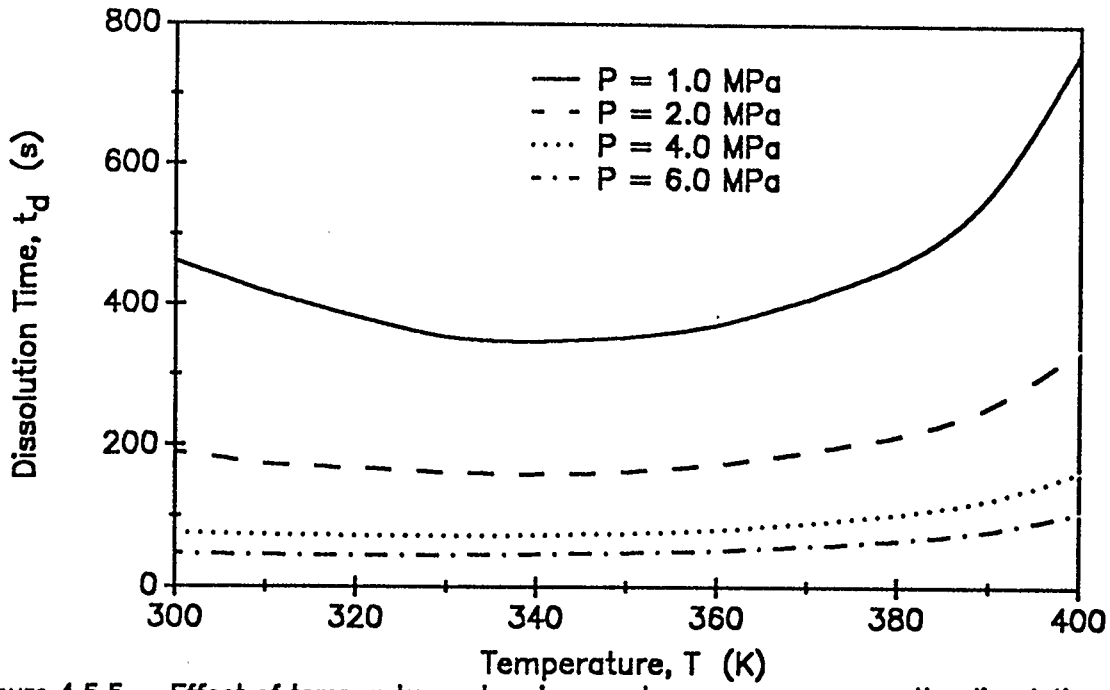

Figure 4.5.5 Effect of temperature, at various system pressures, upon the dissolution of a CO_2 bubble into bitumen assuming Brian–Hales'/Levich's correlations. $m_{b,0} = 5.0 \times 10^{-7}$ kg, X = 0.0.

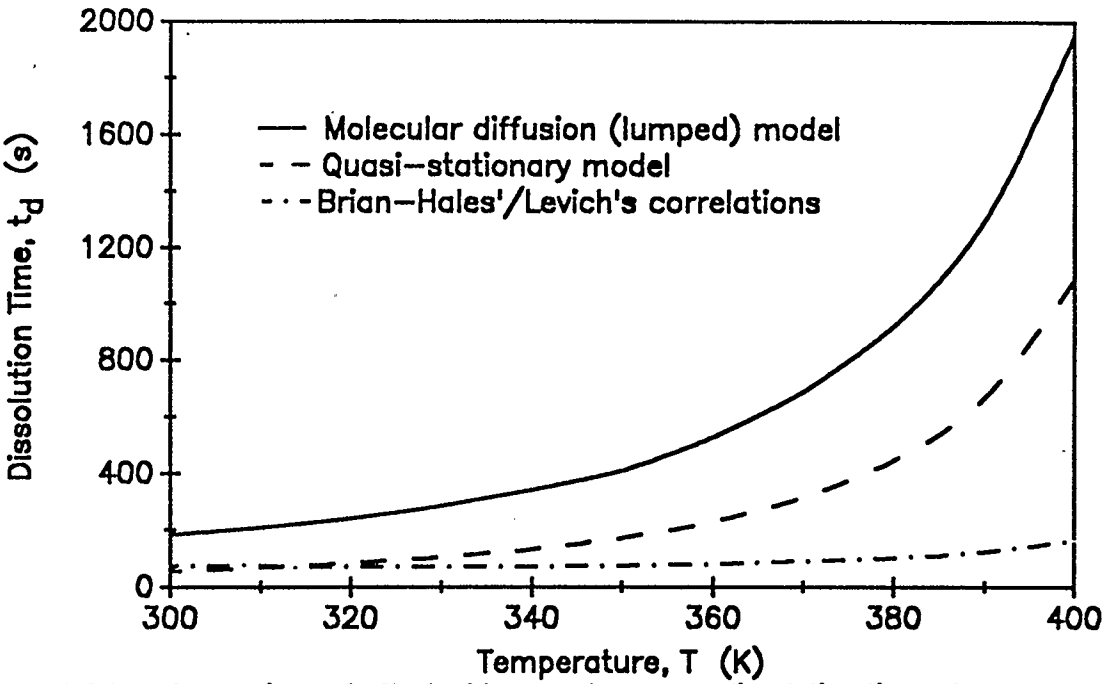

Figure 4.5.6 Comparison of effect of temperature upon dissolution time of a CO_2 bubble under alternative dissolution models. $m_{b,0} = 5.0 \times 10^{-7}$ kg P = 4.0 MPa, X = 0.0.

350 to 400 K in the case of the static bubble modeled by the lumped approach increases the dissolution time by 375 % (410 s to 1951 s), while the dissolution time for the rising bubble modeled utilizing Brian-Hales'/Levich's correlations increased over the same temperature range by only 117 % (75 s to 163 s).

Reduced CO_2 solubility/diffusivity at elevated temperatures is responsible for reducing the effect of molecular diffusivity and hence extending the dissolution time of the static bubble. In the case of the rising bubble, however, the lower bitumen viscosity at the increased temperatures (Section 2.7) results in increased bubble velocities/convective diffusion effects, partially offsetting the reduction in molecular diffusivity. Of note, however, is where convective effects are minimal (at lower temperatures where high bitumen viscosity results in a relatively static bubble) the quasi-stationary approximation results for dissolution time are extremely close to the results obtained from the Brian-Hales/Levich correlations.

The rise height (z_d) for complete bubble dissolution as a function of temperature is shown graphically as Figure 4.5.7. The bubble height increases gradually up to approximately 350 K, as convective effects compensate for reduced diffusivity. Above 350 K, however, the bubble height increases significantly, corresponding to the dramatic increase in time to diffusion and associated reduced bitumen viscosity at

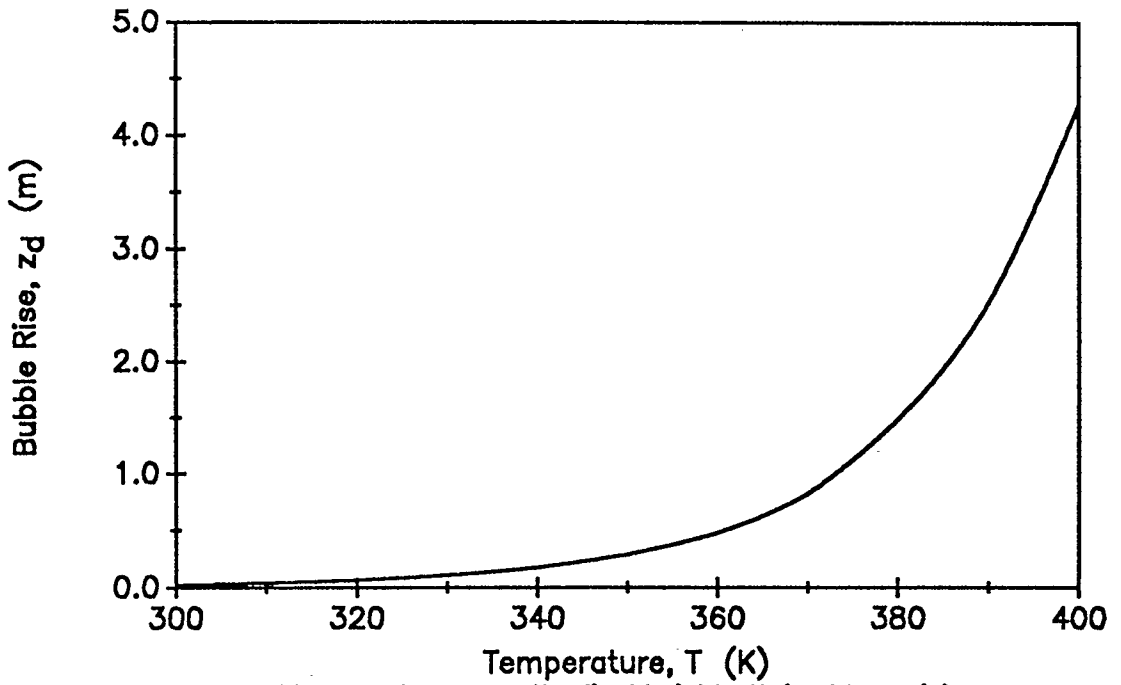

Figure 4.5.7 Effect of temperature upon the final height attained by a rising bubble assuming Brian–Hales'/Levich's correlations. P = 4.0 MPa, $m_{b,0} = 5.0 \times 10^{-7}$ kg, X = 0.0.

elevated temperatures discussed above.

The semi-log plot of the rate of mass transfer from the bubble (Figure 4.5.8) shows a smooth decline corresponding to the reduction of the bubble radius (Figure 4.5.9). The rate of mass transfer shows only a significant decrease when the bubble approaches complete dissolution. Accordingly, the mass flux from the bubble is almost constant throughout the entire dissolution, only increasing dramatically when the bubble radius becomes very small (Figure 4.5.10). The rationale for the end effects has been given previously in Section 4.1.1 and will not be repeated here.

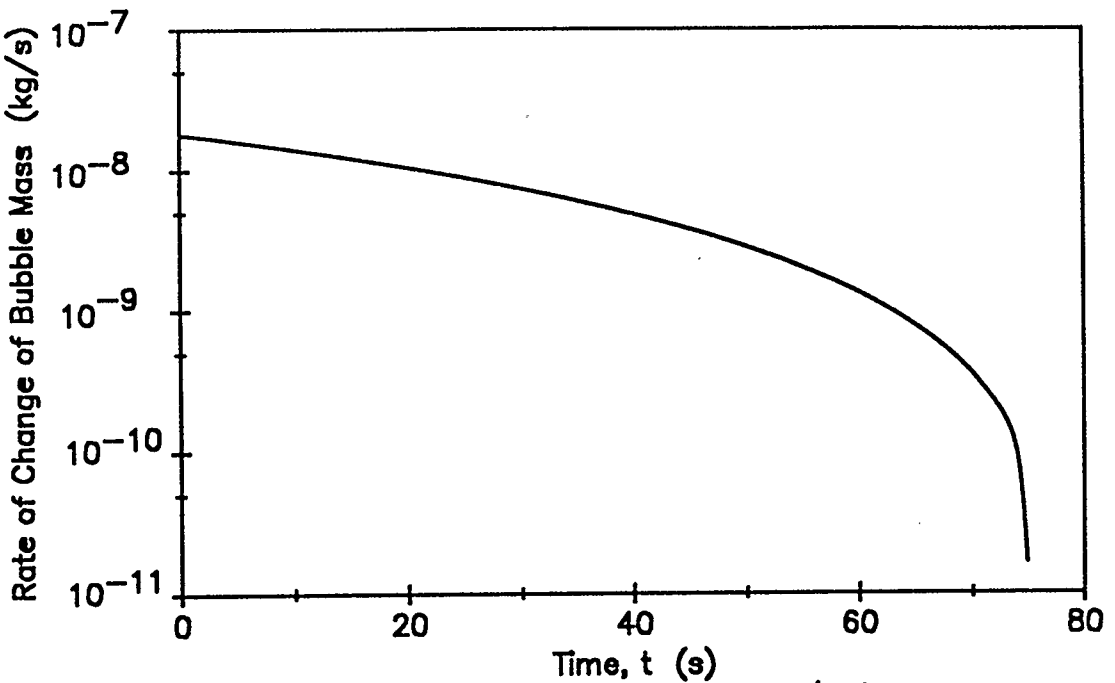

Figure 4.5.8 Rate of change of bubble mass for Brian–Hales'/Levich's model of the dissolution of a CO_2 bubble into a completely sub–saturated bitumen solution. T = 350 K, P = 4.0 MPa.

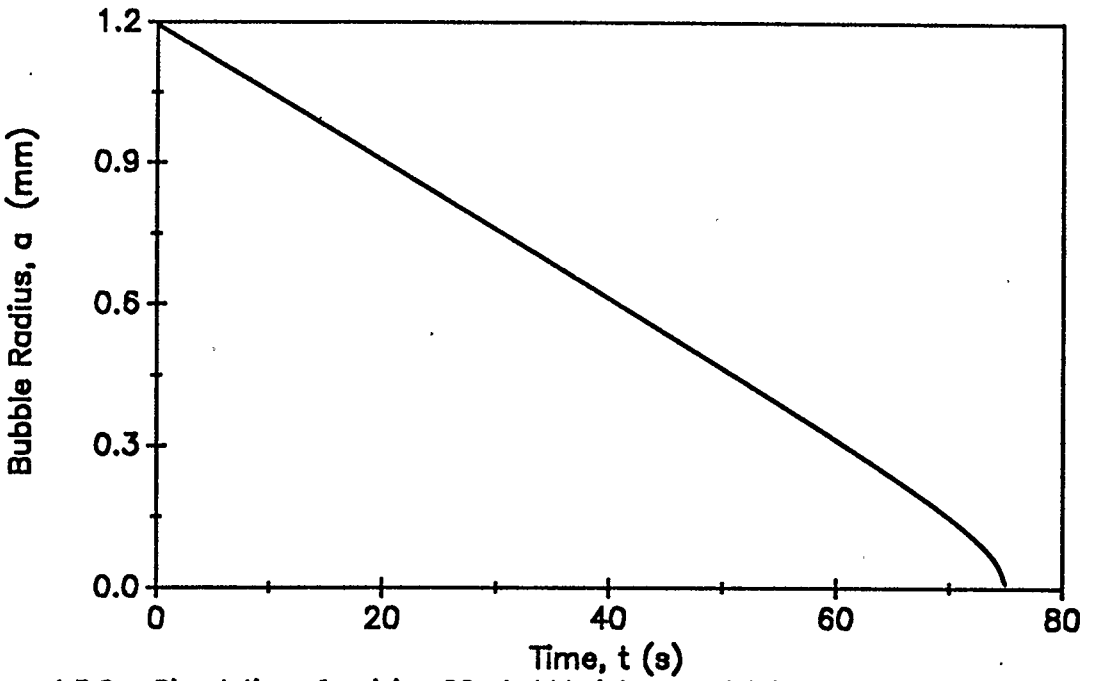

Figure 4.5.9 Dissolution of a rising CO_2 bubble into completely sub-saturated bitumen via Brian-Hales'/Levich's correlations. T = 350 K, P = 4.0 MPa, $m_{b,0} = 5.0 \times 10^{-7}$ kg.

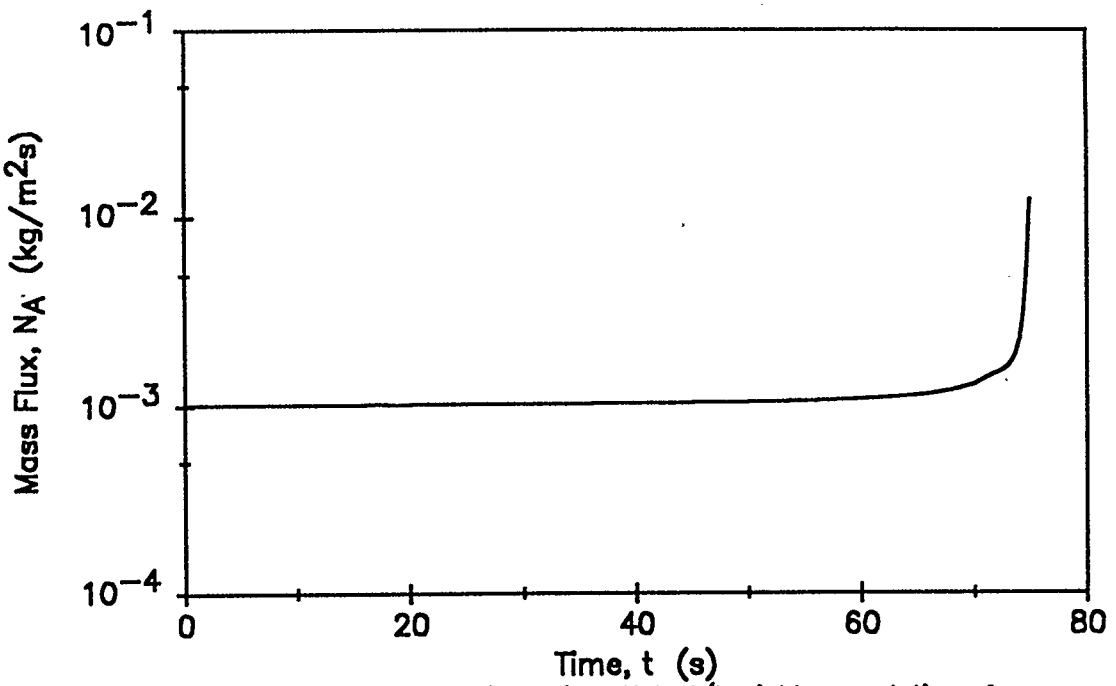

Figure 4.5.10 Mass flux profile assuming Brian–Hales'/Levich's correlations for a rising CO_2 bubble into completely sub–saturated bitumen.
P = 4.0 MPa, T = 350 K, $m_{b,0} = 5.0 \times 10^{-7}$ kg.

4.6 Higbie's Penetration Theory

The second model to be applied to the study of the dissolution of a rising bubble was Higbie's penetration theory. As discussed in Section 2.4, this model assumes that the CO_2 will penetrate only a short distance into a deep packet of liquid bitumen which is sliding along the bubble surface. Higbie's penetration theory assumes the rate of mass transfer to have less dependence upon diffusivity (mass transfer rate varies with the square root of diffusivity - Equation 3.4.3) than the static models (mass transfer rate proportional to diffusivity - Equations 3.1.4 and 3.2.4) or Brian-Hales'/Levich's correlations for the rising bubble (mass transfer rate ranges between proportional to diffusivity to varying with 2/3 power dependent upon Pe_{AB} - Equation 3.3.3). Accordingly, it would be anticipated that the results from the penetration theory would be less influenced by system temperature and pressure related variations in mass solubility and D_{AB} than the other dissolution models.

Results of dissolution time and bubble height for the dissolution of a rising CO_2 bubble ($m_{b,0}$ = 5.0 x 10^{-7} kg) into a completely sub-saturated CO_2-Athabasca bitumen solution, over the same range of system properties (T and P) considered in the analysis of the static bubble, are included as Table 4.6.1. Dissolution times varied from a low of 23 s (at

Table 4.6.1.

Higbie's Penetration Theory Model Dissolution of a Rising CO_2 Bubble Into a Completely Sub-Saturated CO_2-Athabasca Bitumen Solution, Considering Constant Initial Bubble Mass

Model Conditions - $m_{b,0} = 5.0 \times 10^{-7}$ kg, $X = 0.0$

T (K)	P_s (MPa)	t_d (s)	z_d (m)
300	1.0	372.6	0.018
350	1.0	104.4	0.300
400	1.0	106.2	3.280
300	2.0	173.8	0.012
350	2.0	62.8	0.140
400	2.0	68.5	1.530
300	4.0	67.0	0.011
350	4.0	33.8	0.080
400	4.0	42.2	0.700
300	6.0	38.5	0.014
350	6.0	22.7	0.063
400	6.0	31.0	0.440

conditions of T = 350 K and P = 6.0 MPa) to a high of 373 s (at conditions of T = 300 K and P = 1.0 MPa).

Typical dissolution curves (T = 350 K, P = 4.0 MPa), showing bubble radius and mass declines for both rising bubble models, are shown as Figures 4.6.1 and 4.6.2 respectively. The bubble radius predicted from Higbie's penetration theory shows an extremely smooth, constantly decreasing rate of decline throughout all phases of the bubble life, contrasting with the Brian-Hales/Levich model which predicts a constantly increasing rate of decline of the bubble radius, with a significant reduction in radius as the bubble approaches the point of complete dissolution.

Bubble radius decline curves for both static and rising models are given as Figure 4.6.3. Of note is the significant difference in predicted bubble dissolution times depending upon the model selected.

It is probable that a realistic estimate for bubble dissolution is bounded between the Brian-Hales/Levich correlations based model predictions (rising bubble) and the Quasi-Stationary model predictions (static bubble). While it is apparent that the dissolution time predictions from the static models will be somewhat conservative, primarily due to convective effects not being considered, it is probable that

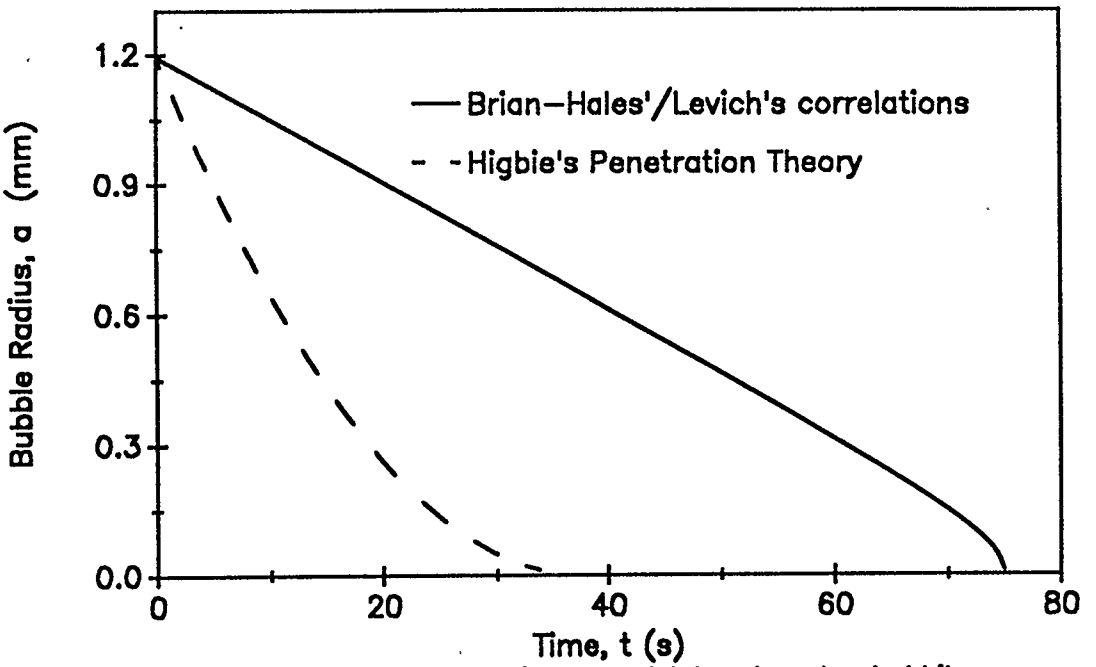

Figure 4.6.1 Dissolution of a CO_2 bubble into completely sub–saturated bitumen using alternative models. T = 350 K, P = 4.0 MPa, $m_{b,0} = 5.0 \times 10^{-7}$ kg

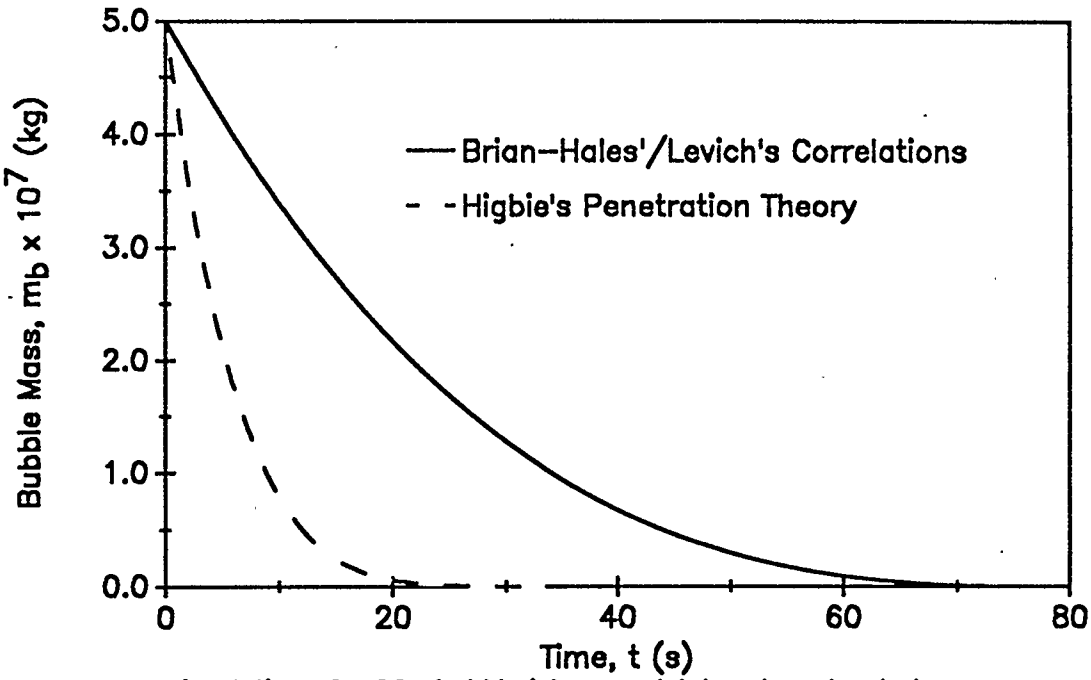

Figure 4.6.2 Dissolution of a CO_2 bubble into completely sub–saturated bitumen using alternative models. T = 350 K, P = 4.0 MPa.

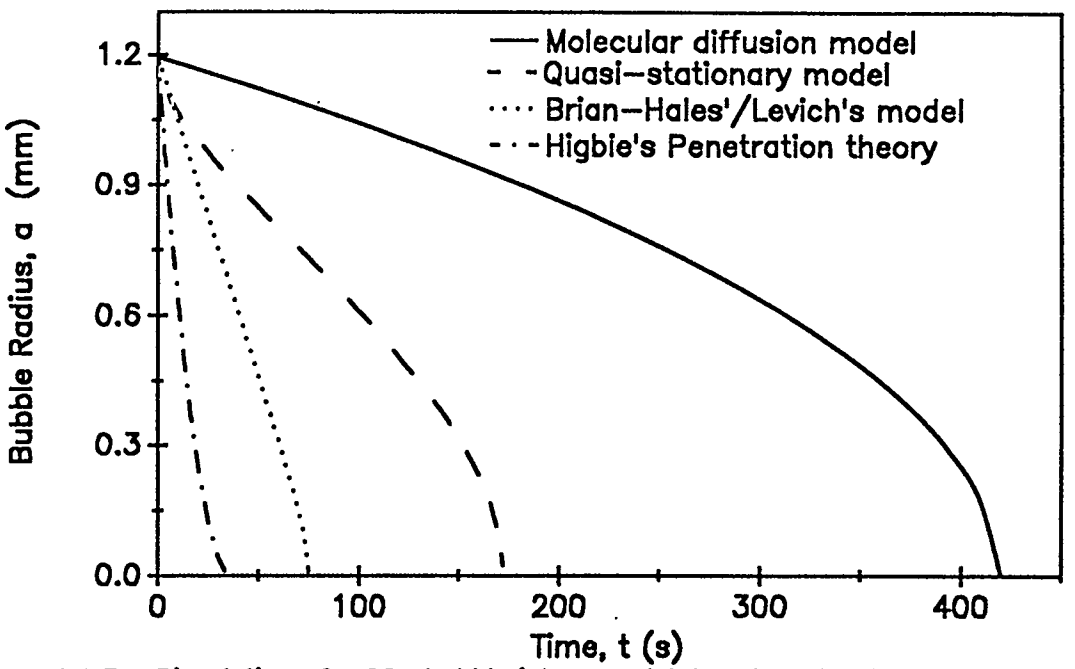

Figure 4.6.3 Dissolution of a CO_2 bubble into completely sub–saturated bitumen using alternative models. T = 350 K, P = 4.0 MPa, $m_{b,0} = 5.0 \times 10^{-7}$ kg.

the rising bubble models provide somewhat optimistic dissolution times due to certain model assumptions. Those model assumptions which lead to the prediction of more rapid bubble dissolution include:

- equilibrium conditions at the bubble interface (resulting in higher assumed gas concentration gradients at the bubble surface),
- solution mass diffusivity based upon interface conditions and assumed constant throughout the solution (as discussed in Section 4.3.1, these assumptions result in an over-estimate of diffusivity in the solution, where x_g is lower than at the bubble interface), and
- solution viscosity based upon interface conditions and assumed constant throughout the solution (these assumptions result in an under-estimate of viscosity away from the bubble interface, resulting in an over-estimate of convective diffusion effects).

The Quasi-Stationary model is suggested as the upper bound on the basis of providing comparable results to the more complex complete set of partial differential equations (Section 2.1). The Brian-Hales/Levich correlations based model is suggested as the lower bound, rather than Higbie's penetration theory model, as of the two, the Brian-Hales/Levich model provides the more conservative (slower) estimate of bubble dissolution.

Higbie's model predicts that, at a given temperature (Figure 4.6.4), increasing the system pressure decreases the bubble dissolution time. The effect of pressure upon the dissolution of the CO_2 bubble, for both rising bubble models, is displayed graphically as Figure 4.6.5. In part due to mass diffusivity effects, it is not surprising that the penetration theory is less affected by variations in system pressure than the Brian-Hales/Levich correlations.

Interpretation of the equations describing mass transfer from the rising bubble as predicted by the Brian-Hales/Levich correlations and Higbie's penetration theory model (Equations 3.3.3 and 3.4.3 respectively) shows that in addition to having a reduced dependence upon mass diffusivity, comparatively the penetration model has a relatively increased dependence upon bubble velocity. The rate of mass transfer of the Brian-Hales/Levich correlations varies approximately with the 1/3 power of velocity, while in the penetration theory it varies with the 1/2 power.

As discussed in Section 2.7 and shown in Table 4.3.1, accompanying an increase in system pressure and mass solubility is a reduction of bitumen viscosity. While the effect of system pressure upon solution viscosity is not as dramatic as temperature effects, it is still significant and in part explains the faster bubble dissolutions predicted by

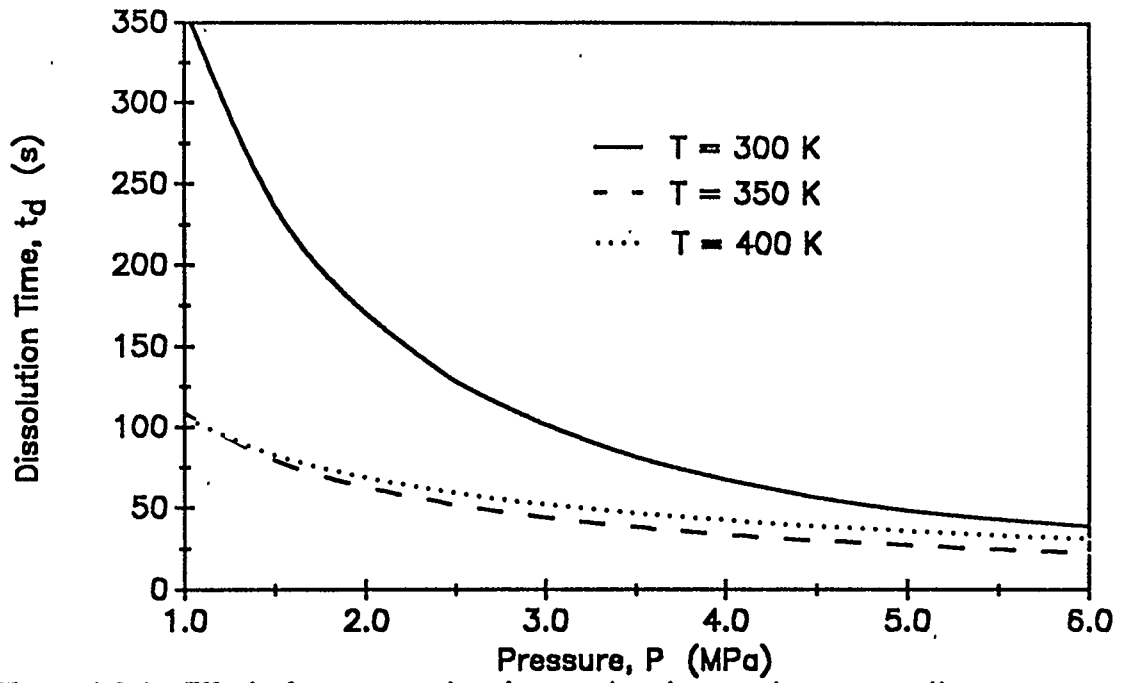

Figure 4.6.4 Effect of pressure, at various system temperatures, upon the dissolution of a rising CO_2 bubble into bitumen assuming Higbie's Penetration Theory model. $m_{b,0} = 5.0 \times 10^{-7}$ kg. X = 0.0.

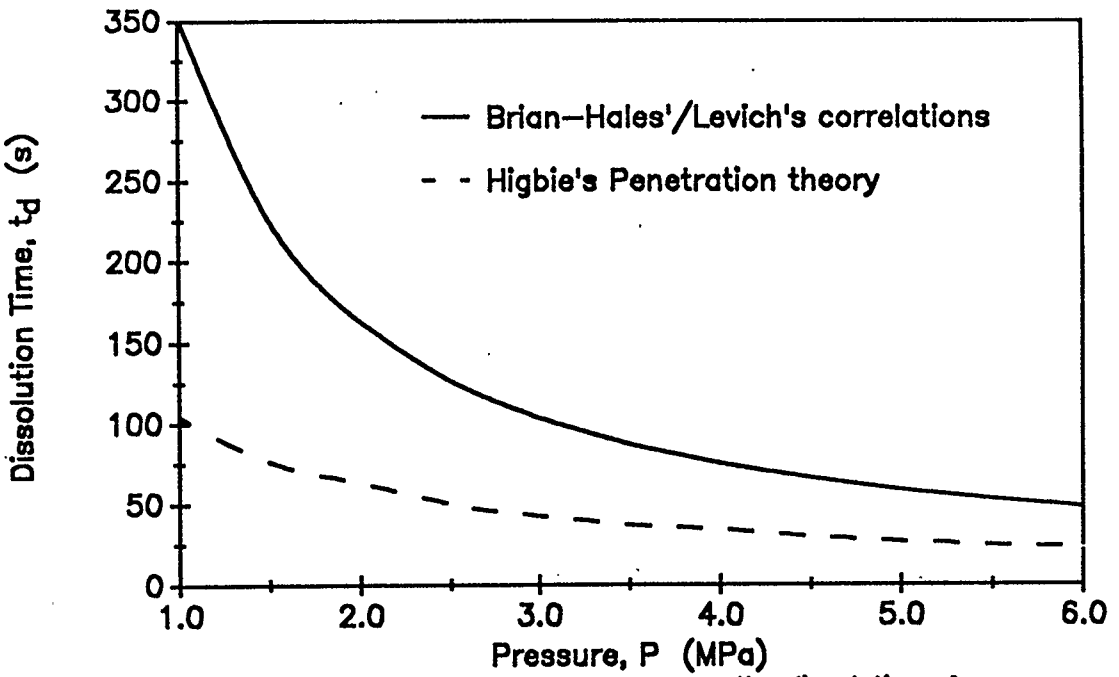

Figure 4.6.5 Comparison of the effect of pressure upon the dissolution of a rising CO_2 bubble under alternate dissolution models. $m_{b,0} = 5.0 \times 10^{-7}$ kg, T = 350 K, X = 0.0.

the penetration theory as compared to Brian-Hales/Levich correlations.

The effect of system pressure upon both static and rising bubbles is presented in Figure 4.6.6. As discussed previously, sensitivity to mass diffusivity (molecular diffusion) and the influence of convective diffusion effects explain the differences in dissolution times shown between static and rising bubbles.

In a similar manner to the model results using the Brian-Hales'/Levich correlations, Higbie's model predicts that, for a given system pressure, a minimum bubble dissolution time is realized at a mid-range temperature (Figure 4.6.7). Dissolution times predicted by Higbie's penetration theory are strongly influenced by temperature at the lower end of the temperature range under consideration, especially at lower system pressures. Conversely dissolution times predicted by Brian-Hales'/Levich's correlations are more influenced by changes in temperature at the upper end of the temperature range under consideration (Figure 4.6.8). This difference suggests that Higbie's penetration theory has a greater dependence upon convective diffusion effects, while dissolution predictions by Brian-Hales'/Levich's correlations are more dependent upon molecular diffusion.

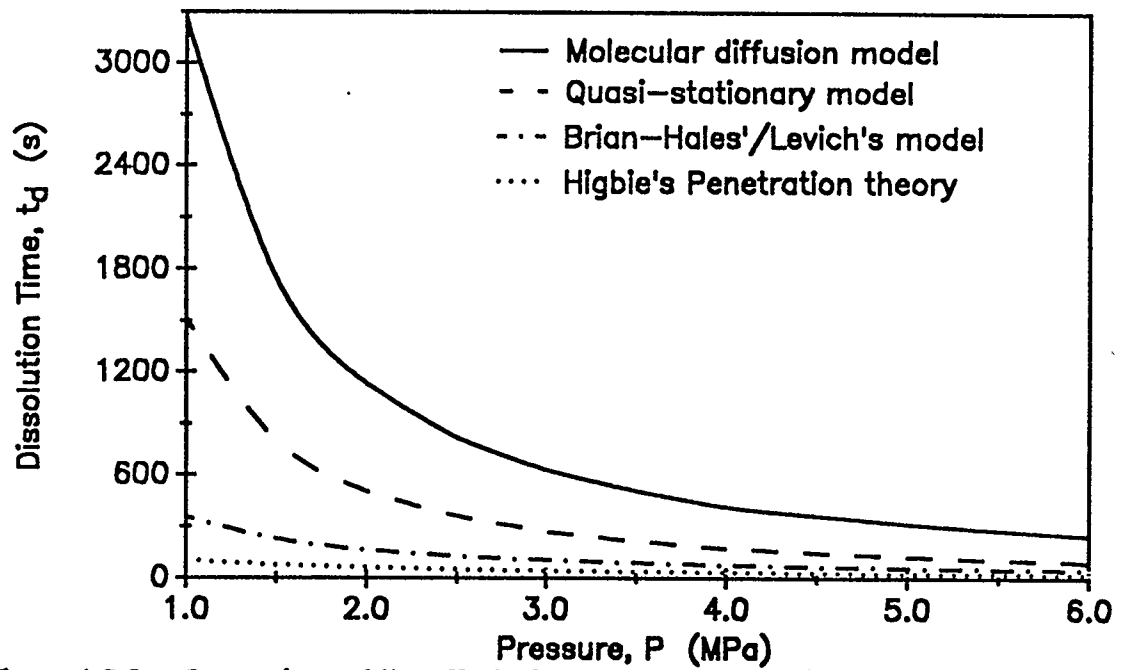

Figure 4.6.6 Comparison of the effect of pressure upon the dissolution of a CO_2 bubble under alternative dissolution models.
$m_{b,0} = 5.0 \times 10^{-7}$kg, T = 350 K, X = 0.0.

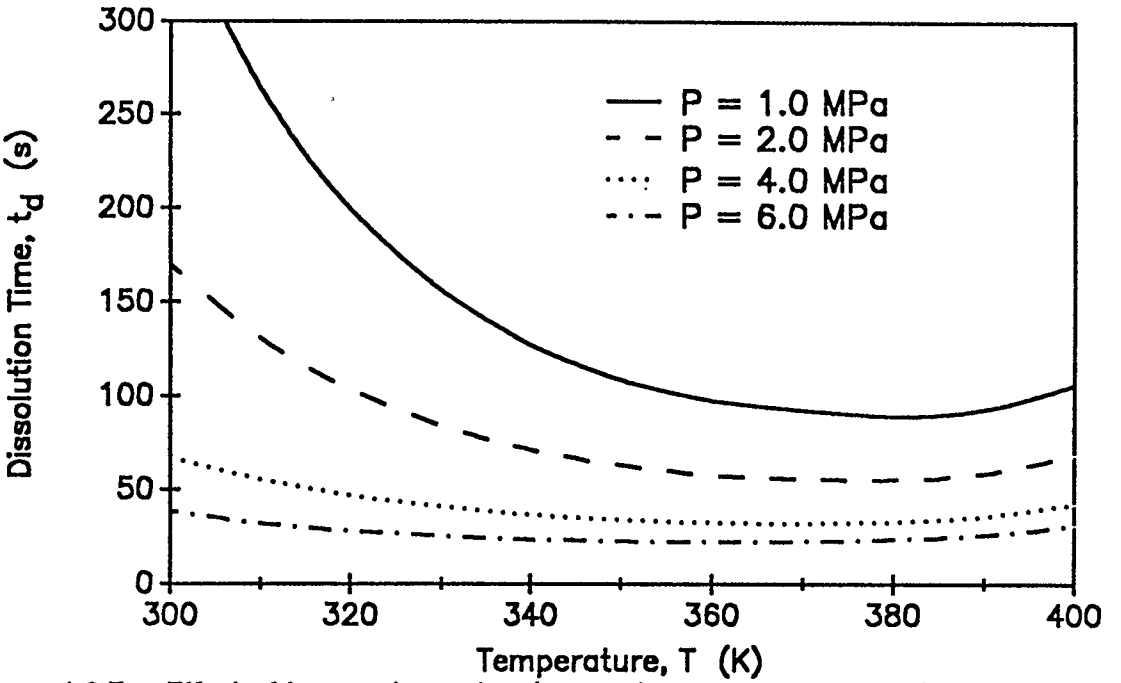

Figure 4.6.7 Effect of temperature, at various system pressures, upon the dissolution of a rising CO_2 bubble assuming Higbie's Penetration Theory. $m_{b,0} = 5.0 \times 10^{-7}$ kg, X = 0.0

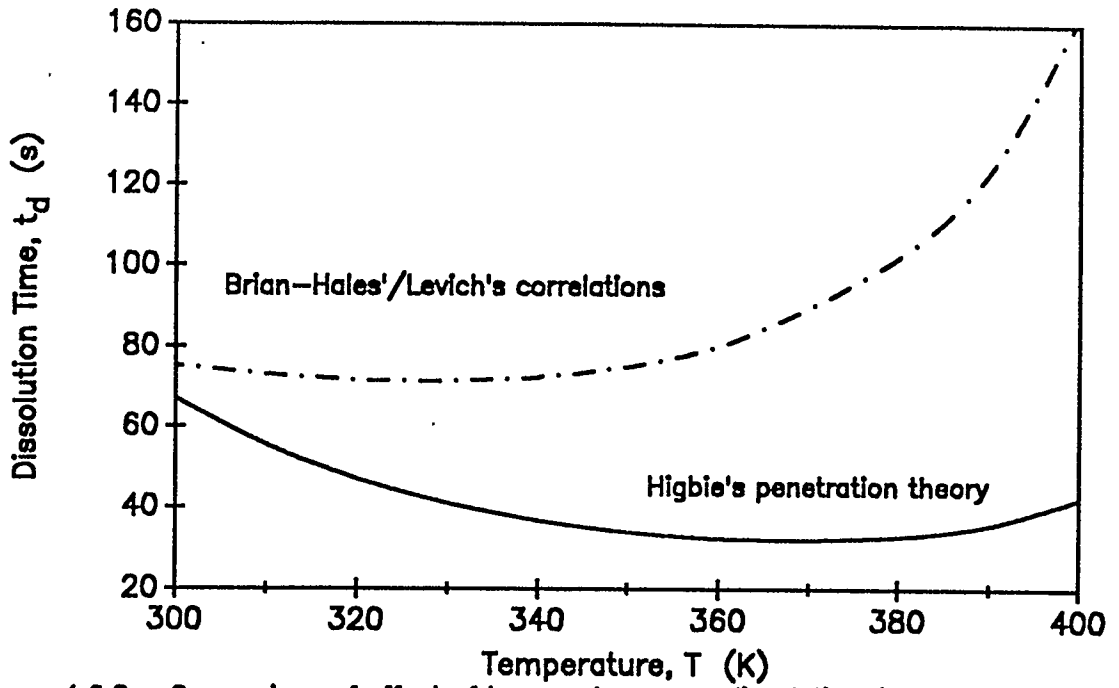

Figure 4.6.8 Comparison of effect of temperature upon dissolution time of a rising CO_2 bubble for different dissolution models.
P = 4.0 MPa, $m_{b,0} = 5.0 \times 10^{-7}$ kg.

For the cases under consideration (completely sub-saturated bitumen, pressure varied between 1.0 to 6.0 MPa), the minimum dissolution time ranged between T = 350 K (at P = 6.0 MPa) to T = 380 K (at P = 1.0 MPa). At temperatures away from the temperature for the minimum dissolution time, the decrease in the combined influence of molecular diffusion effects and convective diffusion effects results in an increased bubbledissolution time.

The effect of system temperature upon both static and rising bubbles is presented in Figure 4.6.9. Where convective influences are minimal (at low system temperatures where solution viscosities are high/bubble velocities low) the difference between predicted dissolution times between the rising bubble models (Brian and Hales' correlations and Higbie's penetration theory) and the quasi-stationary model for a static bubble are minimal.

The final bubble height (z_d) as a function of temperature, for both Brian-Hales/Levich correlation models and Higbie's penetration theory model, are presented in Figure 4.6.10. The greater bubble heights at dissolution predicted by the Brian-Hales/Levich correlations reflect the predicted slower dissolution times.

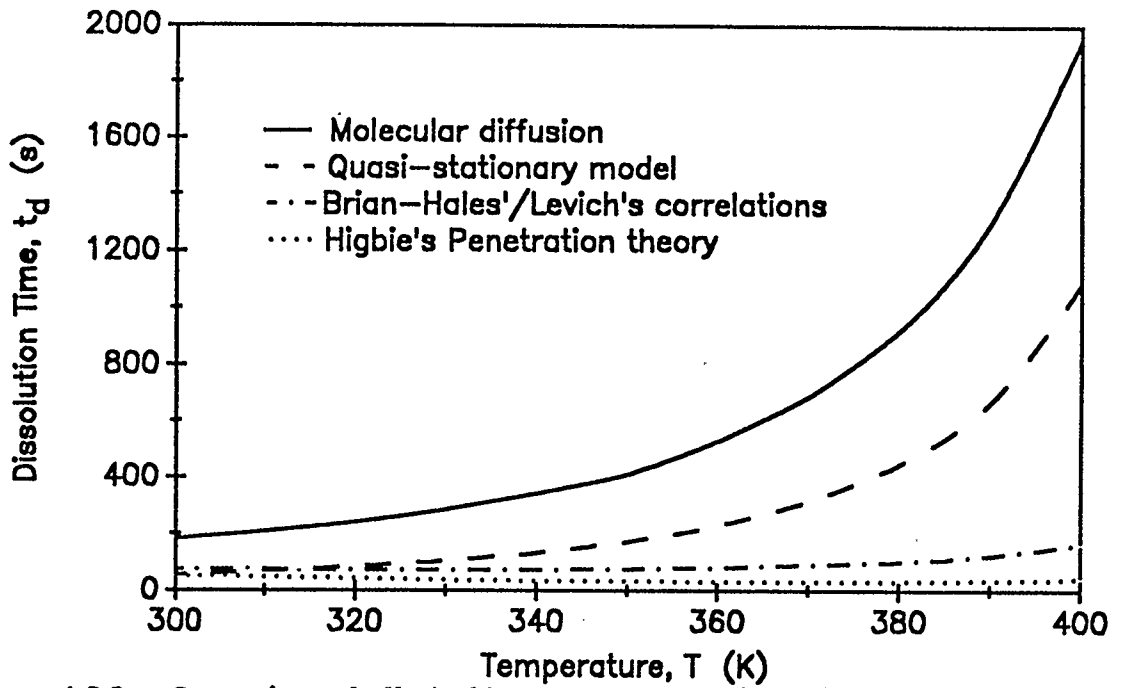

Figure 4.6.9 Comparison of effect of temperature upon dissolution time of a CO_2 bubble under alternative dissolution models. $m_{b,0} = 5.0 \times 10^{-7}$ kg P = 4.0 MPa, X = 0.0.

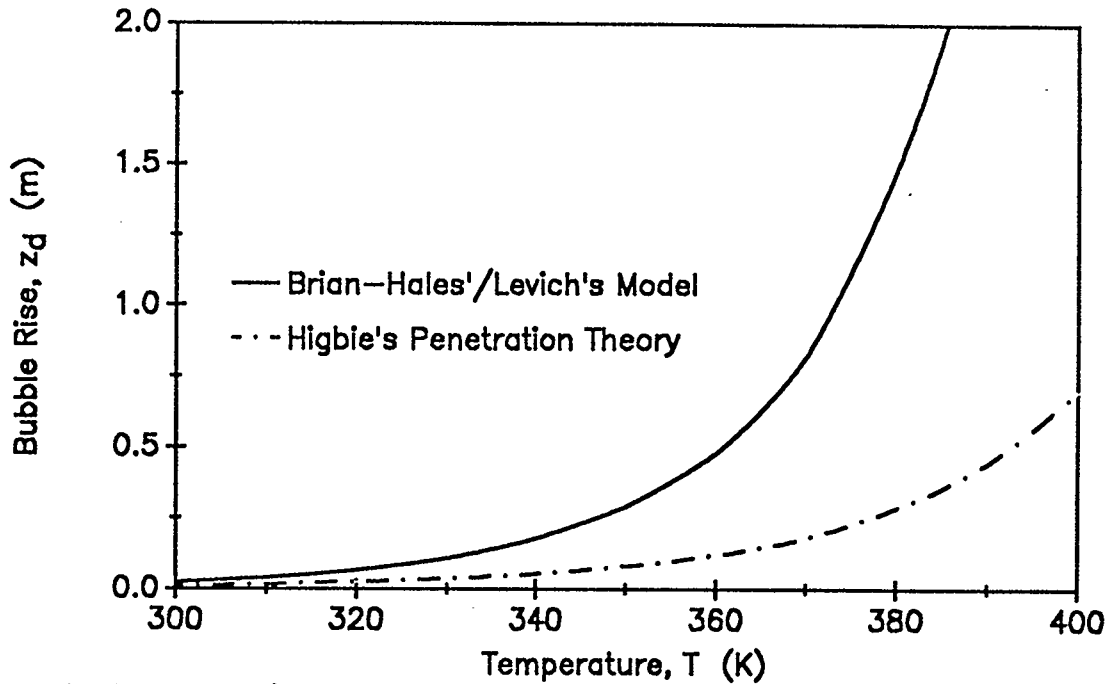

Figure 4.6.10 Comparison of effect of temperature upon the final height attained by a rising bubble under different dissolution models.
P = 4.0 MPa, $m_{b,0} = 5.0 \times 10^{-7}$ kg, X = 0.0.

The semi-log plots showing the rate of change of bubble mass and mass flux versus time (Figures 4.6.11 through 4.6.14) confirm the observations that, as compared to the quasi-stationary and lumped models for a static bubble and the Brian-Hales/Levich correlations for a rising bubble, the penetration model predicts a more rapid, smooth bubble dissolution process with no significant early-time or end-point effects.

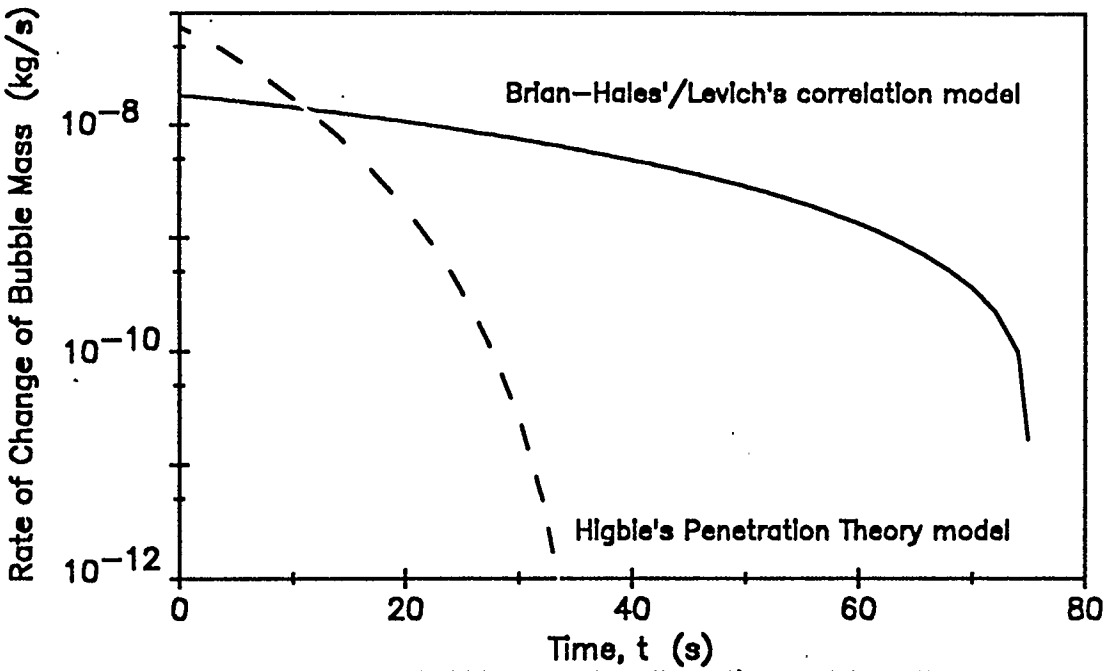

Figure 4.6.11 Rate of change of bubble mass for alternative models of the dissolution of a CO_2 bubble into a completely sub–saturated bitumen solution. T = 350 K, P = 4.0 MPa, $m_{b,0} = 5.0 \times 10^{-7}$ kg.

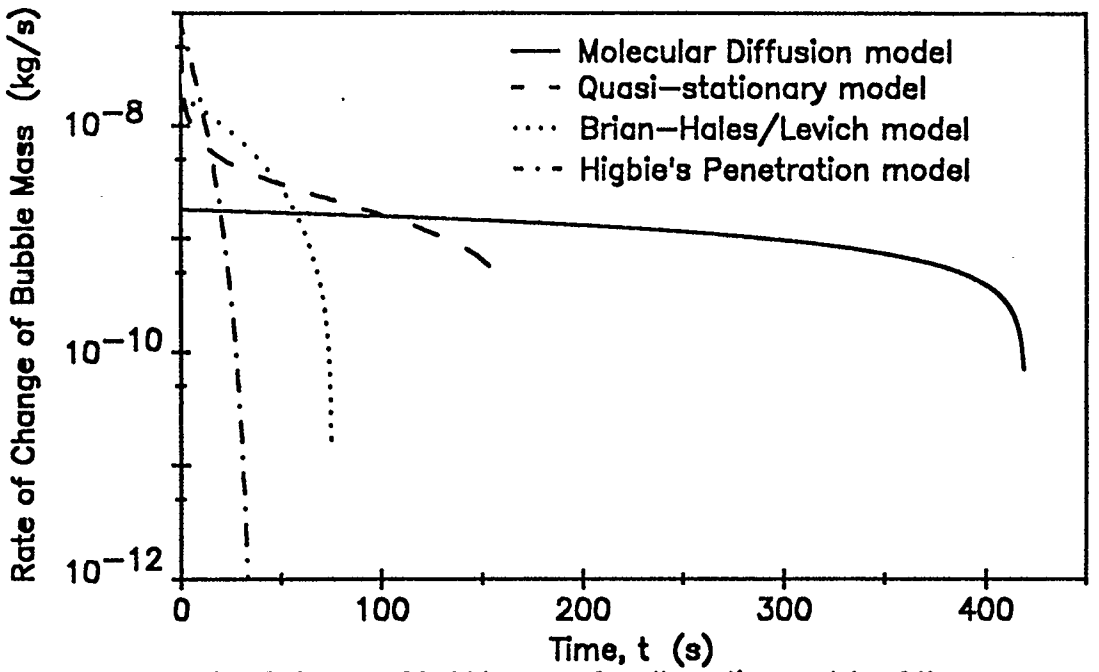

Figure 4.6.12 Rate of change of bubble mass for alternative models of the dissolution of a CO_2 bubble into a completely sub–saturated bitumen solution. T = 350 K, P = 4.0 MPa, $m_{b,0} = 5.0 \times 10^{-7}$ kg.

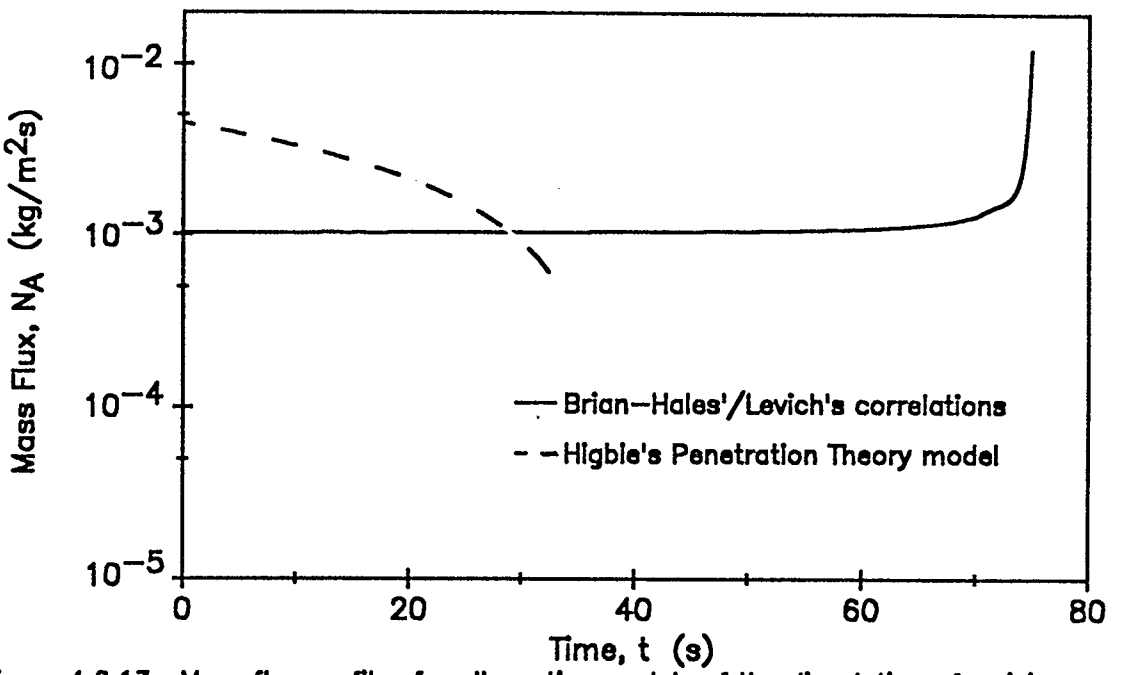

Figure 4.6.13 Mass flux profiles for alternative models of the dissolution of a rising CO_2 bubble into completely sub-saturated bitumen. T = 350 K, P = 4.0 MPa, X = 0.0.

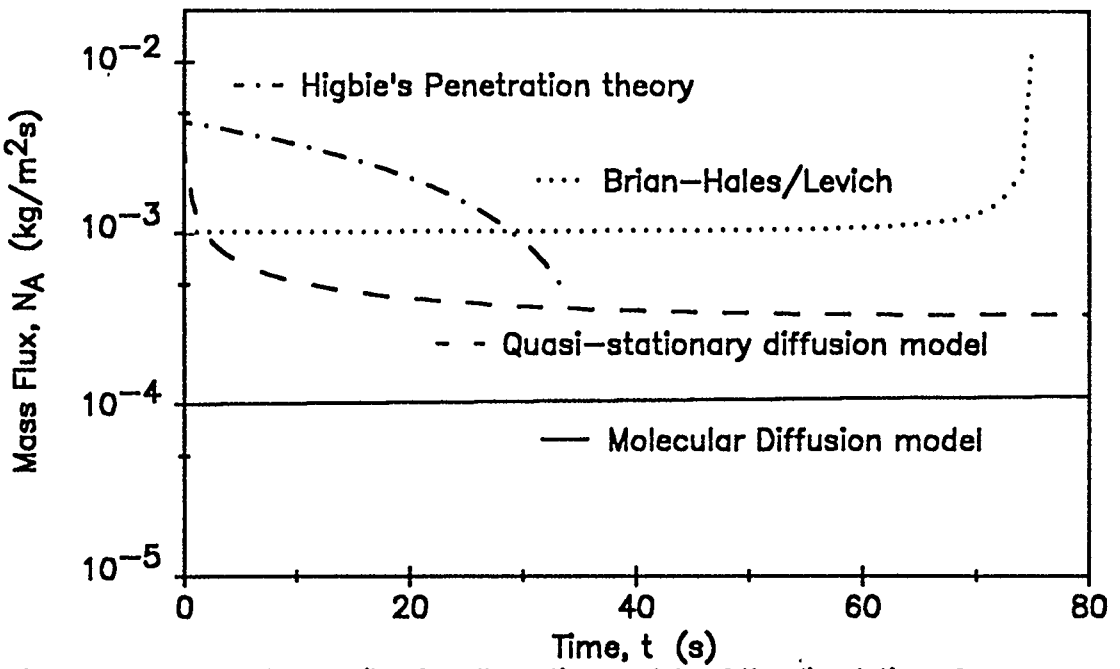

Fig. 4.6.14 Mass flux profiles for alternative models of the dissolution of a CO_2 bubble into completely sub–saturated bitumen. T = 350 K, P = 4.0 MPa., $m_{b,0} = 5.0 \times 10^{-7}$ kg.

CONCLUSIONS AND RECOMMENDATIONS

Models for the dissolution of static and rising bubbles are presented. The models are applied to the problem of dissolution of a single bubble of CO_2 into a solution of Athabasca bitumen. The effects of variation in system conditions (including temperature and pressure) upon model results are evaluated.

Models applied to the dissolution of a static bubble included the more rigorous, analytically based, quasi-stationary model (an approach used successfully in the modelling of the dissolution of O_2 and CO_2 bubbles into glass melts) and the simpler, lumped approach, molecular diffusion model. It was determined that, over the range of temperature and pressures considered, the dissolution times predicted by the quasi-stationary model were lower than the dissolution times predicted by the molecular diffusion model, typically by a factor of approximately 2.

The solubility and mass diffusivity of CO_2 in bitumen are higher at low temperatures and high pressures. As would be anticipated by application of Fick's law, both the quasi-stationary and lumped molecular diffusion models predicted that the dissolution of a static bubble is enhanced by low system temperatures and high system pressures.

It was found that under the conditions considered, surface tension had minimal influence upon dissolution results. Additionally, it was demonstrated that under given CO_2-bitumen solution conditions, the reduced time to bubble dissolution predicted by the quasi-stationary model was constant for bubbles of different initial radius/mass, simplifying the predictions of results of other bubble dissolution cases.

The models based upon Brian-Hales'/Levich's correlations and Higbie's penetration theory were applied to the dissolution of a rising bubble of CO_2 into Athabasca bitumen. The dissolution of the rising bubble reflects the influence of both molecular and convective diffusion effects.

Where convective effects are insignificant (i.e. at low system temperatures), it was found that both of the rising bubble models predicted dissolution times lower than the molecular diffusion model and dissolution times comparable to the quasi-stationary model. Where convective effects are significant, both rising bubble models predicted smaller dissolution times than the static bubble models.

It is probable that a realistic estimate for bubble dissolution is bounded between the Brian-Hales/Levich correlations based model predictions (rising bubble) and the Quasi-Stationary model predictions (static bubble). While it

is apparent that the dissolution time predictions from the static models will be somewhat conservative, primarily due to convective effects not being considered, it is probable that the rising bubble models provide optimistic dissolution times due to model assumptions pertaining to both solution mass diffusivity and solution viscosity. Further investigation / experimental work into the dissolution of CO_2 bubbles into bitumen would be beneficial in providing guidance as to which model provides the most appropriate predictions of bubble dissolution.

Since increases in system temperature and pressure cause a reduction in bitumen viscosity, their overall effect is to enhance convective diffusion. Additionally, an increase in system temperature reduces CO_2 solubility and mass diffusivity, thereby decreasing molecular diffusion. It was demonstrated that the combination of both molecular and convective diffusion effects resulted in the minimum dissolution times being achieved at a temperature which falls in the middle of the temperature range under consideration. That is, there exists a minimum in the dissolution time with respect to temperature.

The relative importance of convective and molecular diffusion effects to each of the rising bubble models, resulted in differences between the model predictions of both the

relationship between system temperature and bubble dissolution time and also the associated minimum dissolution temperatures. It was shown that the model based upon Higbie's Penetration theory has a greater dependence upon convective diffusion effects and a lesser dependence upon molecular diffusion effects than the model based upon the Brian-Hales'/Levich's correlations.

REFERENCES

Advanced Continuous Simulation Language (ACSL) Reference Manual, 4th edn., Mitchell and Gauthier Associates, Concord Mass. (1986).

BIRD, R.B., W.E. STEWART and E.N. LIGHTFOOT, Transport Phenomena, John Wiley and Sons (1960).

BOWMAN, C.W., Molecular and Interfacial Properties of Athabasca Tar Sands, 7th World Petroleum Congress, Mexico (1967).

BRIAN, P.L.T. and HALES, H.B., American Institute of Chemical Engineering Journal, 15, pp.419 (1969).

CARSLAW, H.S. and J.C. JAEGER, Conduction of Heat In Solids , 2nd edn., Clarendon Press, Oxford (1959).

CHEN, Y.W. and P.J. WANG, Dissolution of Spherical Solid Particles in a Stagnant Fluid: an Analytical Solution, *Canadian Journal of Chemical Engineering, 67 (10), pp. 870-872 (1989).*

EPSTEIN, P.S. and M.S. PLESSET, On the Stability of Gas Bubbles in Liquid- Gas Solutions, *Journal of Chemistry and Physics, 18 (11), pp. 1505-1509 (1950).*

HASTINGS, C., Approximations for Digital Computers, Princeton University Press, Princeton (1955)

HEPLER, L.G. and C. HSI, AOSTRA Technical Handbook on Oil Sands, Bitumens and Heavy Oils, Alberta Oil Sands Techn ology and Research Authority, Edmonton (1989).

ISAACS, E.E. and K.F. SMOLEK, Interfacial Tension Behaviour of Athabasca Bitumen/Aqueous Surfactant Systems, *Canadian Journal of Chemical Engineering, 61 (2), pp. 233-240 (1983).*

LEVICH, V.G., Physicochemical Hydrodynamics, Prentice-Hall (1962).

MEHROTRA, A.K. and W.Y. SVRCEK, Correlations for Properties of Bitumen Saturated With CO_2, CH_4 and N_2, and Experiments With Combustion Gas Mixtures, *Journal of Canadian Petroleum Technology, 21 (6), pp. 95-104 (1982).*

MEHROTRA, A.K., A. GARG and W.Y. SVRCEK, Prediction of Mass Diffusivity of CO_2 into Bitumen, *Canadian Journal of Chemical Engineering, 65 (10), pp. 826-832 (1987).*

MEHROTRA, A.K., C.T. YEE and W.Y. SVRCEK, Prediction of Surface Tension of Athabasca Bitumen, *Canadian Journal of Chemical Engineering, 63 (4), pp. 340-343 (1985).*

PERRY, R.H., Perry's Chemical Engineers' Handbook, 6th edn., McGraw-Hill (1984).

READEY, D.W. and A.R. COOPER, Molecular Diffusion With a Moving Boundary and Spherical Symmetry, *Chemical Engineering Science, 21, pp. 917-922 (1966).*

SCHMIDT, T., T.H. LESHCHYSHYN and V.R. PUTTAGUNTA, Diffusivity of Carbon Dioxide into Athabasca Bitumen, *Petroleum Society of CIM, Paper No. 82-33-100 (1982).*

SVRCEK, W.Y. and A.K. MEHROTRA, Gas Solubility, Viscosity and Density Measurements for Athabasca Bitumen, *Journal of Canadian Petroleum Technology, 21 (4), pp. 31-38 (1982).*

WALAS, S.M., Phase Equilibria In Chemical Engineering, Butterworth Publishers (1985).

WEINBERG, M.C., P.I.K. ONORATO and D.R. UHLMANN, Behaviour of Bubbles in Glassmelts: I, Dissolution of a Stationary Bubble Containing a Single Gas, *Journal of the American Ceramic Society, 63 (3-4), pp.175-180 (1980).*

WEINBERG, M.C., Surface Tension Effects in Gas Bubble Dissolution and Growth, *Chemical Engineering Science, 36, pp. 137-141 (1981).*

WELTY, J.R., C.E. WICKS and R.E. WILSON, Fundamentals of Momentum, Heat and Mass Transfer, 3rd edn., John Wiley and Sons (1983).

WYLIE, C.R. and L.C.BARRETT, Advanced Engineering Mathematics, 5th edn., McGraw Hill (1982).

LIST OF APPENDICES

Appendix A

Quasi-Stationary Dissolution Model of an O_2 Bubble Into a Glass Melt - ACSL Source Code - Diffus1.

```
program DIFFUS1
" Quasi-stationary dissolution of gas bubbles into a glass melt. ...
The equation to be integrated drawn from Weinberg pp 138 eqn 12...
Results will be compared to Weinbergs results for x=0.9349"

"    Description of variables which are a function of time            "
"    at - actual bubble radius (m)"
"    t  - actual time (s)"
"    cr - reduced concentration - (c-csi)/(cgi-csi) (dimensionless)"
"    y  - reduced radius - r/a0 (dimensionless)"

 initial

   integer ct
   constant ct = 1
   constant k1 = 3.074          $"k1 = K*Rg*T"
   constant k2 = 5.923e-3       $"k2 = (2*st)/(P0*aic)"
   constant x = 0.9349          $"undersaturation parameter"
   constant diffc = 5.0e-10     $"oxygen m**2/s"
   constant stc = 0.3           $"surface tension (N/m) = 300 dynes/cm"
   constant g = 1.0             $"starting reduced bubble radius"
   variable tr = 1.0e-05        $"reduced time"
   constant pi = 3.14159
   constant gic  = 1.0          $"initial reduced bubble radius  "
   constant tstop = 1.5         $"maximum reduced time"
   constant gmin = 0.01         $"minimum reduced bubble radius"
   constant a0 = 1.00e-3        $"initial actual bubble radius (m)"
   constant rg = 8314           $"univ gas const - (kg*m**2/s**2*kmol*K)"
   constant te = 1673           $"temperature (K)"
   constant p0 = 101.3e3        $"system pressure (Pa - N/m**2)"
   constant c1 = 0.3480242      $"erfc constnts for reduced concentration"
   constant c2 = -0.0958798
   constant c3 = 0.7478556

   array cr(20)
   constant cr=20*0.0

 end $"initial"

 dynamic

  derivative diffu4

   algorithm ialg=4             $"Runge Kutta Method - second order"
   cinterval  cint = 0.001


   k5 = 1./(1. - (1./ ( 3. * (1. + g/k2))))
   g=integ(((-k1*(g*(1.0-x)+k2))/(g+k2))*k5*(1/sqrt(pi*tr)+1/g),gic)

   t = tr * (a0**2.) / diffc
   at = g * a0
   pb = p0 + 2*stc/at           $"bubble pressure (Pa)"

  procedural ( cr = g)          $"concentration profile"
   do 12   ct = 1,20
   y = ct/5.0
   if (y.lt.g) goto 11
   k3 = (y-g) / (2*sqrt(tr))
   k4 = 1 / (1 + 0.47047*k3)
   cr(ct) = (g/y) * (c1*k4 + c2*k4**2 + c3*k4**3) * exp(-(k3**2))
   goto 12
```

```
l1..cr(ct) = 1.0
l2..continue
  end $"procedural"

  end $"derivative"
   termt (tr.gt.tstop.or.g.lt.gmin)
 end $"dynamic"
 terminal
 end $"terminal"
end $"program"
```

Appendix B

Quasi-Stationary Dissolution Model of a Static CO_2 Bubble Into Athabasca Bitumen - ACSL Source Code - Diffus2.

```
program DIFFUS2
"    Models the quasi-stationary dissolution of a static CO2 bubble...
     into Athabasca bitumen...
     Description of variables which are a function of time...
     at - actual bubble radius (m)...
     t  - actual time (s)...
     cr - reduced concentration - (c-csic)/(cgi-csic) (dimensionless)...
     y  - reduced radius - r/aic (dimensionless)...
     The user specifies intial bubble mass rather than radius"

 initial
   integer ct
   constant ct=1
   constant tc = 304.2          $" CO2 critical temperature (K)"
   constant pc = 7.37646e6      $" CO2 critical pressure (Pa)"
   constant ac = 0.225          $" CO2 accentric factor"
   constant g = 1.0             $"starting reduced bubble size"
   constant csic = 0.0         $"initial gas concentration in soln - ml/m"
   variable tr = 1.0e-06        $"initial non zero reduced time"
   constant mwg = 44.01         $"molecular wgt gas - CO2 (kg/kmol)"
   constant mwb = 594.6       $"molecular wgt Athabasca bitumen (kg/kmol)"
   constant pi = 3.14159
   constant gic  = 1.0          $"initial reduced bubble size  "
   constant tstop = 1.5         $"maximum reduced time"
   constant gmin = 0.01         $"minimum reduced bubble size"
   constant mbic = 5.00e-7      $"initial actual bubble mass (kg)"
   constant rg = 8314.          $"univ gas const - (kg*m**2/s**2*kmol*K)"
   constant te = 350.           $"temperature (K)"
   constant ps = 1.e6           $"system pressure (Pa - N/m**2)"
   constant b1 = -0.0073508     $"constants for solubility correlation"
   constant b2 = -14.794
   constant b3 = 6428.5
   constant b4 = 4971.39
   constant c1 = 0.3480242     $"erfc constants for reduced concentration"
   constant c2 = -0.0958798
   constant c3 = 0.7478556


   table diff, 2, 6, 9 / ...
       296, 300, 323, 373, 423, 473, ...
       0.0, 0.001, 0.005, 0.01, 0.05, 0.1, 0.2, 0.3, 0.4,...
       2.3e-14, 4.65e-14, 1.08e-12, 6.25e-11, 4.43e-10, 7.92e-10,...
       1.42e-11, 1.45e-11, 1.58e-11, 7.73e-11, 4.57e-10, 8.50e-10,...
       7.07e-11, 7.22e-11, 7.48e-11, 1.36e-10, 5.14e-10, 9.97e-10,...
       1.41e-10, 1.44e-10, 1.48e-10, 2.10e-10, 5.84e-10, 1.21e-9,...
       7.01e-10, 7.15e-10, 7.32e-10, 7.95e-10, 1.15e-9, 1.48e-9,...
       1.39e-9, 1.42e-9, 1.45e-9, 1.51e-9, 1.84e-9, 2.11e-9,...
       2.72e-9, 2.77e-9, 2.83e-9, 2.90e-9, 3.17e-9, 3.58e-9,...
       3.98e-9, 4.06e-9, 4.15e-9, 4.22e-9, 4.43e-9, 4.81e-9,...
       5.17e-9, 5.27e-9, 5.39e-9, 5.46e-9, 5.62e-9, 6.27e-9 /
"diffusivity (m**2/s) Mehrotra et al - Can.J.Ch.E. 87-09 pp 831 "
"Prediction of Mass Diffusivity of CO2 into Bitumen  "
"Athabasca bitumen used in study"
"Correlating diffusivity to temperature and xg "

    table denl, 1, 4 / ...
        297.6, 314.9, 335.9, 369.7, ...
        1041.1, 1015.3, 1005.9, 984.1 /
"Average gas saturated liquid densities (kg/m3) "
"Svrcek and Mehrotra - Gas solubility, viscosity and density "
"measurements for Athabasca bitumen - JCPT 82-07 "
"Correlating gas saturated liquid density to temperature"
```

```
   table st, 1, 4 / ...
       337.1,348.1,377.1,385.1,...
       26.1e-3,25.5e-3,24.13e-3,23.8e-3 /
 "surface tension ( N/m - Pa m - dyne*e-3/cm )"
 "Prediction of Surface Tension of Athabasca Bitumen"
 "Mehrotra, Yee and Svrcek - CJChE 1985-04"
 "Correlating liquid surface tension to temperature"

   pbic = ps

   a = 0.45724*(rg*tc)**2/pc
   b = 0.07780*rg*tc/pc
   al = (1.+(0.37464+1.54226*ac-0.26992*ac**2)*(1.-(te/tc)**0.5))**2
   aa = a*al*pbic/(rg*te)**2
   bb = b*pbic/(rg*te)
   z0 = -(aa*bb-bb**2-bb**3)
   z1 = aa-3.*bb**2-2.*bb
   z2 = -(1.-bb)
   pp = ((3.*z1)-(z2**2))/3.
   q  = ((27.*z0)-(9.*z2*z1)+(2.*z2**3))/27.
   rr = (pp/3.)**3 + (q/2.)**2
   aaa = ((-q/2.)+(rr**0.5))**(1./3.)
   bbb = ((-q/2.)-(rr**0.5))**(1./3.)
   y1  = aaa + bbb
   zgic = y1 -z2/3.
"As per Walas - Phase Equilibria in Chemical Engineering pp 58...
and Perrys Handbook of Chemical Engineering pp 2-15"

   dengic = mwg*pbic/(rg*te*zgic)
   aic = (mbic*0.75/(pi*dengic))**(1./3.)
   array cr(20)
   constant cr=20*0.0
 end $"initial"

 dynamic
  derivative diffu2
   algorithm ialg=4       $"2'nd order Runge Kutta Method"
   cinterval  cint = 0.001

   k1 = k*rg*te          $"constnt for diffusion equatn to be integrated"
   k2 = (2.*st(te))/(ps*aic)  $"const for diffn equatn to be integrated"

   sol = b1 + b2*pb/1.e6 + b3*pb/(1.e6*te) + b4*(pb/(1.e6*te))**2
"solubility of gas in liquid - (m3/m3)"
"Correlations for Properties of Bitumen Saturated with CO2,"
"CH4, and N2, and Experiments With Combustion Gas Mixtures"
"Mehrotra and Svrcek - JCPT 1982-11 "
"Athabasca bitumen data correlated"

     cgi  = sol / 22.414          $"molar concentration of gas (kmol/m3)"
     dngi = cgi * mwg             $"gas density at interface (kg/m3)"
     dnbi = denl(te) - dngi       $"bitumen density at interface (kg/m3)"
     cbi  = dnbi / mwb            $"molar conc. of bitumen  (kmol/m3)"
     cti  = cbi + cgi             $"molar concentration total (kmol/m3)"
     xg = cgi / cti               $"mole fraction gas at interface"
     xb = cbi / cti               $"mole fraction bitumen at interface"
     k = cgi / pb                 $"Henrys Law coefficient "
     x = csic/(k*ps)              $"undersaturation parameter"
"Surface Tension Effects in Gas Bubble Dissolution and Growth"
"Weinberg -Chemical Eng Sci v36 1981 pp 138"

 procedural ( zg = a,b,al,rg,te,pb)
```

```
   aa = a*al*pb/(rg*te)**2
   bb = b*pb/(rg*te)
   z0 = -(aa*bb-bb**2-bb**3)
   z1 = aa-3.*bb**2-2.*bb
   z2 = -(1.-bb)
   pp = ((3.*z1)-(z2**2))/3.
   q  = ((27.*z0)-(9.*z2*z1)+(2.*z2**3))/27.
   rr = (pp/3.)**3 + (q/2.)**2
   aaa = ((-q/2.)+(rr**0.5))**(1./3.)
   bbb = ((-q/2.)-(rr**0.5))**(1./3.)
   y1  = aaa + bbb
   zg = y1 -z2/3.
   end $"procedural"
"As per Walas - Phase Equilibria in Chemical Engineering pp 58...
and Perrys Handbook of Chemical Engineering pp 2-15"

   pb = ps + 2.*st(te)/at          $"bubble pressure (Pa)"
   deng = pb*mwg/(zg*rg*te)       $"gas density (kg/m3)"

   k5 = 1./(1.-(1./(3.*(1.+g/k2))))
   g=integ(((-k1*(g*(1.0-x)+k2))/(g+k2))*k5*(1./sqrt(pi*tr)+1./g),gic)
   t = tr * (aic**2) / diff(te,xg)
   at = g * aic
   mb = (4./3.)*pi*(at**3)*deng
   gm = mb / mbic

   dmbdt = 4.*pi*(at**2)*deng*((diff(te,xg)/aic)*...
   ((-k1*(g*(1.0-x)+k2))/(g+k2))*k5*(1./sqrt(pi*tr)+1./g))

   flx = abs(dmbdt/(4.*pi*at**2))
   dmbdto = abs(dmbdt)

  procedural ( cr = g)
   do l2   ct = 1,20
   y = ct/5.0
   if (y.lt.g) goto l1
   k3 = (y-g) / (2.*sqrt(tr))
   k4 = 1. / (1. + 0.47047*k3)
   cr(ct) = (g/y) * (c1*k4 + c2*k4**2 + c3*k4**3) * exp(-(k3**2))
   goto l2
l1..cr(ct) = 1.0
l2..continue
  end $"procedural"
  end $"derivative"
   termt (tr.gt.tstop.or.g.lt.gmin)
 end $"dynamic"

 terminal
 end $"terminal"
end $"program"
```

Appendix C

Molecular Diffusion (Lumped) Model Dissolution of a Static CO_2 Bubble Into Athabasca Bitumen - ACSL Source Code - Diffus3.

```
program DIFFUS3
 " This program models the mass transfer from a static bubble assuming"
"  molecular diffusion only, ie Nu = 2.0. Reference WWW pp 651    "
"    Description of variables which are a function of time          "
"    at - actual bubble radius (m)"
"    tr - reduced time (dimensionless)"

 initial
   constant csic = 0.0          $"gas concentration at infinity (kmol/m3)"
   variable t = 0.0             $"initial time"
   constant ac = 0.225          $"CO2 accentric factor"
   constant tc = 304.2          $"CO2 critical temperature (K)"
   constant pc = 7.37646e6      $"CO2 critical pressure (Pa)"
   constant gr = 9.80665        $"gravitational constant (m/s**2)"
   constant mwg = 44.01         $"molecular wgt gas - CO2 (kg/kmol)"
   constant mwb = 594.6       $"molecular wgt Athabasca bitumen (kg/kmol)"
   constant pi = 3.14159
   constant tstop = 150.0       $"maximum  time"
   constant gmin = 0.01         $"minimum reduced bubble radius"
   constant gmmin = 1.0e-6      $"minimum reduced bubble mass"
   constant mbic = 5.0e-07      $"initial bubble mass (kg)"
   constant rg = 8314.          $"univ gas const - (kg*m**2/s**2*kmol*K)"
   constant te = 350.0          $"temperature (K)"
   constant ps = 1.0e6          $"system pressure (Pa - N/m**2)"
   constant b1 = -0.0073508     $"constants for solubility correlation"
   constant b2 = -14.794
   constant b3 = 6428.5
   constant b4 = 4971.39
   constant kc = 2.

   at = aic                     $"actual bubble radius (m)"

   table diff, 2, 6, 9/ ...
       296., 300., 323., 373., 423., 473., ...
       0.0, 0.001, 0.005, 0.01, 0.05, 0.1, 0.2, 0.3, 0.4,...
       2.3e-14, 4.65e-14, 1.08e-12, 6.25e-11, 4.43e-10, 7.92e-10,...
       1.42e-11, 1.45e-11, 1.58e-11, 7.73e-11, 4.57e-10, 8.50e-10,...
       7.07e-11, 7.22e-11, 7.48e-11, 1.36e-10, 5.14e-10, 9.97e-10,...
       1.41e-10, 1.44e-10, 1.48e-10, 2.10e-10, 5.84e-10, 1.21e-9,...
       7.01e-10, 7.15e-10, 7.32e-10, 7.95e-10, 1.15e-9, 1.48e-9,...
       1.39e-9, 1.42e-9, 1.45e-9, 1.51e-9, 1.84e-9, 2.11e-9,...
       2.72e-9, 2.77e-9, 2.83e-9, 2.90e-9, 3.17e-9, 3.58e-9,...
       3.98e-9, 4.06e-9, 4.15e-9, 4.22e-9, 4.43e-9, 4.81e-9,...
       5.17e-9, 5.27e-9, 5.39e-9, 5.46e-9, 5.62e-9, 6.27e-9/
"diffusivity (m**2/s) Mehrotra et al - Can.J.Ch.E. 87-09 pp 831 ...
Prediction of Mass Diffusivity of CO2 into Bitumen ...
Athabasca bitumen used in study ...
Correlation of diffusivity to temperature and xg ...
Range of values ; te - 296 to 473 K, xg - 0.0 to 0.4"

    table denl, 1, 4/ ...
        297.6, 314.9, 335.9, 369.7, ...
        1041.1, 1015.3, 1005.9, 984.1 /
"Average gas saturated liquid densities (kg/m3) ...
Svrcek and Mehrotra - Gas solubility, viscosity and density ...
measurements for Athabasca bitumen - JCPT 82-07 ...
Correlation of solubility to temperature ...
Range of values ; te - 297 to 369 K"

   table st, 1, 4 / ...
       337.1, 348.1, 377.1, 385.1, ...
       26.1e-3, 25.5e-3, 24.13e-3, 23.8e-3 /
```

```
"surface tension ( N/m - Pa m - dyne*e-3/cm )...
Prediction of Surface Tension of Athabasca Bitumen...
Mehrotra, Yee and Svrcek - CJChE 1985-04 ...
Range of values ; te - 337 to 385 K"


  pbic = ps

  a = 0.45724*(rg*tc)**2/pc
  b = 0.07780*rg*tc/pc
  ap = (1.+(0.37464+1.54226*ac-0.26992*ac**2)*(1.-(te/tc)**0.5))**2
  aa = a*ap*pbic/(rg*te)**2
  bb = b*pbic/(rg*te)
  z0 = -(aa*bb-bb**2-bb**3)
  z1 = aa-3.*bb**2-2.*bb
  z2 = -(1.-bb)
  pp = ((3.*z1)-(z2**2))/3.
  q  = ((27.*z0)-(9.*z2*z1)+(2.*z2**3))/27.
  rr = (pp/3.)**3 + (q/2.)**2
  aaa = ((-q/2.)+(rr**0.5))**(1./3.)
  bbb = ((-q/2.)-(rr**0.5))**(1./3.)
  y1  = aaa + bbb
  zgic = y1 - z2/3.
"As per Walas - Phase Equilibria in Chemical Engineering pp 58...
and Perrys Handbook of Chemical Engineering pp 2-15"

  dengic = mwg*pbic/(rg*te*zgic)
  aic=(mbic*0.75/(pi*dengic))**(1./3.)

  algorithm ialg=4          $" Runge Kutta Method - second order"
  nsteps   nstp = 1
  cint = 0.1

end $'initial'

dynamic
  gm = mb /mbic
  tr = t * diff(te,xg) / (aic**2)
  at = (0.75*mb/(pi*deng))**(1./3.)
  g = at / aic
  flx = abs(dmbdt/(4.*pi*at**2))
  dmbdto = abs (dmbdt)
 derivative mass

  sol = b1 + b2*pb/1.e6 + b3*pb/(1.e6*te) + b4*(pb/(1.e6*te))**2
"solubility of gas in liquid - (m3/m3)...
Correlations for Properties of Bitumen Saturated with CO2,...
CH4, and N2, and Experiments With Combustion Gas Mixtures...
Mehrotra and Svrcek - JCPT 1982-11 ...
Athabasca bitumen data correlated...
Range of values ; te - 298 to 369 K, pb - 1.7 to 6 MPa"

procedural (zg = a,b,ap,rg,te,pb)
  aa = a*ap*pb/(rg*te)**2
  bb = b*pb/(rg*te)
  z0 = -(aa*bb-bb**2-bb**3)
  z1 = aa-3.*bb**2-2.*bb
  z2 = -(1.-bb)
  pp = ((3.*z1)-(z2**2))/3.
  q  = ((27.*z0)-(9.*z2*z1)+(2.*z2**3))/27.
  rr = (pp/3.)**3 + (q/2.)**2
  aaa = ((-q/2.)+(rr**0.5))**(1./3.)
```

```
   bbb = ((-q/2.)-(rr**0.5))**(1./3.)
   y1  = aaa + bbb
   zg = y1 - z2/3.
 end $"procedural"
 "As per Walas - Phase Equilibria in Chemical Engineering pp 58...
 and Perrys Handbook of Chemical Engineering pp 2-15"

     cgi  = sol / 22.414          $"molar concentration of gas (kmol/m3)"
     dngi = cgi * mwg             $"gas density at interface (kg/m3)"
     dnbi = denl(te) - dngi       $"bitumen density at interface (kg/m3)"
     cbi  = dnbi / mwb            $"molar conc. of bitumen  (kmol/m3)"
     cti  = cbi + cgi             $"molar concentration total (kmol/m3)"
     xg = cgi / cti               $"mole fraction gas at interface"
     pb = ps + 2.*st(te)/at       $"bubble pressure (Pa)"
     deng = pb*mwg/(zg*rg*te)     $"gas density (kg/m3)"


   dmbdt = -2.0*pi*at*diff(te,xg)*(cgi-csic)*mwg*kc
   mb = integ(dmbdt,mbic)
   " Single sphere models for mass transfer kg/s"

 end $'derivative mass'

   termt (t.gt.tstop.or.g.lt.gmin.or.gm.lt.gmmin)
 end $'dynamic'
 terminal
 end $'terminal'
end $'program'
```

Appendix D

Brian-Hales'/Levich's Correlation Model Dissolution of a Rising CO_2 Bubble Into Athabasca Bitumen - ACSL Source Code - Diffus4.

```
program DIFFUS4
 " This program models the mass transfer from a rising bubble using"
" Brian and Hales correlation ( Pe < 10000 ) or Levichs correlation"
" ( Pe > 10000 ). Terminal velocity utilized  "

 initial
   constant zic = 0.0          $"initial bubble height (m)"
   constant gm = 1.0           $"initial reduced mass"
   constant g = 1.0            $"initial reduced radius"
   constant vt = 0.0           $"initial terminal velocity (m/s)"
   constant flx = 0.0          $"initial mass flux(kg/m2s)"
   constant csic = 0.0         $"gas concentration at infinity (kmol/m3)"
   variable t = 1.0e-06        $"initial non zero time"
   constant ac = 0.225         $"CO2 accentric factor"
   constant tc = 304.2         $"CO2 critical temperature (K)"
   constant pc = 7.37646e6     $"CO2 critical pressure (Pa)"
   constant gr = 9.80665       $"gravitational constant (m/s**2)"
   constant mwg = 44.01        $"molecular wgt gas - CO2 (kg/kmol)"
   constant mwb = 594.6        $"molar wgt Athabasca bitumen (kg/kmol)"
   constant pi = 3.14159
   constant tstop = 1000.0     $"maximum time (s)"
   constant mbic = 5.0e-07     $"initial bubble mass (kg)"
   constant gmin = 0.01        $"minimum reduced bubble radius"
   constant gmmin = 1.0e-6     $"minimum reduced bubble mass"
   constant rg = 8314.         $"univ gas const - (kg*m**2/s**2*kmol*K)"
   constant te = 300.0         $"temperature (K)"
   constant ps = 1.0e6         $"system pressure (Pa - N/m**2)"
   constant reic = 5.e-09      $"minimum Reynolds number"
   constant a1 = 0.815991      $"constants for viscosity correlation"
   constant a2 = -0.0044495
   constant a3 = 0.076639
   constant a4 = -34.5133
   constant b1 = -0.0073508    $"constants for solubility correlation"
   constant b2 = -14.794
   constant b3 = 6428.5
   constant b4 = 4971.39

   table diff, 2, 6, 9/ ...
       296., 300., 323., 373., 423., 473., ...
       0.0, 0.001, 0.005, 0.01, 0.05, 0.1, 0.2, 0.3, 0.4,...
       2.3e-14, 4.65e-14, 1.08e-12, 6.25e-11, 4.43e-10, 7.92e-10,...
       1.42e-11, 1.45e-11, 1.58e-11, 7.73e-11, 4.57e-10, 8.50e-10,...
       7.07e-11, 7.22e-11, 7.48e-11, 1.36e-10, 5.14e-10, 9.97e-10,...
       1.41e-10, 1.44e-10, 1.48e-10, 2.10e-10, 5.84e-10, 1.21e-9,...
       7.01e-10, 7.15e-10, 7.32e-10, 7.95e-10, 1.15e-9, 1.48e-9,...
       1.39e-9, 1.42e-9, 1.45e-9, 1.51e-9, 1.84e-9, 2.11e-9,...
       2.72e-9, 2.77e-9, 2.83e-9, 2.90e-9, 3.17e-9, 3.58e-9,...
       3.98e-9, 4.06e-9, 4.15e-9, 4.22e-9, 4.43e-9, 4.81e-9,...
       5.17e-9, 5.27e-9, 5.39e-9, 5.46e-9, 5.62e-9, 6.27e-9/
"diffusivity (m**2/s) Mehrotra et al - Can.J.Ch.E. 87-09 pp 831 ...
Prediction of Mass Diffusivity of CO2 into Bitumen ...
Athabasca bitumen used in study ...
Correlation of diffusivity to temperature and xg ...
Range of values ; te - 296 to 473 K, xg - 0.0 to 0.4"

    table denl, 1, 4/ ...
        297.6, 314.9, 335.9, 369.7, ...
        1041.1, 1015.3, 1005.9, 984.1 /
"Average gas saturated liquid densities (kg/m3) ...
Svrcek and Mehrotra - Gas solubility, viscosity and density ...
measurements for Athabasca bitumen - JCPT 82-07 ...
Correlation of solubility to temperature ...
```

```
Range of values ; te - 297 to 369 K"

   table st, 1, 4 / ...
       337.1, 348.1, 377.1, 385.1, ...
       26.1e-3, 25.5e-3, 24.13e-3, 23.8e-3 /
 "surface tension ( N/m - Pa m - dyne*e-3/cm )...
 Prediction of Surface Tension of Athabasca Bitumen...
 Mehrotra, Yee and Svrcek - CJChE 1985-04 ...
 Range of values ; te - 337 to 385 K"

   pbic = ps
   a = 0.45724*(rg*tc)**2/pc
   b = 0.07780*rg*tc/pc
   ap = (1.+(0.37464+1.54226*ac-0.26992*ac**2)*(1.-(te/tc)**0.5))**2
   aa = a*ap*pbic/(rg*te)**2
   bb = b*pbic/(rg*te)
   z0 = -(aa*bb-bb**2-bb**3)
   z1 = aa-3*bb**2-2.*bb
   z2 = -(1.-bb)
   pp = ((3.*z1)-(z2**2))/3.
   q  = ((27.*z0)-(9.*z2*z1)+(2.*z2**3))/27.
   rr = (pp/3.)**3 + (q/2.)**2
   aaa = ((-q/2.)+(rr**0.5))**(1./3.)
   bbb = ((-q/2.)-(rr**0.5))**(1./3.)
   y1  = aaa + bbb
   zgic = y1 - z2/3.
 "As per Walas - Phase Equilibria in Chemical Engineering pp 58...
 and Perrys Handbook of Chemical Engineering pp 2-15"

   dengic = mwg*pbic/(rg*te*zgic)
   aic = (mbic*0.75/(pi*dengic))**(1./3.)
   at=aic                          $"initial bubble radius (m)"
   deng=dengic
   zg = zgic

 end $'initial'

 dynamic

   algorithm ialg=4          $" Second order Runge-Kutta method"
   cinterval cint = 0.01

   gm = mb / mbic
   g = at / aic
   deng = pb*mwg/(zg*rg*te)          $"gas density (kg/m3)"
   vt = (abs(gr*(denl(te)/deng-1.)*(at*deng)/(0.375*cd*denl(te))))**0.5
   flx = abs(dmbdt/(4.*pi*at**2))
   dmbdto = abs(dmbdt)

 procedural (zg = a,b,ap,rg,te,pb)
   aa = a*ap*pb/(rg*te)**2
   bb = b*pb/(rg*te)
   z0 = -(aa*bb-bb**2-bb**3)
   z1 = aa-3.*bb**2-2.*bb
   z2 = -(1.-bb)
   pp = ((3.*z1)-(z2**2))/3.
   q  = ((27.*z0)-(9.*z2*z1)+(2.*z2**3))/27.
   rr = (pp/3.)**3 + (q/2.)**2
   aaa = ((-q/2.)+(rr**0.5))**(1./3.)
   bbb = ((-q/2.)-(rr**0.5))**(1./3.)
   y1  = aaa + bbb
   zg = y1 - z2/3.
```

```
 end $"procedural"
 "As per Walas - Phase Equilibria in Chemical Engineering pp 58...
 and Perrys Handbook of Chemical Engineering pp 2-15"

  derivative vel

   sol = b1 + b2*pb/1.e6 + b3*pb/(1.e6*te) + b4*(pb/(1.e6*te))**2
"solubility of gas in liquid - (m3/m3)...
Correlations for Properties of Bitumen Saturated with CO2,...
CH4, and N2, and Experiments With Combustion Gas Mixtures...
Mehrotra and Svrcek - JCPT 1982-11 ...
Athabasca bitumen data correlated...
Range of values ; te - 298 to 369 K, pb - 1.7 to 6 MPa"

   cgi  = sol / 22.414          $"molar concentration of gas (kmol/m3)"
   dngi = cgi * mwg                $"gas density at interface (kg/m3)"
   dnbi = denl(te) - dngi       $"bitumen density at interface (kg/m3)"
   cbi  = dnbi / mwb               $"molar conc. of bitumen  (kmol/m3)"
   cti  = cbi + cgi              $"molar concentration total (kmol/m3)"
   xg = cgi / cti                  $"mole fraction gas at interface"
   pb = ps - denl(te)*gr*z + 2.*st(te)/at      $"bubble pressure (Pa)"
   re = max(denl(te)*vt*2.*at/visc,reic)       $"Reynolds number"
   sc = visc / (denl(te)*diff(te,xg))       $"Schmidt number"
   pe = re * sc                             $" Peclet number"

   visc=10.**(10.**(a1 + a2*(te-273.1) + a3*pb*1.e-6 + a4*pb*...
      1.e-6/te))* 1.e-3
"dynamic viscosity (Pa*s) of gas saturated bitumen...
Correlations for Properties of Bitumen Saturated with CO2...
CH4, and N2, and Experiments with Combustion Gas Mixtures...
Mehrotra and Svrcek - JCPT 1982-11...
Range of values; te - 298 to 369 K, pb - 1.7 to 6 MPa"

   z = integ(vt,zic)

  procedural  ( cd = re )
   if (re.lt.0.9) cd = 24./re
   if (re.ge.0.9) cd = 18.5/(re**0.6)
  end $'procedural'

  procedural  ( kc = pe )
   if (pe.lt.1.0e4) kc = sqrt(4. + 1.21*(pe**(2./3.)))
   if (pe.ge.1.0e4) kc = 1.01*(pe**(1./3.))
  end $'procedural'

   dmbdt = -2.0*pi*at*diff(te,xg)*(cgi-csic)*mwg*kc
   mb = integ(dmbdt,mbic)
   " Single sphere models for mass transfer kg/s"
   at = (0.75*mb/(pi*deng))**(1./3.)

  end $'derivative '

   termt (t.gt.tstop.or.g.lt.gmin.or.gm.lt.gmmin)
  end $'dynamic'
  terminal
  end $'terminal'
 end $'program'
```

Appendix E

Higbie's Penetration Theory Model Dissolution of a Rising CO_2 Bubble Into Athabasca Bitumen - ACSL Source Code - Diffus5.

```
program DIFFUS5
" This program models the mass transfer from a rising bubble using ...
  Higbies penetration theory. Reference WWW pp 616...
    Description of variables which are a function of time ...
    at - actual bubble radius (m)...
    tr - reduced time (dimensionless)"

 initial


   constant gm = 1.0          $"initial reduced mass"
   constant g = 1.0           $"initial reduced radius"
   constant vt = 0.0          $"initial terminal velocity (m/s)"
   constant flx = 0.0         $"initial mass flux(kg/m2s)"
   constant vic = 0.0         $"initial bubble velocity (m/s)"
   constant zic = 0.0         $"initial bubble height (m)"
   constant csi = 0.0         $"gas concentration at infinity (kmol/m3)"
   constant ac = 0.225        $"CO2 accentric factor"
   constant tc = 304.2        $"CO2 critical temperature (K)"
   constant pc = 7.37646e6    $"CO2 critical pressure (Pa)"
   constant gr = 9.80665      $"gravitational constant (m/s**2)"
   variable t = 0.0           $"time    (sec)"
   constant mwg = 44.01       $"molecular wgt gas - CO2 (kg/kmol)"
   constant mwb = 594.6       $"molecular wgt Athabasca bitmn (kg/kmol)"
   constant pi = 3.14159
   constant tstop = 100       $"maximum  time"
   constant gmin = 0.01       $"minimum reduced bubble radius"
   constant gmmin = 1.0e-6    $"minimum reduced bubble mass"
   constant mbic = 5.0e-7     $"initial bubble mass (kg)"
   constant rg = 8314.        $"univ gas const - (kg*m**2/s**2*kmol*K)"
   constant te = 300.0        $"temperature (K)"
   constant ps = 1.0e6        $"system pressure (Pa - N/m**2)"
   constant reic = 5.e-09     $"minimum Reynolds number"
   constant a1 = 0.815991     $"constants for viscosity correlation"
   constant a2 = -0.0044495
   constant a3 = 0.076639
   constant a4 = -34.5133
   constant b1 = -0.0073508   $"constants for solubility correlation"
   constant b2 = -14.794
   constant b3 = 6428.5
   constant b4 = 4971.39



   table diff, 2, 6, 9 / ...
         296, 300, 323, 373, 423, 473, ...
         0.0, 0.001, 0.005, 0.01, 0.05, 0.1, 0.2, 0.3, 0.4,...
         2.3e-14, 4.65e-14, 1.08e-12, 6.25e-11, 4.43e-10, 7.92e-10,...
         1.42e-11, 1.45e-11, 1.58e-11, 7.73e-11, 4.57e-10, 8.50e-10,...
         7.07e-11, 7.22e-11, 7.48e-11, 1.36e-10, 5.14e-10, 9.97e-10,...
         1.41e-10, 1.44e-10, 1.48e-10, 2.10e-10, 5.84e-10, 1.21e-9,...
         7.01e-10, 7.15e-10, 7.32e-10, 7.95e-10, 1.15e-9, 1.48e-9,...
         1.39e-9, 1.42e-9, 1.45e-9, 1.51e-9, 1.84e-9, 2.11e-9,...
         2.72e-9, 2.77e-9, 2.83e-9, 2.90e-9, 3.17e-9, 3.58e-9,...
         3.98e-9, 4.06e-9, 4.15e-9, 4.22e-9, 4.43e-9, 4.81e-9,...
         5.17e-9, 5.27e-9, 5.39e-9, 5.46e-9, 5.62e-9, 6.27e-9 /
"diffusivity (m**2/s) Mehrotra et al - Can.J.Ch.E. 87-09 pp 831 "
"Prediction of Mass Diffusivity of CO2 into Bitumen  "
"Athabasca bitumen used in study"
"Correlation of diffusivity to temperature and xg"

    table denl, 1, 4 / ...
```

```
          297.6, 314.9, 335.9, 369.7, ...
          1041.1, 1015.3, 1005.9, 984.1 /
"Average gas saturated liquid densities (kg/m3) "
"Svrcek and Mehrotra - Gas solubility, viscosity and density "
"measurements for Athabasca bitumen - JCPT 82-07 "
"Correlation of solubility to temperature"

  table st, 1, 4 / ...
       337.1, 348.1, 377.1, 385.1, ...
       26.1e-3, 25.5e-3, 24.13e-3, 23.8e-3 /
 "surface tension ( N/m - Pa m - dyne*e-3/cm )"
 "Prediction of Surface Tension of Athabasca Bitumen"
 "Mehrotra, Yee and Svrcek - CJChE 1985-04"

  pbic = ps

  a = 0.45724*(rg*tc)**2/pc
  b = 0.07780*rg*tc/pc
  ap = (1.+(0.37464+1.54226*ac-0.26992*ac**2)*(1.-(te/tc)**0.5))**2
  aa = a*ap*pbic/(rg*te)**2
  bb = b*pbic/(rg*te)
  z0 = -(aa*bb-bb**2-bb**3)
  z1 = aa-3*bb**2-2.*bb
  z2 = -(1.-bb)
  pp = ((3.*z1)-(z2**2))/3.
  q  = ((27.*z0)-(9.*z2*z1)+(2.*z2**3))/27.
  rr = (pp/3.)**3 + (q/2.)**2
  aaa = ((-q/2.)+(rr**0.5))**(1./3.)
  bbb = ((-q/2.)-(rr**0.5))**(1./3.)
  y1  = aaa + bbb
  zgic = y1 - z2/3.
"As per Walas - Phase Equilibria in Chemical Engineering pp 58...
and Perrys Handbook of Chemical Engineering pp 2-15"

  dengic = mwg*pbic/(rg*te*zgic)
  aic = (mbic*0.75/(pi*dengic))**(1./3.)
  at=aic                        $"initial bubble radius (m)"
  deng=dengic
  zg = zgic


 end  $"initial"

dynamic
  gm = mb / mbic
  g = at / aic
  deng = pb*mwg/(zg*rg*te)          $"gas density (kg/m3)"
  vt = (abs(gr*(denl(te)/deng-1.)*(at*deng)/(0.375*cd*denl(te))))**0.5
  flx = abs(dmbdt/(4.*pi*at**2))
  dmbdto = abs(dmbdt)

procedural (zg = a,b,ap,rg,te,pb)
  aa = a*ap*pb/(rg*te)**2
  bb = b*pb/(rg*te)
  z0 = -(aa*bb-bb**2-bb**3)
  z1 = aa-3.*bb**2-2.*bb
  z2 = -(1.-bb)
  pp = ((3.*z1)-(z2**2))/3.
  q  = ((27.*z0)-(9.*z2*z1)+(2.*z2**3))/27.
  rr = (pp/3.)**3 + (q/2.)**2
  aaa = ((-q/2.)+(rr**0.5))**(1./3.)
  bbb = ((-q/2.)-(rr**0.5))**(1./3.)
```

```
    y1  = aaa + bbb
    zg = y1 - z2/3.
  end $"procedural"
  "As per Walas - Phase Equilibria in Chemical Engineering pp 58...
  and Perrys Handbook of Chemical Engineering pp 2-15"

    cinterval  cint = 1.0e-02
    algorithm ialg = 4          $"Runge Kutta Method - second order"

  derivative vel

    sol = b1 + b2*pb/1.e6 + b3*pb/(1.e6*te) + b4*(pb/(1.e6*te))**2
 "solubility of gas in liquid - (m3/m3)"
 "Correlations for Properties of Bitumen Saturated with CO2,"
 "CH4, and N2, and Experiments With Combustion Gas Mixtures"
 "Mehrotra and Svrcek - JCPT 1982-11 "
 "Athabasca bitumen data correlated"

      cgi  = sol / 22.414           $"molar concentration of gas (kmol/m3)"
      dngi = cgi * mwg              $"gas density at interface (kg/m3)"
      dnbi = denl(te) - dngi        $"bitumen density at interface (kg/m3)"
      cbi  = dnbi / mwb             $"molar conc. of bitumen  (kmol/m3)"
      cti  = cbi + cgi              $"molar concentration total (kmol/m3)"
      xg = cgi / cti                $"mole fraction gas at interface"
      pb = ps - denl(te)*gr*z + 2.*st(te)/at      $"bubble pressure (Pa)"
      re = max(denl(te)*vt*2.*at/visc,reic)       $"Reynolds number"

  visc=10.**(10.**(a1 + a2*(te-273.1) + a3*pb*1.e-6 + a4*pb*1.e-6/te...
        ))*1.e-3
 "dynamic viscosity (Pa*s) of gas saturated bitumen "
 "Correlations for Properties of Bitumen Saturated with CO2"
 "CH4, and N2, and Experiments with Combustion Gas Mixtures"
 "Mehrotra and Svrcek - JCPT 1982-11"


    z = integ(vt,zic)


   procedural  ( cd = re )       $"drag coefficient"
    if (re.lt.0.9) cd = 24./re
    if (re.ge.0.9) cd = 18.5/(re**0.6)
    end $"procedural"

    dmbdt = -4.*mwg*(cgi-csi)*at*sqrt(pi*diff(te,xg)*vt*2.*at)
    mb = integ(dmbdt,mbic)
    " Penetration model for mass transfer kg/s"

    at = (0.75*mb/(pi*deng))**(1./3.)

   end $"derivative"
    termt (t.gt.tstop.or.g.lt.gmin.or.gm.lt.gmmin)
  end $"dynamic"
  terminal
  end $"terminal"
end $"program"
```